A STUDY ON MILLING OF GLASS FIBER REINFORCED POLYMER

by
DEBOJYOTI BANDYOPADHYAY

Examination Roll No. **M4MEC19027**
Registration No. **140885 of 2017-2018**

A thesis submitted in the partial fulfillment
of the requirements for the degree of
Master of Mechanical Engineering

FACULTY OF ENGINEERING AND TECHNOLOGY
JADAVPUR UNIVERSITY
Kolkata – 700032
2019

A STUDY ON MILLING OF
GLASS FIBER REINFORCED POLYMER

by
DEBOJYOTI BANDYOPADHYAY

Examination Roll No. **M4MEC19027**
Registration No. **140885 of 2017-2018**

A thesis submitted in the partial fulfillment of the requirements for the degree of
Master of Mechanical Engineering

FACULTY OF ENGINEERING AND TECHNOLOGY
JADAVPUR UNIVERSITY
Kolkata – 700032
2019

DEDICATED TO

MY BELOVED SISTER

Ms. DEBOSMITA BANERJEE

AND

MY THESIS ADVISOR

Prof. ASISH BANDYOPADHYAY

JADAVPUR UNIVERSITY
FACULTY OF ENGINEERING AND TECHNOLOGY
CERTIFICATE OF RECOMMENDATION

Date:

I, hereby recommend that the thesis presented under my supervision by Sri. Debojyoti Bandyopadhyay entitled "**A STUDY ON MILLING OF GLASS FIBER REINFORCED POLYMER"** be accepted in partial fulfillment of the requirements for the Degree of Master of Mechanical Engineering during the academic session 2018-2019.

To the best of my knowledge, the matter embodied in this thesis has not been submitted to any other university/ institute for the award of any degree or diploma.

_____

Dr. Asish Bandyopadhyay
Professor,
Mechanical Engineering Department.
(Thesis Supervisor)

_____

COUNTERSIGNED

Dr. Gautam Majumdar
Professor and Head,
Mechanical Engineering Department.

_____

Prof. Chiranjib Bhattacharjee
Dean,
Faculty of Engineering and Technology
Jadavpur University.

JADAVPUR UNIVERSITY
FACULTY OF ENGINEERING AND TECHNOLOGY

CERTIFICATE OF APPROVAL*

The foregoing thesis is hereby approved as a creditable study of an engineering subject carried out and presented in a manner satisfactory to warrant its acceptance as a prerequisite to the degree for which it has been submitted. It is understood that by this approval the undersigned do not endorse or approve any statement made, the opinion expressed or conclusion drawn therein but approve the thesis only for the purpose for which it has been submitted.

_____

COMMITTEE OF THE FINAL EXAMINATION FOR EVALUATION OF THESIS

_____

*Only in case the thesis is approved

DECLARATION OF ORIGINALITY AND COMPLIANCE OF ACADEMIC ETHICS

I, hereby declare that this thesis contains literature survey and original research work by the undersigned candidate, as part of my Master of Mechanical Engineering during academic session 2018-2019.

All information in this document has been obtained and presented in accordance with academic rules and ethical conduct.

I also declare that, as required by this rules and conduct, I have fully cited and referenced all material and results that are not original to this work.

Name : Debojyoti Bandyopadhyay
Roll Number : M4MEC19027 (Examination Roll No.)
: 001711202026 (Class Roll No.)
Thesis Title : A study on Milling of Glass Fiber Reinforced Polymer.

Date:

_____

Debojyoti Bandyopadhyay

ACKNOWLEDGEMENT

The author would like to express his deepest sense of gratitude and heartiest appreciation to his respected thesis advisor Dr. Asish Bandyopadhyay, Professor, Mechanical Engineering Department, Jadavpur University for his intellectual support, guidance and encouragement for which the author has always been confident of attaining his goals. The author wants to offer special thanks to Dr. Gautam Majumdar, Professor and Head, Mechanical Engineering Department and Dr. Titas Nandi, Professor and Workshop Superintendent, Mechanical Engineering Department for giving him the opportunity to complete this thesis work. The author also expresses his sincere gratitude to all faculty members of Mechanical Engineering Department for their blessing and advice during the thesis work.

The author would like to thank Mr. Sushanta Kumar Ghoku, Ph.D. Research Scholar of Jadavpur University, Mr. Abhijit Haldar, Jr. Mechanic, G. C. Sen Memorial Machine Tool Research Laboratory and Mr. Soumyabrata Chakravarty, M.Tech Student, Jadavpur University, who helped him to conduct the experiments. Also, the author is indebted to Dr. Nikhil Kumar, Prof. Suman Nihar, Prof. Abhishek Mandal and Mr. Angshuman Roy for their constant help during this work. The author would like to thank all the staff members of Blue Earth Machine Shop, Mechanical Engineering Department, Jadavpur University for helping him during the research work.

The author is also thankful to all other batch mates for their support.

Date:

_____

(Debojyoti Bandyopadhyay)

CONTENTS Pages

CHAPTER – 2

CHAPTER – 3

CHAPTER – 4

CHAPTER- 1

1. INTRODUCTION

Many of our modern technologies require materials with unusual combinations of properties that cannot be met by the conventional metal alloys, ceramics and polymeric materials. This is especially true for materials that are needed for aerospace, underwater and transportation applications. Engineers are continuously searching for structural materials that have low densities are strong, stiff with high abrasion and impact strength. Frequently, strong materials are relatively dense; also, increasing the strength or stiffness generally results in a decrease in impact strength. Material property combinations and ranges have been, and yet being, extended by the development of composite materials. A composite is considered to be any multiphase material that exhibits a significant proportion of the properties of both constituent phases such that a better combination of properties is realized. According to this principle of combined action, better property combinations are fashioned by the judicious combination of two or more distinct materials. In designing composite materials, scientists and engineers have ingeniously combined various metals, ceramics, and polymers to produce a new generation of extraordinary materials. Most composites have been created to improve combinations of mechanical characteristics such as stiffness, toughness, and ambient and high temperature strength.

There are many naturally occurring composites, such as wood and bones. Wood consists of strong cellulose fiber held together by lignin matrix. Bones consists of short and soft collagen fibers embedded in mineral matrix. One simple scheme for the classification of composite materials is shown in Fig- 1.1.

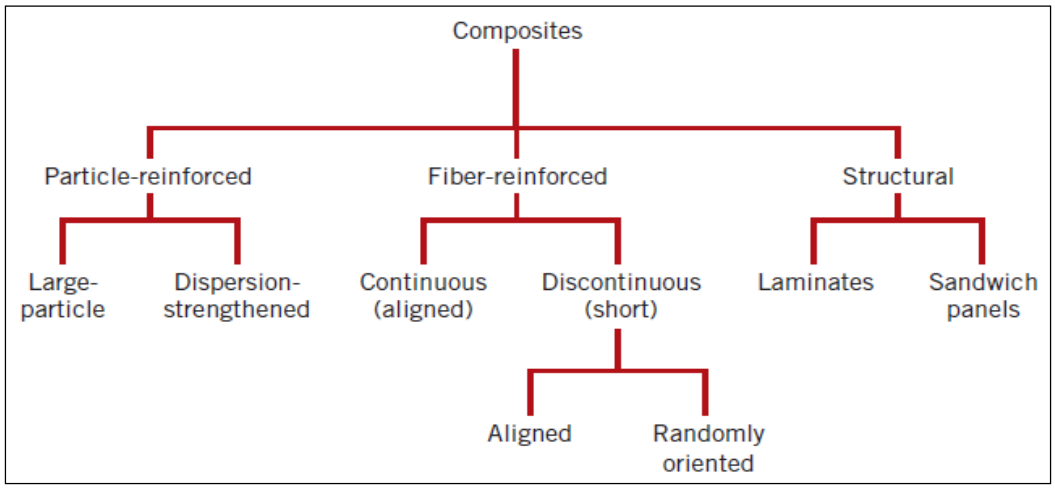

Fig-1.1 Various composite materials [55]

Among many types of composite materials, fiber-reinforced polymer (FRP) composites have been attractive and extensively used. Glass fiber reinforced polymers (GFRP) are widely used composite materials in aerospace, wind power stations, hybrid cars, marine industries etc,

applications due to their outstanding properties like high strength, low weight and high fatigue strength. Composite materials thus far can be defined as materials consisting of two or more constituents (phases) that combine at macroscopic level and are not soluble in each other. Modern synthetic composites using reinforced fibers (one phase) and matrices (another phase) of varies type have been introduced as replacement materials to metals in civilian, military and aerospace applications.

While the advantages of composite materials over conventional materials are obvious, one must not overlook their limitations. There is an apparent lack of knowledge and experience that limits their fast incorporation into existing and new designs. The high cost of materials and complexities in their manufacturing is perhaps the most serious problems that designers with composites have to deal with. Components fabricated from composite materials are endeavored to be made net shape. This is made possible because of the fact that many components are built layer by layer out of contoured to- dimensional plies that closely captures the final shape of the product. Even though composite components are often made net shape, some machining is often unavoidable. In many cases excess material is added to compensate for material conformity to complex mold shapes and for locating and featuring performs. Resin flashing may also result after molding and curing of fiber- resin performs. This excess materials has to be removed my machining. Machining is also indispensible process for shaping parts from stocking composite materials and for finishing close-tolerance components. Some of the common machining processes used are edge trimming, turning, drilling and grinding. Despite the existing experience and knowledge in machining traditional materials such as metals, it has been challenge to maintain consistent results in terms of machining quality for composite material.

Due to fiber arrangements or orientation, poor surface finish which includes fiber pullout, matrix delamination and subsurface damage and matrix polymer failures is usually observed if improper machining conditions are applied. Secondly tool sharpness is greatly affected by the abrasiveness of the fiber embedded in composite materials. Inadequate sharpness accounted for the increase in tool forces and heat generation on machined surface. These result in performance degradation of machined part and put a restriction on widespread usage of FRP composites. In current aircraft manufacturing, milling and drilling are critical for finishing trimmed edges of panels, cutting windows or openings, or making accurate holes to rivet pieces together. Machining of composites is vastly different from that of metals, despite the fact that mostly metal machining tools and technology are used for composites. Unlike metals, composites are inhomogeneous and their interaction with the cutting tool during machining is a complex phenomenon that is not well understood. Machining may adversely affect the quality of the composite part due to defects such as delamination, cracking, fiber pull out and burning during machining. The abrasiveness of reinforcement fibers and the need to shear them neatly put additional requirement and constraints on selection of tool materials and geometry. Milling is the important operations for slots and hole making in engineering field. During the milling operation, the process parameters like rotational speed, feed rate, depth of cut and cutter diameter etc greatly affect the delamination and surface quality. The delamination is a major problem associated with the milling of chopped glass fibers reinforced polyester composites. The milling by the optimal milling process parameters is most

important in machining shop, than the “trial and error” method, to achieve the desire goals. Because the “trial and error” method is not efficient and that can be time consuming and also increases the cost and loss efficiency.

As the understanding of machining of GFRP for drilling and turning is matured, the focus research must now switch to the complex milling operation. Since the use of FRP composites finds tremendous increase in wide range of applications, one can expect broader industrial applications of milling such materials. Hence in this work an attempt has been made to study the side and face milling on Glass Fiber Reinforced Polymer.

1.1 MACHINE TOOL VIBRATION

One common problem with milling is the occurrence of vibration. Excessive vibration is quickly translated into degraded milling performance. Work piece quality suffers and cost rises. So it is very essential to diagnose and check vibration. To achieve this goal, understanding relating to dynamic behavior of the milling machine has to be précised and clear. Study in this regard is still being continued. In so far, as the effect of process parameters on milling cutter vibration is concerned, the publications are rare. Even if chatter doesn’t occur, machine cutter does vibrate and this vibration behavior may be influenced by the parameters of the process, but little work has so far been done in this regard.

A machine tool, as viewed from one point, is designed to achieve basically two objectives. (1) Production desired orientation to the cutter with respect to the work piece (2) Imparting desired cutting and feed motions to the work piece. The accuracy of operations and relative motions is necessary for obtaining the desired dimensional and finishing accuracy on the work-piece. However, due to a variety of reasons it is impossible to obtain error free orientations or relative motions. The chief cause of this is the absence of proper dynamic rigidity of the machine tool-work system. The overall performance of the machine tool depends primarily upon the static and dynamic behavior of the machine structure. This in turn is dependent upon the individual elements and joints, which make up the structure. With the ever-increasing demands for high productivity, precision working and good surface quality in machining, the design of the basic structure is receiving more attention. At the same time attempts are being made in this field to reduce the vibration during the metal-cutting operation by selecting ne tool material, modifying cutting parameters (geometry) of the cutting tool itself.

The design of the machine tool structure differs from that of the other structures in that, the allowable limits of deflection are very small and the areas involved are, however relatively large, resulting in development of stresses in members far below the material permissible stress. Hence, the governing factors of machine tool structures are static stiffness to reduce deflection under heavy loads applied to the structure and dynamic stiffness to prevent resonance vibrations under high working frequencies.

Modern trends in machine tool development have put on maximum thrust on accuracy and reliability. In today's world of intense competition, achievement of greater accuracy and productivity at the same time has made it impossible to design machine tools only from static considerations. So, the principle criteria to be taken into consideration in developing new machine tools are: accuracy, case operation and safety, productivity and economy in production. Operation accuracy of machine tools to produce components to specifications is affected by the geometrical, kinematic and dynamic stability of the machine tools. Hence, the dimensional and surface qualities of the work piece produced depend on dynamic characteristics of the machine tools under action of cutting forces and torque developed due to above or during vibrations (self-excited or forced) developed during operations.

Consideration of dynamic instability of the machine tools has become a bare necessity in modern machine tool design industry worldwide. Any relative vibratory motion present between the cutting tool and the job will have a negative effect on the performance of the machine tools. Machine tool vibration has harmful effect on tool life which subsequently lowers the productivity and increases cost of production. The requisite operational excellence of machine tools is obtained by incorporation sufficient static and dynamic rigidity of the machine tool along with adding vibration-proof features, such as attaching visco-elastic damping layers to the machine tool structure, adding vibration isolators etc.

1.2 TYPES OF VIBRATION IN MACHINE TOOLS

During operation, machine tools are subjected to static and dynamic loads, which may act in the following manners:
(a) Dynamic behavior of machine tools solely caused by acting load during the action period of the load (Free vibration),
(b) Dynamic behavior started by a load but persistent after load is withdrawn (Free Vibration),
(c) Dynamic behavior through interaction of structural dynamics of machine tool and forced generated the chip removal process (self-excited vibration).

1.3 DYNAMIC STABILITY OF MACHINE TOOLS

Dynamic stability of a system is attained when the masses of a distributed system vibrate with decreasing amplitudes towards the original state of equilibrium, while the reverse is true for dynamically unstable system. Thus dynamic stability signifies transient response characteristics of the system.

Dynamic rigidity is the ratio of amplitude of vibratory force to the vibratory displacement at a given frequency. This is the measure of resistance to vibration of the structure of the system. In effect, dynamic rigidity refers to the steady state vibrations.

One major type of dynamic instability in a machine tools is the occurrence of self-excited vibrations, frequency termed as **chatter**. Hence, the structure of any machine tool has considerable effect on its dynamic stability and it has the immense importance in analysis and design of machine tools.

1.4 SOURCES OF VIBRATIONS IN MACHINE TOOL

Six main sources for vibration identified are:

1. Transmission of vibration from vibrating foundation due to external sources of vibration,
2. Defects, faulty arrangements and unbalance in driving mechanism,
3. Periodically discontinuous cutting process,
4. Machine tool chatter,
5. Varying nature of cutting forces due to non-homogeneity of work piece material and
6. Build-up edges changing the instantaneous rake angle of the cutting tool.

1.5 MACHINE TOOLS AS A DYNAMIC SYSTEM

A machine tool can be approximated as an elastic system constituting an aggregation of machine-fixture-tool- work piece complex (MFTW) and the working processes occurring (cutting, friction, electro-dynamic and other processes in the elastic system) at the time of machining.

All the factors affecting the elastic system can be represented in the form of a diagram (Fig- 1.2), which is valid for the case in which the deformation of the elastic system does not lead to vibration in the magnitude of force. In many cases, the relative positions of the components of the system are changed by the deformation stated above, which constitutes a movable joint or association, and thereby change the conditions under which the working process operates. This, in turn, changes the acting forces. The variation of forces with deformation of the system contradicts the proposition of considering those forces as external (Fig- 1.3) depicts this phenomenon).

This interaction of the MFTW elastic system with criteria forces, thermal effects, properties of cutter and work-piece materials etc should also be taken care of. The remaining forces, independent of the deformations of the elastic system, are external in reference to the system. Their effects are shown by downward arrow marked f(t) in Fig- 1.3, supposed to be time varying. These include forces due to impacts and vibrations transmitted from outside through the foundation or originated in the system itself because of inaccurate alignment of drive-mechanisms, faulty meshing of gears or other defects in manufacturing of parts and their assemblies.

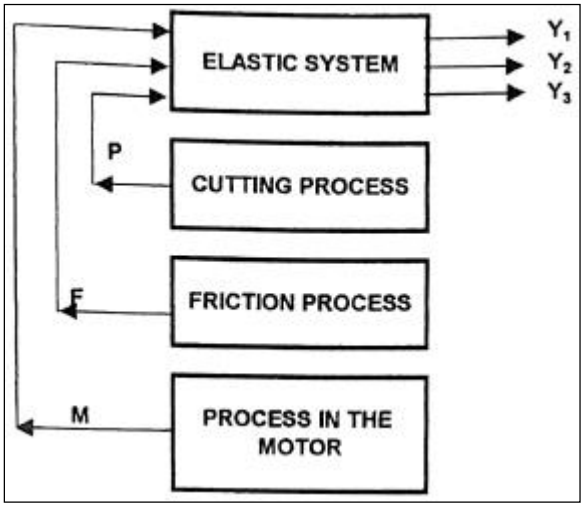

Fig- 1.2 Open circuit Dynamic system of a machine tool [53]

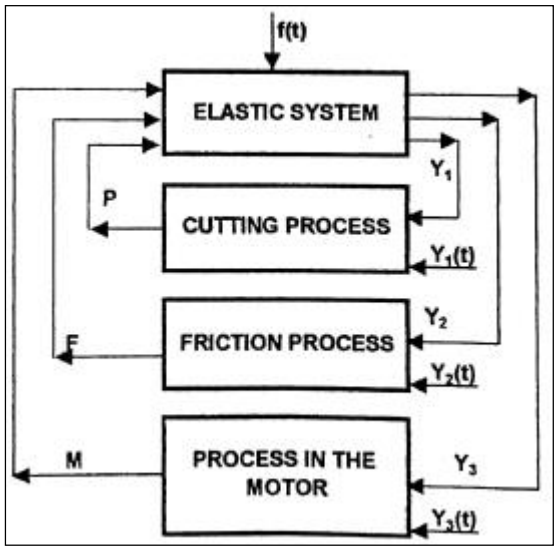

Fig- 1.3 Closed circuit Dynamic system of a machine tool [53]

A physical quantity describing the action on the given element or system, is called the input coordinate of the system, the result of the action – the output coordinate. For example, the inputs of an elastic system are the forces acting (P, F, M, f(t)) and the output generated is the deformation (Y1, Y2, Y3 and their time varying counterparts resulting from the time varying forces). A dynamic system as machine tool becomes discontinuous if one of the linkages between the elements is disconnected.

1.6 SOME FUNDAMENTALS OF VIBRATION

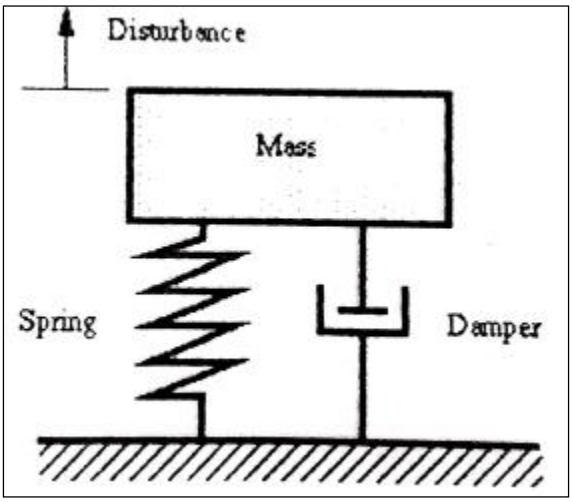

Fig- 1.4 Free vibration of a SDOF system with viscous damping [57]

To understand the concept of dynamic stability, a simple dynamic system, consisting of a mass, a spring and a damper is considered. The spring is modeled as a linear spring, which provides a restoring force. The damper is modeled as a viscous damper, which provides a damping force proportional to the relative displacement and acting to the direction against velocity vector. If there is driving force acting on the mass and the system vibrates under the driving force, which is called forced vibration. Otherwise, the system may vibrate under initial displacement and/or initial velocity, which is called free vibration. Free vibration of a SDOF system with viscous damping is shown in Fig- 1.4.

The equation of motion is as given below:

$$m\,(d^2x/dt^2) + c\,(dx/dt) + Kx = 0 \qquad (1.1)$$

The solution consists of one transient part and steady state part, given by,

$$x = Ae^{[-(c/2m)+ j\omega]t} \qquad (1.2)$$

for, c>0, the transient part dies down i^{th} only steady state oscillations ($Ae^{i\omega t}$) remaining. Such systems are termed as dynamically stable. Here, c<0, the system becomes dynamically unstable as the system amplitudes increases exponentially. At the threshold of stability, c=0, free undamped vibrations results.

UNDAMPED FREE RESPONSE (c = 0)

Free vibration occurs because there is an initial disturbance to the system. Fig- 1.5 is showing a system under undamped free vibration. The initial disturbance is referred to as initial conditions, which can be either a displacement of the mass, or an initial velocity of mass, or both. Frequency

of the system is determined by the mass and spring constant of the system. Initial conditions cannot change vibration frequency. This is why it is called natural frequency. Vibration amplitude and phase angle is determined by initial conditions. Theoretically, an undamped free vibration system will vibrate forever once it is started. Equation of motion is:

$m\ddot{x} + kx = 0$, for initial conditions $x(0) = x_0$, $\dot{x}(0) = 0$ (1.3)

The solution of the equation is: $x(t) = [x_0^2 + (\dot{x}/\dot{w}_R)^2]^{1/2} \sin(\omega_R t + \Phi)$ (1.4)

Where $\Phi = \tan^{-1}\left(\frac{x_0\,\omega_R}{\dot{x}_0}\right)$ and $\omega_R = \sqrt{k/m}$

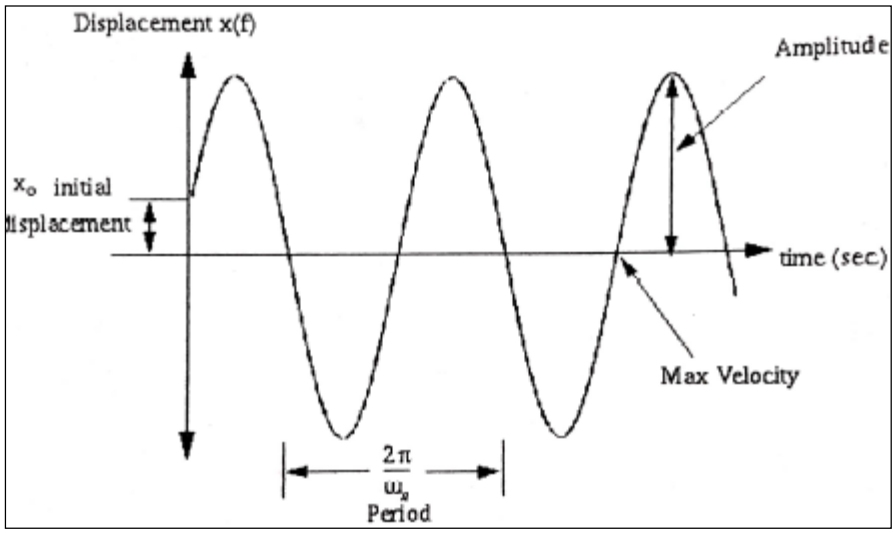

Fig- 1.5 Undamped free vibrations [53]

DAMPED FREE RESPONSE:

Physically, there is no such a vibrating system that vibrates forever, that means there is always some kind of damping in the system that dissipates energy. For mathematical simplicity, the damping is modeled as viscous damping. Depending on the magnitude of damping, a damped system can be under damped, critically damped or over damped. Critical damping coefficient is determined by the system mass and spring constant. Under critical damping, damping ratio is unity. Critical damping separates non-oscillatory motion from oscillatory motion. When damping ratio is greater than 1, which is called over damping, the system does not oscillate. For damping ratio less than 1, which is called under damping, the system oscillates with decaying magnitudes, as shown in Fig- 1.6 For most physical system, damping ratio are less than 1. Actually, most physical systems have damping ratio less than 0.1. With damping in the free vibration system, the mass always restores its equilibrium position even it is distributed. The greater the damping, the less time is taken to restore its equilibrium position. So in most cases, adequate damping is desirable.

The equation of motion is:

$m\ddot{x}+c\dot{x}+kx = 0$, for initial condition: $x(0)=X_0$, $\dot{x}(0)= v_0$ (1.5)

The solution of equation is: $x(t) = Ae^{-T_d\xi\omega_0}\ (\omega_0 t +\Phi)$ (1.6)

where $\omega_d= \omega_0\sqrt{1-\xi^2}$,

$\omega_n = \sqrt{k/m}$, $\xi = \frac{c}{2\sqrt{km}}$ (1.7)

$$A= \frac{\sqrt{(v_0+ x_0\xi\omega_0)^2+(x_0\omega_d)^2}}{\omega_d} \quad (1.8)$$

and $\Phi = \tan^{-1}\left(\frac{x_0\omega_d}{v+\xi\omega_n x_0}\right)$

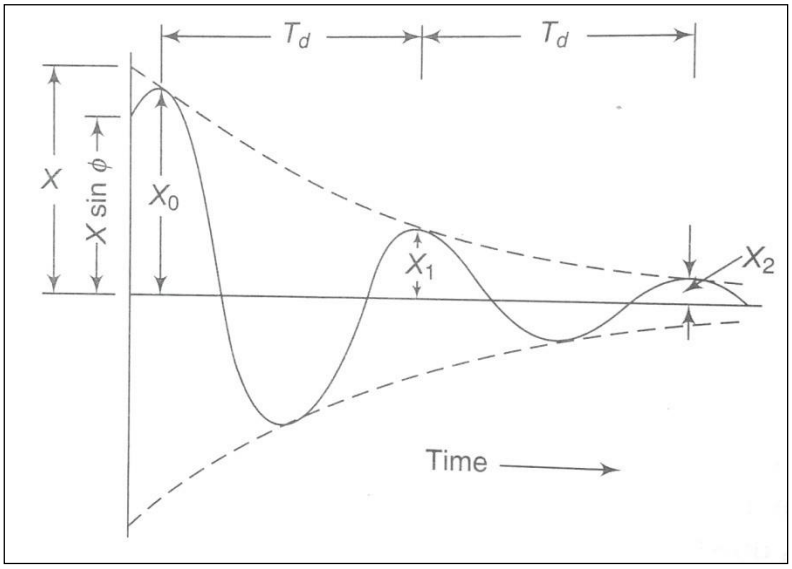

Fig- 1.6 Damped free vibration [57]

FORCED RESPONSE OF SDOF:

When there is a driving force acting on single degree of freedom (SDOF) system, the system's vibrating frequency is determined by driving force frequency and damping ratio. One is mostly interested in the magnitude and phase shift of the response. Their characteristics are indicated in the system's frequency response function. When driving frequency is close to system's natural frequency, forced vibration magnitude is large. Hen driving force frequency is equal to natural

frequency. Forced vibration reaches its maximum magnitude, this is called resonance. Under resonance, the response's phase shift is 90^0. The greater the damping ratio, lesser the forced vibration magnitude. Dynamic stability deals with studying behavior of the system, which in steady state condition or uniform motion, under the effect of dynamic disturbance. Example is chatter free machining process or uniform feed motion performed by machine tool and acted on by time-varying cutting forces. If the disturbance superposed on the uniform motion dies away after a certain period of time and the uniform motion is restored, the system is considered dynamically stable. Fig- 1.7 is showing transmutability of a system under forced vibration.

Vibrations in metal cutting operations can make it impossible to meet the surface finish requirement, generate excessive amounts of noise and lead to premature tool failure due to edge chipping. Forced vibration, in general, results from the continuing application of external periodic force (typical sources include spindle imbalance, gear drive irregularities, electric motor, oil pump and machine tools in the vicinity). Under certain condition, vibrations can occur, which are not attributed to external excitation. For example, for c<o, in free vibration of an SDOF system, the transient part superposed on steady state movement becomes self-excited.

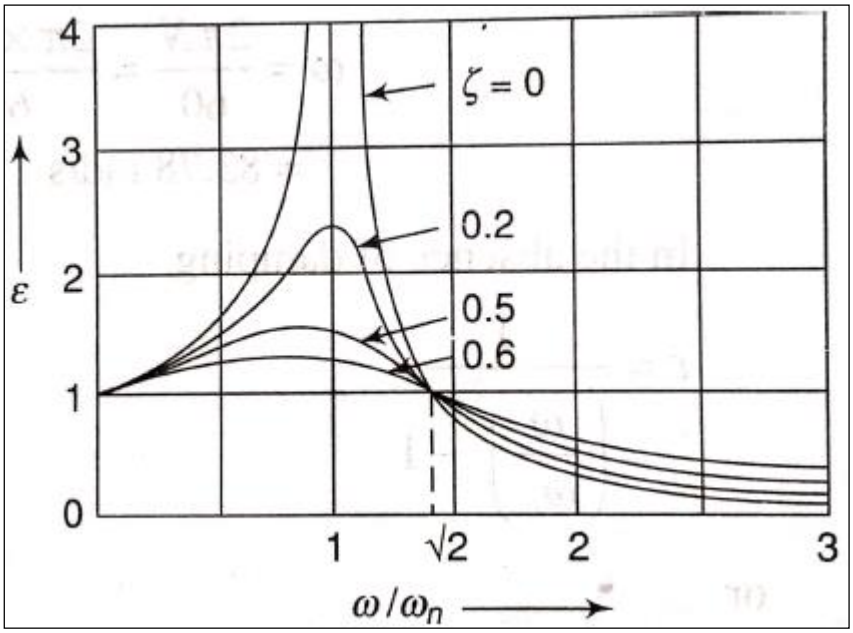

Fig- 1.7 Forced vibration [57]

The investigation of self-excited vibrations indicate that dynamic stability prevails in an elastic system, when the energy dissipation by existing positive dumping is larger or at least equals the energy input by the negative dumping effect of self-excited vibrations. It is important that, forces generating self-excited vibration are always velocity dependent.

Machine tool structures and their damping contribute to the dynamic stability of the system. So, stability analysis of machine tools require the study of mathematical models explaining machine

tool chatter, study of structural design of machine tools structure designs and their effects on stability, the study of cutting process dynamics etc.

1.7 EFFECTS OF VIBRATION

The effects of vibration can be considered on four main points:

a) The effect of vibration on machine tool.
b) The effect of vibration on cutting conditions.
c) The effect of vibration on the work piece.
d) The effect of vibration on tool life.

Effect of Vibration on machine tool:

The effect of vibration on machine tool can be disastrous. If the frequency of vibration coincides with the natural frequency of any mode the machine tool, it may result in complete or partial destruction of the machine tool. Besides, undue vibration may also decrease the life of machine tools.

Effect of vibration on the cutting conditions:

There are mainly three effects on the cutting conditions. They are-
a) **Chip thickness variation effect**: The uncut chip thickness, which remains constant during a vibration free cutting, is not at all constant when vibration is present. Due to the vibration of chip thickness cutting force also varies.
b) **Penetration rate variation effect**: Due to vibration the penetration rate or feed rate also varies. Due to this variation the penetration rate also varies.
c) **Cutting speed variation effect**: The cutting speed also varies due to vibration.

Effect of vibration on the workpiece:

The major effect of vibration on the work piece is worsened surface finish. This is very important for milling machines, because milling operation is a finishing operation. Again when vibration becomes excessive then dimensional accuracy of the job may also be affected. It has been proved that the chatter marks lead to calculation of chatter vibration frequency. Chatter marks themselves are considered as proofs for the effect of vibration on the surface of the work piece.

Effect of vibration on Tool life:

It is known that cutting variables are affected by the vibration, as such it is expected that the tool vibration will affect tool life, because tool life is a function of cutting variables only. From Taylor's tool life equation:

$$VT^n = C, \quad (1.9)$$

where, V= Cutting velocity,
T= Tool life,
n and C are constants.
As cutting velocity is affected by vibration, so tool life must be affected by vibration.

1.8 SELF-EXICTED VIBRATION

Self-excited vibration results from the instability, which may be effected by reasons inherent in any machining operation. Under some cutting conditions, mainly in cuts with small width, vibrations do not occur and cutting process is stable. Increase in chip width may lead to instability I the cutting process. This instability is caused by the interaction of the structural dynamics and the forces generated in chip removal process. In any process, where substantial energy is transmitted and mechanical damping is lowered, a very small portion of the energy is sufficient to maintain large amplitude of vibrations. It must be noted, in self-excited vibrations, initially the instability has no forces associated with it. But such forces build up over a period of time. It is generally considered that cutting conditions and machine tool structures must be selected so as to avoid chatter. Fig- 1.8 is showing the block diagram of self-excited machine tool chatting system.

The basic process is represented by a close loop system that includes two fundamental components, the cutting process and the vibratory system of the machine tool, and the mutual directional orientation of the two. It indicated that the vibration 'Y' between tool and work piece influences the cutting process so as to cause a vibration 'P' of the cutting force which acting on the vibratory system of the machine tool, create again vibration 'Y'. The mutual orientation '3' of the two fundamental components occurs since machine surface has a definite location in space with definite direction of vibration in its individual modes. By changing '3' the condition for stable machining change by changed mutual influence of the 2 components of the process.

Den Hartog [56] defined the characteristics of self-excited vibrations as "In a self-excited vibration, the motion is created and controlled by the motion itself and when the motion stops, the alternating force disappears, while in forced vibration, the sustaining alternating force exists independently of the motion and persists even when the vibratory motion stops".

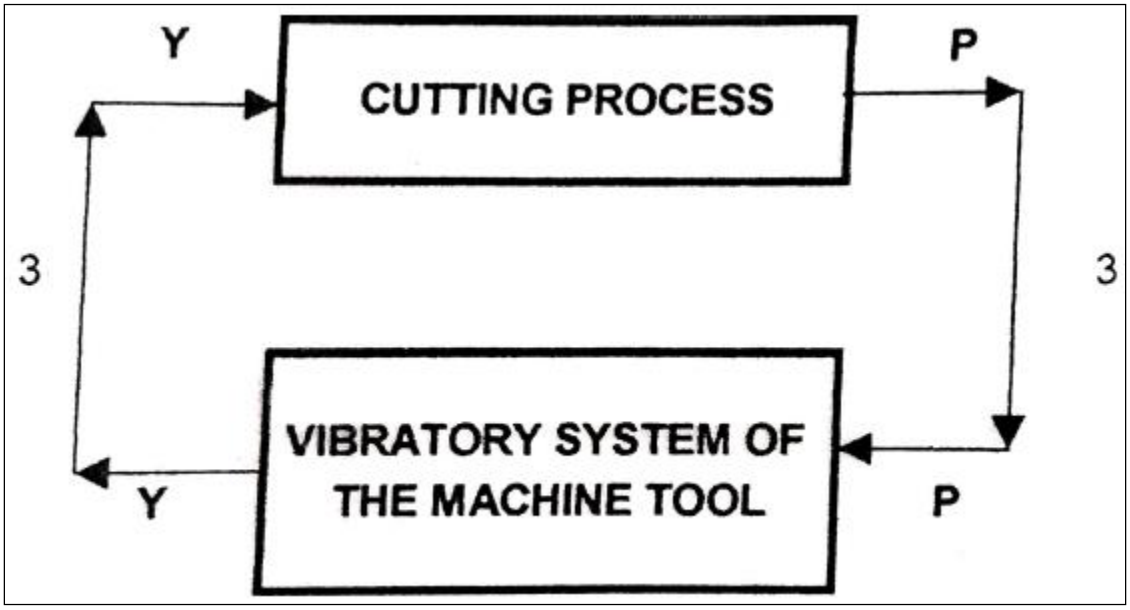

Fig- 1.8 Block diagram of self-excited machine tool chatter [53]

Chatter is undesirable because of its adverse effect on the surface finish, accuracy and tool life. Chatter is also counter- productive as it causes reduction of metal removal rates, while compared with vibration free performance, in absence of any alternate remedies. Other vibration phenomenon occurring on machine tool due to forced (induced unbalance, drive- errors etc) or free (induced by shock) can be overcome by methods long employed in other branches of mechanical engineering. But physical causes underlying chatter are not still fully understood and hence it is very difficult to find any remedy for fighting reduction of metal removal rates with consequent lowering the output. Also, inconsistency in chatter phenomenon makes it's impossible to visualize the tendency of the machine tool to exhibit chatter effect, during design and development stage. The results of chatter research to be discussed below can be divided into two main groups:

a) Chatter elementary theory that simplifies the dynamic behavior of the structure by assuming it to be idealized systems with one or two degree of freedom. This can be further divided into two parts: (i) theory with one degree of freedom (ii) the theory of mode coupling. The former is applicable only when the modes of the machine tool structure are ell separated and the system can be approximated by one or more systems with one degree of freedom. It is assumed that the relative vibration x occurring between work and the tool and having the direction of a principal vibration disturbs the steady state cutting process, this in turn generates a cutting force element dP. From dP equivalent damping of the dynamic cutting process is calculated and added to frame damping. A cutting condition for which the overall damping obtained this way is negative is unstable and causes chatter. Mode coupling theory points out that the stability of a machine tool can be influenced not only by stiffness and damping also by changes in mutual relationship of

individual natural modes of vibration and their directional orientation. This contributed to improvement of machine tool stability without addition of considerable weight.

b) As to the theory of chatter with several degrees of freedom, the dynamic characteristics of the structure are incorporated through harmonic response data determined experimentally. This however needs complex theoretical apparatus and experimental technique.

Basic theory of self-excitation had certain simplifications as listed below:

1. The vibratory system of a machine tool is assumed to be linear.
2. The direction of the variable component of the cutting force is constant.
3. The variable component of the cutting force depends only on vibration in the direction of the normal to the surface being cut.
4. The value of the variable component of the cutting force varies proportionately and instantaneously with vibration displacement.
5. The frequency of the vibration and the mutual phase shift of undulation in subsequent overlapping cut are not influenced by the relationship of wave length to the length of cut, this corresponds to an infinite length of every cut. Fig- 1.9 is showing schematically the various interrelations between different theories and models.

The basic theory of Tlusty [36] differs from the methods used by authors namely Kudinov, Tobias and Peters in that graphical solution of the limit of stability was performed not on the complex plane but in the real plane. This idea of cross receptance between the cutting force directions with the principal direction of deformation of the machine permitted an understanding of how the limit of stability depends on the individual modes of the structure and led to the suggestions of adequate changes of the structure. The above simplification prompted the development of closed loop self-excitation equation.

The tool and the work piece belong to the vibratory system of the machine tool. The cutting force acts between them. Tlusty and Polacek assumed real coupling coefficient, r, expressing the degree of coupling between modal vibration of the machine tool structure and the cutting force variation. The final form of the lowest or critical limit of stability condition in the basic theory can be expressed as:

$$(½)xb_{lim}r = -G_{min} \qquad (1.10)$$

b_{lim}= limiting width of the chip

G_{min}= minimum value of the real part of cross receptance

One important conclusion drawn from the above equation is, coupling between vibration and force is proportional to the chip width b for a given set of cutting conditions and tool geometry. Thus the minimum value of b for which cutting stability limit is reached is depend on the value

of minimum value of real receptance 'G' of the vibratory system. This minimum must be negative as b and r both are positive.

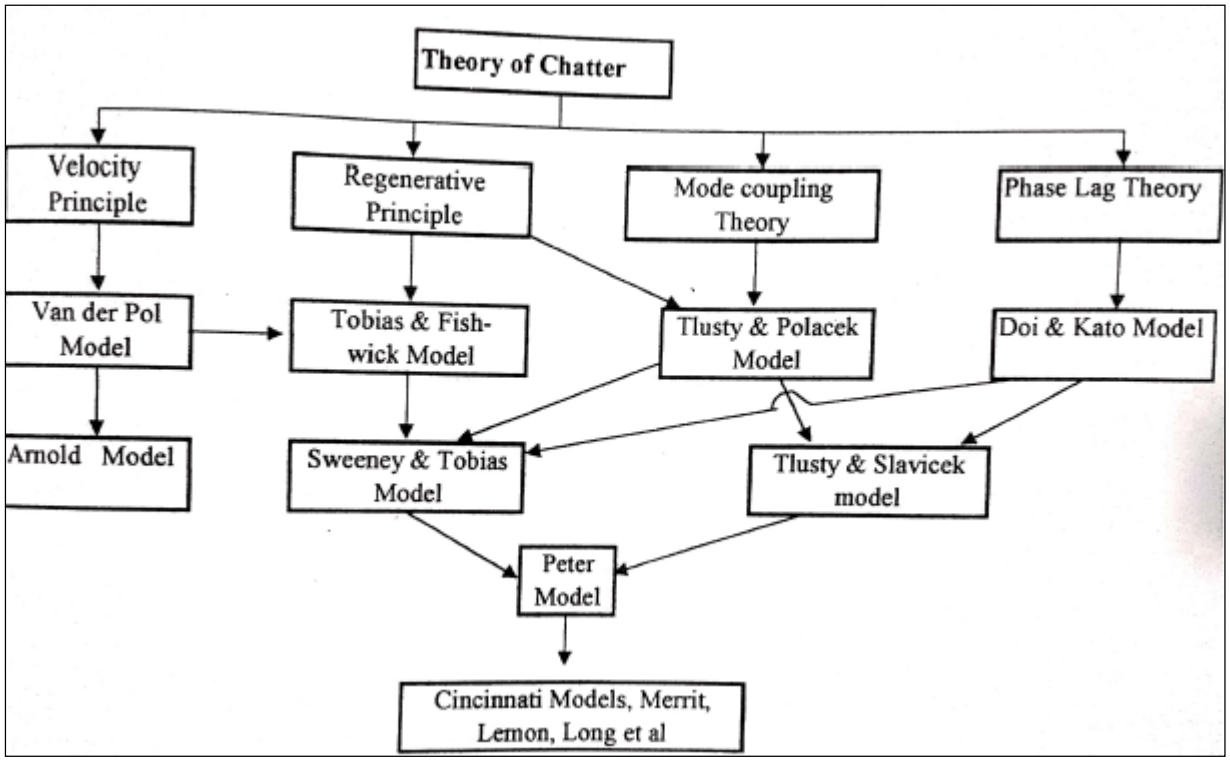

Fig- 1.9 Interrelation between different theories and models [53]

But as argued by some investigators in the field of machine tool chatters research, by assuming real one possible source of energy for self-excitation as excluded. Earlier works in the field explained chatter on the assumption of a cutting force characteristic depend on and in-phase with velocity in the direction of vibration. Some investigators did not use these simplifications and assumed a possible phase shift between the chip thickness variation and the vibration due to exciting force. This meant that the coupling coefficient would not be a real value but complex one. This assumption reveals the influence of change in cutting speed on the limit of depth of cut. As a machine tool is used with various speed and various work pieces, various cutter teeth pitches, and diameters each having same effect as aped change for final design of machine tool. The most favorable combination of these parameters must be accounted for the reducing the self-excited vibration.

'Tobias and Peters' acceptance of complex coupling coefficient leads to the solution in the complex plane, making the resolution of the solution into individual moods and analysis of the roles of machine components in chatter impossible.

Hence, the complex coupling coefficient is represented as $R = re^{i\varrho}$, where ϱ is the phase shift between chip thickness variation and force. The cutting force becomes,

$$P(t) = -bR(y(t)- y(t-\tau)), \quad (1.11)$$

and the stability criterion for the chatter becomes,

$$-(1/2)xbr = G\cos\varrho - H\sin\varrho, \quad (1.12)$$

this equation proves that, the limiting value of r for stability is an algebraic function of real part G and imaginary part H of the cross receptance and a trigonometric function of phase shift ϱ, which is turn is a function of the chatter frequency ω. Substantial improvements have been made in the field of computational aids for accurately fielding the natural frequencies and mode shapes of machine tool structure and their different variants. Advent of high speed computers have made it possible to find accurate results in least possible time, using efficient vibration analysis techniques as finite element method. The same method can be well used in determining the parameters affecting the cutting process dynamics of the metal cutting tools. The main advantage of this method is the simulation of the machine tools and metal cutting tools without actually binding them. Though, one limitation is the determination of the exact direction of modal vibrations with sufficient reliability.

1.9 VIBRATION ELIMINATION AND DESIGN OF MACHINE TOOLS

Stiffness of machine tool elements an also the overall stiffness of the machine tools are very important in elimination of structural vibration. Stiffness and damping capacities are the two predominant features for determining the dynamic characteristics of the machine tools and components. Dimensional accuracy is dependent on the static stiffness and should be tackled at the design stage. The intensity of vibration is reduced by introducing damping at the conceptual stage of design of machine tools. By comparing the rigidity of several cross sections of equal cross sectional area, a hollow rectangular section is found to have the best in bending and torsion. Ribs and partitions increase the strength of hollow machine frames. The rigidity of an element of a machine tool is determined by a progressive application of loads. While the static compliance (inverse of rigidity) of a machine tool is defined by x/P (displacement to force ratio), the dynamic compliance is a function of natural frequency and damping given by:

$$x/P = 1/K[1-r\,2 +2j\xi r] \quad (1.13)$$

Increase in stiffness may reduce x at a given frequency but does not reduce vibrational amplitude in the range of natural frequency increased by increasing K. In the range of natural frequency, only damping is effective. At resonance, the dynamic magnification factor (DMF) is given by $(½)\xi$ and hence the result of reducing DMF by a direct increase in ξ.

In machine tools, the main sources of damping are:

a) Internal friction of the vibrating structure; structural damping.
b) Rubbing between moving surfaces at the junction
c) Presence of surrounding air (very negligible)

Many researchers have emphasized the use of welded steel components for machine tool structures to enhance damping. Intensifying the rubbing effects between mating surfaces can also enhance damping. That stiffness is a major requirement for the accuracy of a modern machine tool is not questioned, but the damping is as important and should be introduced from the design inception stage of the machine is rather a recent point of view, brought up by latest studies of machine tool dynamics.

Although a machine tool does not behave as a single degree of freedom system, it is often possible to consider different modes as more or less uncoupled. For every mode a dynamic compliance can be computed as shown above. The inverse of it is called dynamic stiffness. The dynamic admittance is the velocity to force ratio versus frequency:

v/P = 1/[cj(ωm-k)/ω]. The inverse of this is the dynamic impedance, which at resonance frequency $\omega_n = \sqrt{k/m}$ is equal to damping constant c.

Physically this equation means that under static condition, ω= 0, the exciting force is balanced by the elastic restoring force (-kx). At resonance, the damping force (-cx) is the only one to balance the driving force: at resonance the elastic restoring force (-kx) and (-mx) are in quadrature with the driving force. This explains our earlier statement that, an increase in stiffness does not limit the vibration the vibration impedance in the range of resonance frequencies. It may increase the natural frequency, but only damping plays important part in the dynamic behaviour of the machine. Damping saves energy dissipation; it supposes a relative displacement between elements around an intermediate layer with high dissipative properties. This would require the damping ratio ξ (c/2√k/m) to be increased by 10 to 20 times to 0.5 from that of a conventional machine tool, as stated by Peters [20]. Orynski [47] referred plastic or rubber as damping material used in shear. Peters et al studied PVC plastics and concluded that, damping ratio is practically independent of the preload of the strips and of the surface of them. The spring constant was found to be variable depending upon surface, thickness, surface to thickness ratio and the preload. This feature of visco-elastic damping materials allowed them to tune the spring constant selecting the dimensions and directional preloading.

1.10 COMPOSITE

Composite materials are composed of mixtures of two or more distinct constituents or phases separated by a distinct interface. For a material to be called a "composite material" it must satisfy the following conditions:

1. It is fabricated (naturally occurring composites such as wood and bones are excluded)
2. It is composed of two or more physically and/or chemically different and suitably arranged constituents. This arrangement of constituents is added into the composite during early manufacturing stages. Metal alloys that produce second phase or inter-metallic precipitates during solidification or during subsequent heat treatment are not considered as composites.
3. The constituents are present in reasonable proportions.
4. It has characteristics that are not described by any of the constituent alone.

Composites are made up of individual materials referred to as constituent materials. There are two main categories of constituent materials: matrix (binder) and reinforcement. At least one portion of each type is required. The matrix material surrounds and supports the reinforcement materials by maintaining their relative positions. The reinforcements impart their special mechanical and physical properties to enhance the matrix properties. A synergism produces material properties unavailable from the individual constituent materials, while the wide variety of matrix and strengthening materials allows the designer of the product or structure to choose an optimum combination.

Engineered composite materials must be formed to shape. The matrix material can be introduced to the reinforcement before or after the reinforcement material is placed into the mould cavity or onto the mould surface. The matrix material experiences a melding event, after which the part shape is essentially set. Depending upon the nature of the matrix material, this melding event can occur in various ways such as chemical polymerization for a thermoset polymer matrix, or solidification from the melted state for a thermoplastic polymer matrix composite. A variety of moulding methods can be used according to the end-item design requirements. The principal factors impacting the methodology are the natures of the chosen matrix and reinforcement materials. Another important factor is the gross quantity of material to be produced. Large quantities can be used to justify high capital expenditures for rapid and automated manufacturing technology. Small production quantities are accommodated with lower capital expenditures but higher labor and tooling costs at a correspondingly slower rate.

Many commercially produced composites use a polymer matrix material often called a resin solution. There are many different polymers available depending upon the starting raw ingredients. There are several broad categories, each with numerous variations. The most are known as polyester, vinylester, epoxy, phenolic, polyimide, polyamide, polypropylene, PEEK, and others. The reinforcement materials are often fibers but also commonly ground minerals. The various methods described below have been developed to reduce the resin content of the final product, or the fiber content is increased. As a rule of thumb, lay up results in a product containing 60% resin and 40% fiber, whereas vacuum infusion gives a final product with 40% resin and 60% fiber content. The strength of the product is greatly dependent on this ratio.

1.11 FIBER REINFORCED COMPOSITE

Technologically, the most important composites are those in which the dispersed phase is in the form of a fiber. Design goals of fiber-reinforced composites often include high strength and/or stiffness on a weight basis. These characteristics are expressed in terms of specific strength and specific modulus parameters, which correspond, respectively, to the ratios of tensile strength to specific gravity and modulus of elasticity to specific gravity. Fiber-reinforced composites with exceptionally high specific strengths and moduli have been produced that use low-density fiber and matrix materials. Fig- 1.10 is showing types of different reinforcement arrangements in composites

Fiber-reinforced composites are sub-classified by fiber length. For short fiber, the fibers are too short to produce a significant improvement in strength. Fiber provides strength, dimensional stability and heat resistance. Additives provide color and determine surface finish and affect many other properties such as weathering and flame retardance.

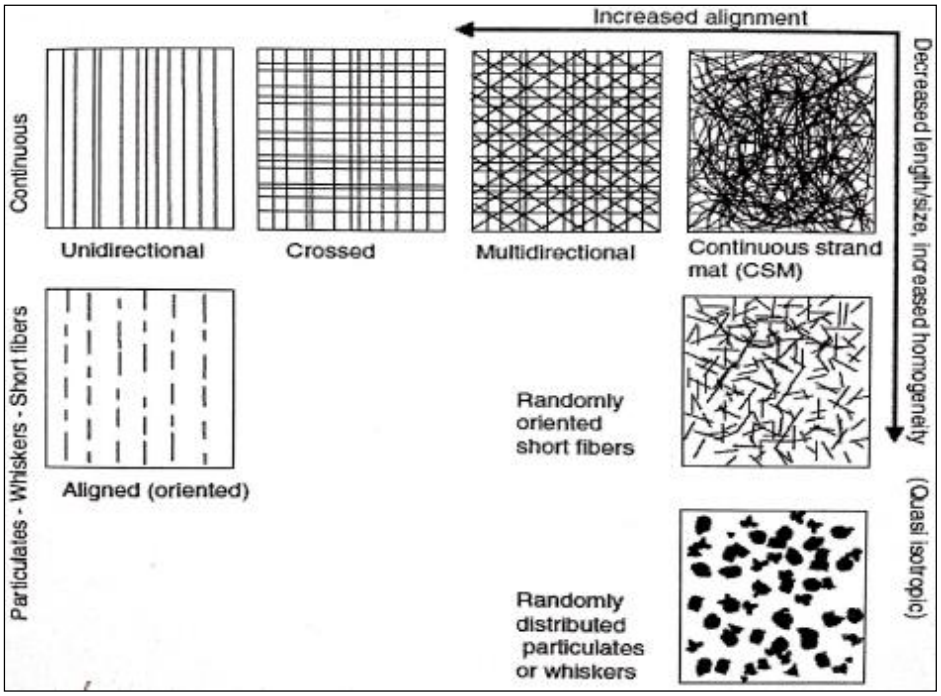

Fig- 1.10 Types of different reinforcement arrangements in composites [52]

Influence of fiber length

The mechanical characteristics of a fiber-reinforced composite depend not only on the properties of the fiber, but also on the degree to which an applied load is transmitted to the fibers by the matrix phase. Important to the extent of this load transmittance is the magnitude of the interfacial bond between the fiber and matrix phases. Under an applied stress, this fiber–matrix bond ceases at the fiber ends yielding a matrix deformation pattern as shown schematically in Figure 1.11; in other words, there is no load transmittance from the matrix at each fiber extremity.

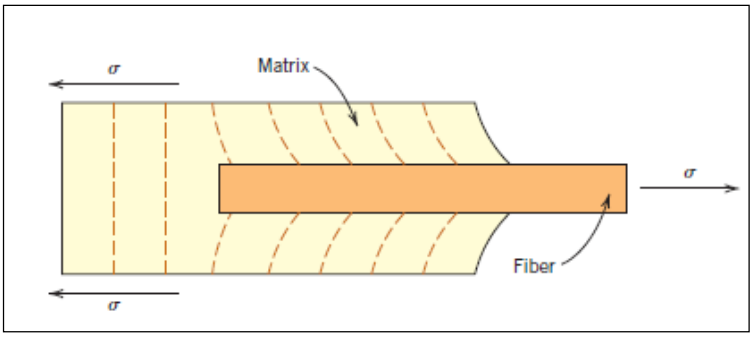

Fig - 1.11 Deformation pattern in matrix surrounding a fiber that is subjected to an applied tensile load [55]

Some critical fiber length is necessary for effective strengthening and stiffening of the composite material. This critical length l_c is dependent on the fiber diameter d and its ultimate (or tensile) strength σ_f, and on the fiber–matrix bond strength (or the shear yield strength of the matrix, whichever is smaller) τ_c according to Fig- 1.11.

$$l_c = \frac{\sigma_f^*}{2\tau_c} d \tag{1.14}$$

For a number of glass and carbon fiber–matrix combinations, this critical length is on the order of 1 mm, which ranges between 20 and 150 times the fiber diameter. When a stress equal to is applied to a fiber having just this critical length, the stress–position profile shown in Fig- 1.12a results; that is, the maximum fiber load is achieved only at the axial center of the fiber. As fiber length l increases, the fiber reinforcement becomes more effective; this is demonstrated in Fig- 1.12b, a stress–axial position profile for l>lc when the applied stress is equal to the fiber strength. Fig- 1.12c shows the stress–position profile for l<lc.
Fibers for which (normally l>>lc) are termed continuous; discontinuous or short fibers have lengths shorter than this. For discontinuous fibers of lengths significantly less than lc, the matrix deforms around the fiber such that there is virtually no stress transference and little reinforcement by the fiber. These are essentially the particulate composites as described earlier. To effect a significant improvement in strength of the composite, the fibers must be continuous.

Influence of fiber orientation and concentration

The arrangement or orientation of the fibers relative to one another, the fiber concentration, and the distribution all have a significant influence on the strength and other properties of fiber-reinforced composites. With respect to orientation, two extremes are possible: (1) a parallel alignment of the longitudinal axis of the fibers in a single direction, and (2) a totally random alignment. Continuous fibers are normally aligned (Fig- 1.13a), whereas discontinuous fibers may be aligned (Fig- 1.13b), randomly oriented (Fig- 1.13c), or partially oriented. Better overall composite properties are realized when the fiber distribution is uniform.

Tensile Stress–Strain Behavior—Longitudinal Loading (Continuous and Aligned Fiber Composites)

Mechanical responses of this type of composite depend on several factors, including the stress–strain behaviors of fiber and matrix phases, the phase volume fractions, and the direction in which the stress or load is applied. Furthermore, the properties of a composite having its fibers aligned are highly anisotropic, that is, dependent on the direction in which they are measured. Let us first consider the stress–strain behavior for the situation wherein the stress is applied along the direction of alignment the direction of alignment, the longitudinal direction, which is indicated in Fig- 1.13a.

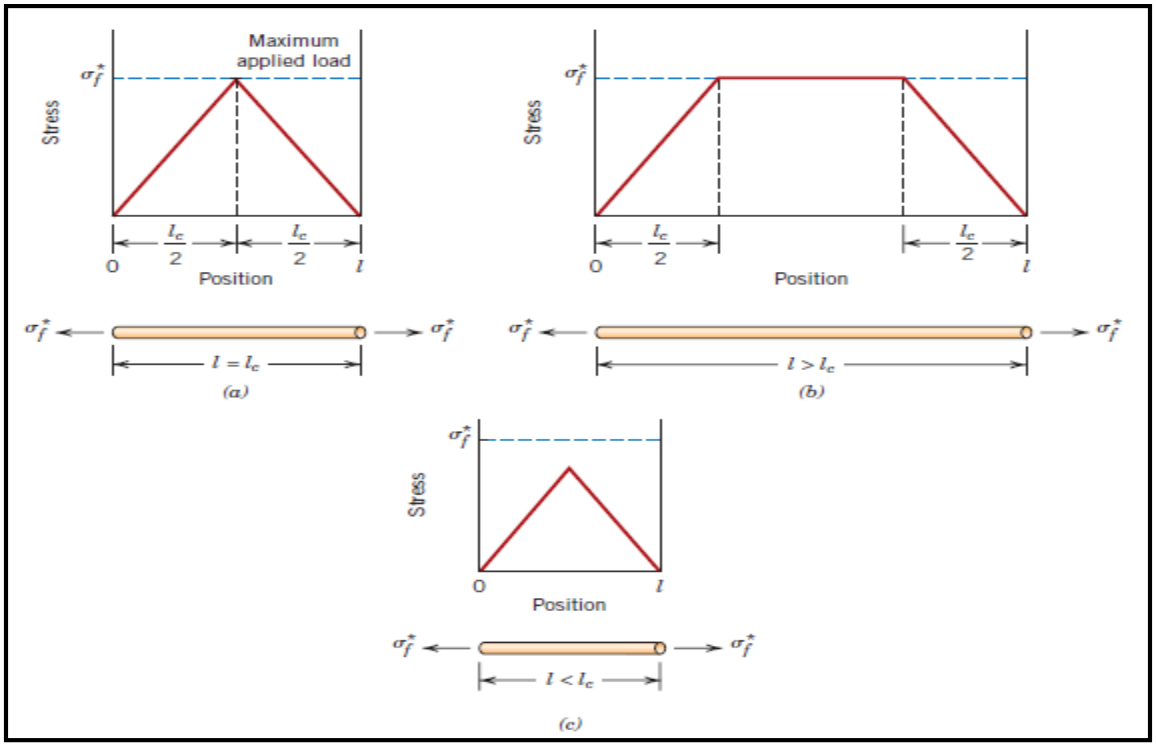

Fig -1.12 Stress- position profiles when fiber length l (a) is equal to critical length lc, (b) is greater than critical length and (c) is less than critical length [53]

To begin, assume the stress-strain behaviors for fiber and matrix phases that are represented schematically in Fig- 1.14a; in this treatment we consider the fiber to be totally brittle and the matrix phase to be reasonably ductile. Also indicated in this figure are fracture strengths in tension for fiber and matrix, σ_f^* and σ_m^* respectively, and their corresponding fracture strains, ε_f^* and ε_m^* furthermore, it is assumed that $\varepsilon_f^* > \varepsilon_m^*$ which is normally the case.

A fiber-reinforced composite consisting of these fiber and matrix materials will exhibit the uniaxial stress–strain response illustrated in Fig- 1.14b; the fiber and matrix behaviors from Fig- 1.14a are included to provide perspective. In the initial Stage I region, both fibers and matrix deform elastically; normally this portion of the curve is linear. Typically, for a composite of this type, the matrix yields and deforms plastically (at ε_{ym} Fig- 1.14b) while the fibers continue to stretch elastically, inasmuch as the tensile strength of the fibers is significantly higher than the yield strength of the matrix. This process constitutes Stage II as noted in the figure; in this stage is ordinarily very nearly linear, but of diminished slope relative to Stage I. Furthermore, in passing from Stage I to Stage II, the proportion of the applied load that is borne by the fibers increases.

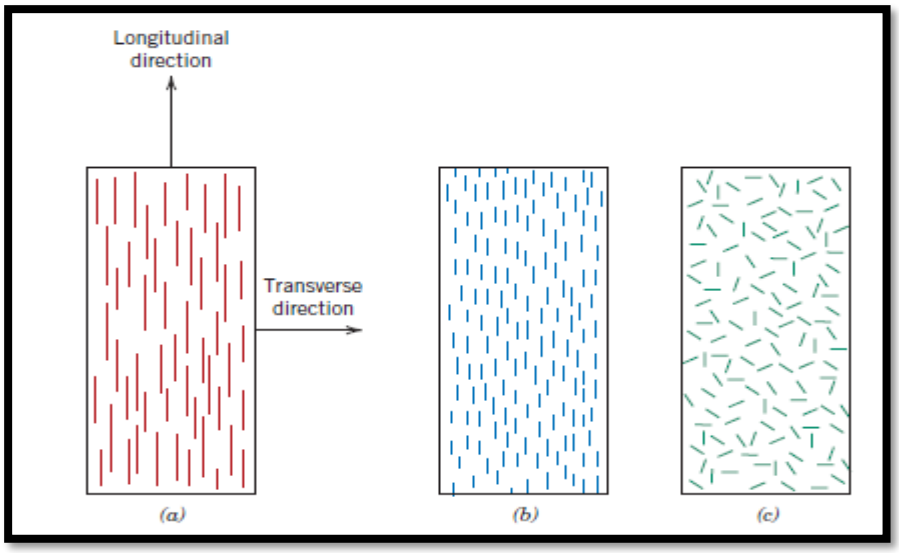

Fig- 1.13 Schematic representation of (a) continuous and aligned, (b) discontinuous and aligned and (c) discontinuous and randomly oriented [55]

The onset of composite failure begins as the fibers start to fracture, which corresponds to a strain of approximately ε_f^* as noted in Fig- 1.14b. Composite failure is not catastrophic for a couple of reasons. First, not all fibers fracture at the same time, because there will always be considerable variations in the fracture strength of brittle fiber materials. In addition, even after fiber failure, the matrix is still intact inasmuch as $\varepsilon_f^* < \varepsilon_m^*$ (Fig- 1.14a). Thus, these fractured fibers, which are shorter than the original ones, are still embedded within the intact matrix and consequently are capable of sustaining a diminished load as the matrix continues to plastically deform.

Elastic Behavior—Longitudinal Loading

Let us now consider the elastic behavior of a continuous and oriented fibrous composite that is loaded in the direction of fiber alignment. First, it is assumed that the fiber–matrix interfacial bond is very good, such that deformation of both matrix and fibers is the same (an iso-strain situation).

Under these conditions, the total load sustained by the composite F_c is equal to the sum of the loads carried by the matrix phase F_m and the fiber phase F_f:

$$F_c = F_m + F_f \qquad (1.15)$$

Let us now consider the elastic behavior of a continuous and oriented fibrous composite that is loaded in the direction of fiber alignment. First, it is assumed that the fiber–matrix interfacial bond is very good, such that deformation of both matrix and fibers is the same (an isostrain situation). Under these conditions, the total load sustained by the composite Fc is equal to the sum of the loads carried by the matrix phase F_m and the fiber phase F_f,

$\sigma_c Ac = \sigma_m A_m + \sigma_f A_f$ (1.16)

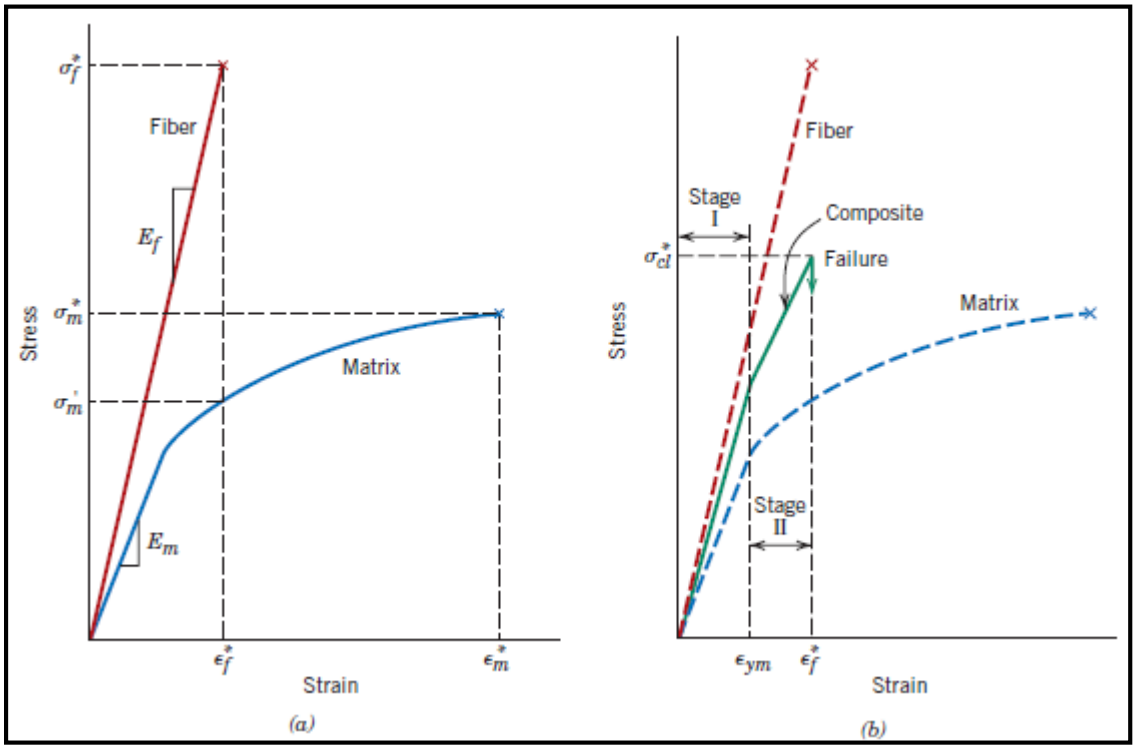

Fig-1.14 (a) Schematic stress-strain curves for brittle fiber and ductile matrix materials
(b) Schematic stress-strain curve for an aligned FRC [55]

and then, dividing through by the total cross-sectional area of the composite, *Ac*, we have

$$\sigma_c = \sigma_m \frac{A_m}{A_c} + \sigma_f \frac{A_f}{A_C} \quad (1.17)$$

where, (A_m/A_c) and (A_f/A_c) are the area fractions of the matrix and fiber phases, respectively. If the composite, matrix, and fiber phase lengths are all equal, (A_m/A_c) is equivalent to the volume fraction of the matrix, V_m, and likewise for the fibers, $V_f = (A_f/A_c)$.

$\sigma_c = \sigma_m V_m + \sigma_f V_f$ (1.18)

The previous assumption of an iso-strain state means that

$\varepsilon_c = \varepsilon_m = \varepsilon_f$ (1.19)

and when each term is divided by its respective strain,

$$\frac{\sigma_c}{\varepsilon_c} = \frac{\sigma_m}{\varepsilon_m} V_m + \frac{\sigma_f}{\varepsilon_f} V_f \quad (1.20)$$

Furthermore, if composite, matrix, and fiber deformations are all elastic, then and the E_s being the moduli of elasticity for the respective phases. An expression for the modulus of elasticity of a continuous and aligned fibrous composite in the direction of alignment (or longitudinal direction), E_{cl}, as

$$E_{cl} = E_m V_m + E_f V_f \quad (1.21)$$

$$E_{cl} = E_m(1- V_f) + E_f V_f \quad (1.22)$$

Since, the composite consists of only matrix and fiber phases; that is, $V_m + V_f = 1$.

Thus, E_{cl} is equal to the volume-fraction weighted average of the moduli of elasticity of the fiber and matrix phases. Other properties, including density, also have this dependence on volume fractions.

It can also be shown, for longitudinal loading that the ratio of the load carried by the fibers to that carried by the matrix is:

$$\frac{F_f}{F_m} = \frac{E_f V_f}{E_m V_m} \quad (1.23)$$

Longitudinal Tensile Strength

We now consider the strength characteristics of continuous and aligned fiber–reinforced composites that are loaded in the longitudinal direction. Under these circumstances, strength is normally taken as the maximum stress on the stress–strain curve; often this point corresponds to fiber fracture, and marks the onset of composite failure. Failure of this type of composite material is a relatively complex process, and several different failure modes are possible. The mode that operates for a specific composite will depend on fiber and matrix properties, and the nature and strength of the fiber–matrix interfacial bond.

If we assume that, $\varepsilon_f^* < \varepsilon_m^*$, which is the usual case, then fiberswill fail before the matrix. Once the fibers have fractured, most of the load thatwas borne by the fibers is now transferred to the matrix. This being the case, it is possible to adapt the expression for the stress on this type of composite into the following expression for the longitudinal strength of the composite, σ_{cl}^*;

$$\sigma_{cl}^* = \sigma_m' (1-V_f) + \sigma_f^* V_f \quad (1.24)$$

Here σ_m' is the stress in the matrix at fiber failure and σ_f^* is the fiber tensile strength.

1.12 CONSTITUENTS OF COMPOSITE

Composite materials are formed by combining two or more materials that have quite different properties. The different materials work together to give the composite unique properties, but within the composite they do not dissolve or blend into each other.

A composite material composite of two phases:

1. **Matrix phase**: The primary phase having a continuous character is called matrix. Matrix is usually more ductile and less hard. It consists of any of the three basic material type's polymers, ceramics or metals. The matrix forms the bulk part.

2. **Reinforcement**: The secondary phase is implanted in the matrix in a discontinuous form. The dispersed phase is usually harder and stronger than the continuous phase and is called reinforcement. It functions to strengthen the composites and improves the overall mechanical properties of the matrix. Much of strength of FRP/ composite is due to type, amount and arrangements of the fiber reinforcement. E-glass is the mostly commonly used fiber reinforcement. It is strong, has good heat resistance and high electrical properties. For more critical needs, S-glass offers higher heat resistance and about one third higher tensile strength (at a high cost) than that of E-glass. Fibers are usually produced by drawing a liquid material from an orifice or by pulling a precursor, which result in aligning its crystal or molecules along the length of the fiber and thus imparting significantly higher strength and stiffness along the axis. Most materials are stronger and stiffer in the fibrous form than in any other form. This is because fewer and smaller flaws would exist in a smaller volume of the material than in larger volume. Material failure usually commences at a larger flow and fracture strength drastically decreases with an increase in flaw size. Particles have no preferred orientation and their shape is less important than the fibers. Their size varies from less than a micron to less than a millimeter. Whiskers are pure single crystals manufactured by chemical vapor deposition, thus whiskers are anisotropic. Table -1 is showing properties of reinforcement fibers.

All fibers reinforcements originate as single filament. A large number of filaments are formed simultaneously and gathered into strand. A surface treatment is then applied to facilitate subsequent processing, maintain fiber integrity and provide compatibility with specific resin systems. After this treatment, the strands are further processed into various forms of reinforcement for use in moulding FRP composites.

1.13 PROPERTIES AND ADVANTAGES OF COMPOSITE

High strength to weight ratio: Fiber composites are extremely strong for their weight. By refining the laminate many characteristics can be enhanced. A common laminate of say 3mm Chopped strand material is quite flexible compared to say a 3 mm ply. However, it will bend a long way more than the ply before yielding. Stiffness should not be confused with Strength. A carbon fiber laminate on the other hand, will have a stiffness of many times that of mild steel of the same thickness, increased ultimate strength, yet only be less than (¼) of its weight.

Table- 1 Properties of reinforcement fibers [52]

characteristics	PAN-based carbon		Kevlar-49	E-glass	S-glass
	HM	HS			
Diameter (μm)	5-8	6-8	8-14	10-20	10-20
Density (Kg/m^3)	1.81	1.78	1.44	2.62	2.46-2.49
Young's modulus (GPa)					
Parallel to fiber axis	400	230	131	80-81	88-91
Perpendecular to fiber axis	12	20	70	--	--
Tensile strength (GPa)	2.5-4.5	3.8-4.2	3.6-4.1	3.1-3.8	4.38-4.59
Strain to failure (%)	0.6	2.0	2.8	4.6	5.4-5.8
Coefficient of thermal Expansion ($10^{-6}K^{-1}$)					
Parallel to fiber axis	-0.5	-0.6	-4.3	6.0	2.9
Perpendecular to fiber axis	7.0	10.0	41	--	--
Thermal conductivity (W/m K)	70	11	0.04-1.4	10-13	1.1-1.4
Specific Heat (kJ/kg K)	0.7-0.9	--	0.769	0.45	0.41

Light weight: A standard Fiberglass laminate has a specific gravity in the region of 1.5, compared to Alloy of 2.7 or steel of 7.8. When you then start looking at Carbon laminates, strengths can be many times that of steel, but only a fraction of the weight.

Fire resistance: The ability for composites to withstand fire has been steadily improving over the years. There are two types of systems to be considered:

Fire Resistant - More difficult and made with the likes of Phenolic Resins. These are difficult to use, are cured with formaldehyde, and require a hi-degree of post curing to achieve true fire resistance.

Fiberglass Developments Ltd. produces a Fire Door as part of our Steridor TM range. Use of special Phenolic resin has allowed us to create the only fully tested Composite door in Australasia. Fire rated by BRANZ to 4 hours, this door is also approved by MAF as meeting all their Hygiene requirements.

Electrical properties: Fiberglass Developments Ltd produced the Insulator Support straps for the Tranz Rail main trunk electrification.

Chemical weathering resistance: Composite products have good weathering properties and resist the attack of a wide range of chemicals. This depends almost entirely on the resin used in manufacture, but by careful selection resistance to all but the most extreme conditions can be

achieved. Because of this, composites are used in the manufacture of chemical storage tanks, pipes, chimneys and ducts, boat hulls and vehicle bodies.

Color: Almost any shade of any color can be incorporated into the product during manufacture by pigmenting the gel coat used. Costs are therefore reduced by no further finishing or painting.

We do not however, recommend dark colors. These produce excessive heat on the surface which can lead to the surface deteriorating and showing print through, where the Resin matrix cures more and shrinks, bringing the fibers to the surface. In extreme cases delamination can occur.

Translucency: Polyester resins are widely used to manufacture translucent mouldings and sheets. Light transmission of up to 85% can be achieved.

Design flexibility: Because of the versatility of composites, product design is only limited by your imagination.

Low thermal conductivity: Fiberglass Developments has been involved in the development and production of specialized meat containers which maintain prime cuts of chilled meat at the correct temperature for Export markets. They are manufactured using the RTM process, with special reinforcing and foam inserts.

Manufacturing economy: Fiberglass development produces several models of fuel pump covers for Fuel quip. Fiberglass is an ideal material for producing items of this type for many reasons, including being very economical.

1.14 APPLICATION OF COMPOSITE

Table-2 is showing the various applications of composites. Table-3 is showing the use of FRP and suitability for marine application.

Table-2 Application of Composites

Application area	Examples
Aerospace	Spacecraft, Satellite, rocket vehicle case etc.
Aircraft	Access door, stiffness, floor beams etc.
Chemical	Pipes, tanks, pressure vessels etc.
Construction	Brides and walkways including docs, handrails, cable, frames etc.
Domestic	Chair, table, shower unit etc.
Electrical	Panel, housing, switchgear etc.
Leisure	Finishing rods, bi-cycle frames, golf clubs etc.
Marines	Hulks, docs, interior panels etc.
Medical	Wheel chair, orthofies, medical equipments etc.
Transportation	Body panels, dash board, frames etc.

Table-3 FRP use and suitability for marine application

Marine/off-shore application	FRP Suitability	
	Advantages	Examples
Boating/sports related	Moisture resistance, ease of use and repair, high strength/stiffness, light weight, corrosion resistance	Boats, seating and storage compartments, fishing rods etc.
Naval applications	High strength/stiffness, light weight, corrosion resistance, ease of navigation, longer service life	Ships decks, aircraft landing platforms, cabins, gun housings, walking platforms, rails etc.
Off-shore applications	Moisture resistance, ease of use, high strength/stiffness, corrosion resistance, ease of construction, longer service	Piles, retaining walls, pedestrian walkways, bridges, pavement panels for oil fields and off-shore structures

1.15 THE MILLING PROCESS

In milling, material is removed from work-piece by rotating cutter head that may have more than one active cutting edge. The types of milling operation that are most common in machining of FRPs are peripheral milling or profile and end milling but in the present work the side and face milling operation has been selected.

i) Peripheral milling uses the edges on the periphery of the tool. The machine surface is parallel to the axis of rotation of cutter and the engagement into the work-piece is in radial direction of the cutter. Peripheral milling is approximately called edge trimming because tool diameter is usually small and the axial engagement covers the entire thickness of the work piece.

ii) End milling is similar to peripheral milling, except that the axial engagement may be less than the thickness of the part and slot is obtained. The machine most commonly used is vertical milling machine but for side and face milling horizontal milling machine is used. Fig- 1.15 is showing an end milling operation.

iii) Side and face milling is done by side and face milling cutter. Side and face milling cutters can handle long, deep, open slot in most efficient manner and provide the best stability and productivity for this type of milling.

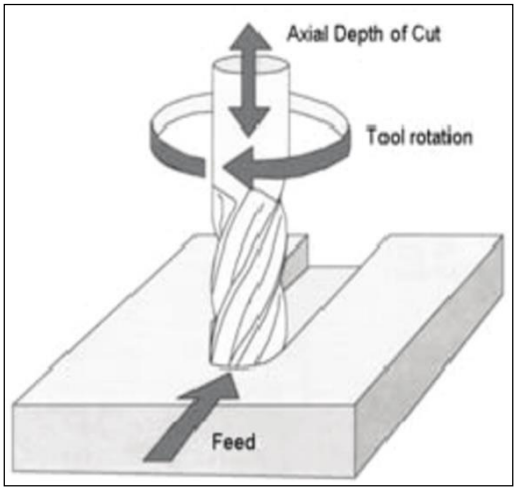

Fig- 1.15 End Milling Operation

They can also be built into a 'gang' to machine more than one surface in the same plane at the same time. The milling machine provides the primary motion to the spindle (to which the cutter is held) and feed motions to the machine tables (to which the work-piece is held). The milling operation may be classified as conventional milling (or up cut milling) and climb milling (or down cut milling) operation depending on how the edges approach the work-piece. Fig- 1.16 is showing a side and face milling cutter.


Fig- 1.16 Photographic view of Side and Face Milling Cutter

In the up cut milling the direction of the cutting speed of the edge in contact with work-piece is opposite to the direction of feed. In down-milling, the direction of cutting speed is the same as that of the feed. The resulting chip area in both the cases has a "comma" shape and length of the chip is described by a torchoid that results from the superposition of peripheral motion and feed motion. In up-milling the cutting edge begins engaging the chips at the thin section of the comma shape. This results in low engagement forces and in lifting up the work piece. In down-milling the cutting edge engages the chip at the thick section of the comma shape. The engagement forces are high and result in pushing the work-piece against the work holding surface. Cutting forces in milling are also not continuous. In up-milling the forces gradually increases from zero at the beginning of tool engagement to a maximum when the cutting edges about to leaves the work-piece.

1.16 MILLING OF GFRP

Milling is the one of the most frequently used material removal processes in manufacturing parts made of FRPs. However unlike of metals which are characterized by high material removal rates, milling of FRPs is conducted at much lower scale. The reason for this is that FRPs components are largely made near net shape and any subsequent milling is limited mainly to deburring and trimming as well as for achieving the contour shape accuracy. In milling, the cutting tool is rotating and quite often more than one cutting edge is engaged in cutting at the same time. This adds complexity to the milling processes in terms of fiber orientation, chip size and cutting forces that continuously vary with tool rotation. The machinability of FRPs in milling is mainly characterized by tool wear, surface roughness and delamination.

1.17 FIBER ORIENTATION IN MILLING UNIDIRECTIONAL FRPs

The peculiar aspects of cutting with rotating tool such as in milling, drilling and abrasive cutting, as opposed to linear orthogonal machining is that the fiber orientation angle, θ, is not constant, but varies continuously with cutting edge position around the cutter axis. In milling the chip thickness also varies with cutting edge position. Fig- 1.17(a, b) shows the scheme of up-milling and in Fig- 1.17(c, d) shows the down milling operation. Consider for example Fig. 1.17a up-milling of unidirectional laminate with fiber orientation $\psi<90°$. The cutting edge position is indicated by the engagement angle Φ, measured from vertical line. At the current cutting edge position, the fiber is subjected to tensile and bending stresses. The fiber orientation angle (θ) is measured clockwise from cutting velocity vector. Then for the case in Fig. 1.17a and for $\Phi \leq \psi$ it can be shown that

$$\theta = \psi - \Phi \text{ for } \Phi \leq \psi \qquad (1.25)$$

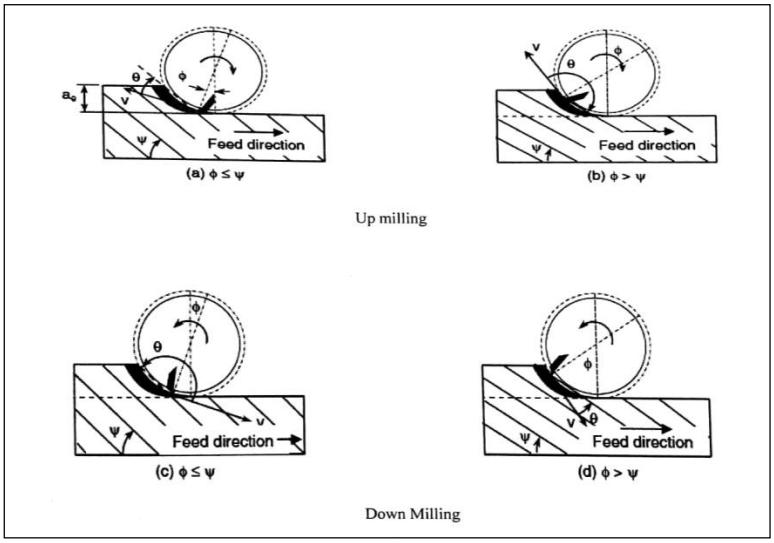

Fig- 1.17 Schematic view of Up and Down milling

As the tool engagement angle increases and become equal to laminate orientation, $\Phi = \psi$, the fiber orientation angle become equal to zero. With further increase in engagement angle so that,

$\psi > \Phi$ as shown in Fig- 1.17(b), the fibers will subject to compression and bending. The fiber orientation angle for this case is given by

$$\theta = \Pi + \psi - \Phi \text{ for } \Phi > \psi \quad (1.26)$$

Similarly, for don milling Fig- 1.17(c, d) it can be shown that:

$$\theta = \Pi + (\Phi - \psi) \quad \Phi \leq \psi \quad (1.27)$$

$$\theta = \Phi - \psi \quad \Phi > \psi \quad (1.28)$$

Because of this continuous evolution of fiber orientation angle and the associated chip formation modes, the characteristics of the instantaneous cutting forces (frequency and magnitude) will vary from one cutting edge position to another as shown in Fig- 1.17. The change in uncut chip thickness will also affect the magnitudes of the cutting forces. The quality of the machined surface would depend on the fiber orientation at cutting edge entry for up milling and at cutting edges exits for down milling. Since $\Phi = 0$ for both these position, the quality of the machined surface is function of angle ψ for up milling and the angle $(\Pi - \psi)$ for down milling.

1.18 MECHANICS OF UP-MILLING USING A STRAIGHT-FLUTED MILLING CUTTER

Fig- 1.17 schematically visualizes the display of cutting force components in milling by using a straight fluted plain milling cutter under straight-tooth engagement. At any angular position ψ of the tooth, the milling force R can be resolved into tangential component F_T and a radial component F_R. The same force R can also be resolved into force components F_Z and F_Y as indicated. Therefore,

$$R = F_T + F_R = F_Z + F_Y \quad (1.29)$$

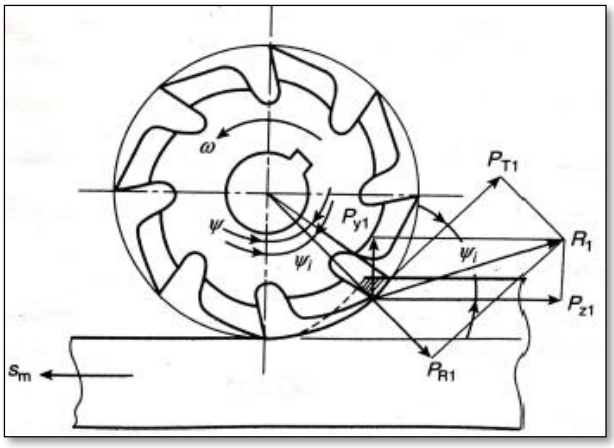

Fig- 1.18 Cutting forces in Up-milling by straight-toothed plain milling cutter under single-tooth engagement [54]

The magnitudes of forces P_T and P_R are useful for the determination of cutting torque and power requirement and for the design of the cutters, arbor, spindle etc. whereas the magnitudes of the forces F_Z and F_Y (and also F_X where it exists) are essentially used for machine tool design. The relationships among these force components can be derived from Fig. 1.18 as,

(a) F_Z and $F_Y = f(F_T, F_R, \psi)$ (1.30)

$F_Z = F_T \cos\psi + F_R \sin\psi$ (1.31)

$F_Y = F_T \sin\psi - F_R \cos\psi$ (1.32)

where, ψ is the angle of engagement of the i'th tooth.

(b) F_T and $F_R = f(F_Z, F_Y, \psi)$ (1.33)

$F_T = F_Z \cos\psi + F_Y \sin\psi$ (1.34)

$F_R = F_Z \sin\psi - F_Y \cos\psi$ (1.35)

1.19 SURFACE ROUGHNESS

Surface roughness often shortened to roughness, is a component of surface texture. It is quantified by the deviations in the direction of the normal vector of a real surface from its ideal form. If these deviations are large, the surface is rough; if they are small, the surface is smooth. In surface metrology, roughness is typically considered to be the high-frequency, short-wavelength component of a measured surface. However, in practice it is often necessary to know both the amplitude and frequency to ensure that a surface is fit for a purpose.

Roughness plays an important role in determining how a real object will interact with its environment. In tribology, rough surfaces usually wear more quickly and have higher friction coefficients than smooth surfaces. Roughness is often a good predictor of the performance of a mechanical component, since irregularities on the surface may form nucleation sites for cracks or corrosion. On the other hand, roughness may promote adhesion. Generally speaking, rather than scale specific descriptors, cross-scale descriptors such as surface fractality provide more meaningful predictions of mechanical interactions at surfaces including contact stiffness and static friction. Fig- 1.19 is showing a schematic representation of a machined surface.

Although a high roughness value is often undesirable, it can be difficult and expensive to control in manufacturing. For example, it is difficult and expensive to control surface roughness of fused deposition modeling (FDM) manufactured parts. Decreasing the roughness of a surface usually increases its manufacturing cost. This often results in a trade-off between the manufacturing cost of a component and its performance in application.

Roughness can be measured by manual comparison against a "surface roughness comparator" (a sample of known surface roughness), but more generally a surface profile measurement is made with a profilometer. These can be of the contact variety (typically a diamond stylus) or optical (e.g.: a white light interferometer or laser scanning confocal microscope).

However, controlled roughness can often be desirable. For example, a gloss surface can be too shiny to the eye and too slippery to the finger (a touchpad is a good example) so a controlled roughness is required. This is a case where both amplitude and frequency are very important.

There are many different roughness parameters in use, but Ra is by far the most common, though this is often for historical reasons and not for particular merit, as the early roughness meters could only measure R_a. Other common parameters include R_z, R_q and R_{sk}. Some parameters are used only in certain industries or within certain countries. For example, the R_k family of parameters is used mainly for cylinder bore linings, and the Motif parameters are used primarily in the French automotive industry. The MOTIF method provides a graphical evaluation of a surface profile without filtering waviness from roughness. A motif consists of the portion of a profile between two peaks and the final combinations of these motifs eliminate ″insignificant″ peaks and retains ″significant″ ones. Please note that R_a is a dimensional unit that can be micrometer or micro-inch.

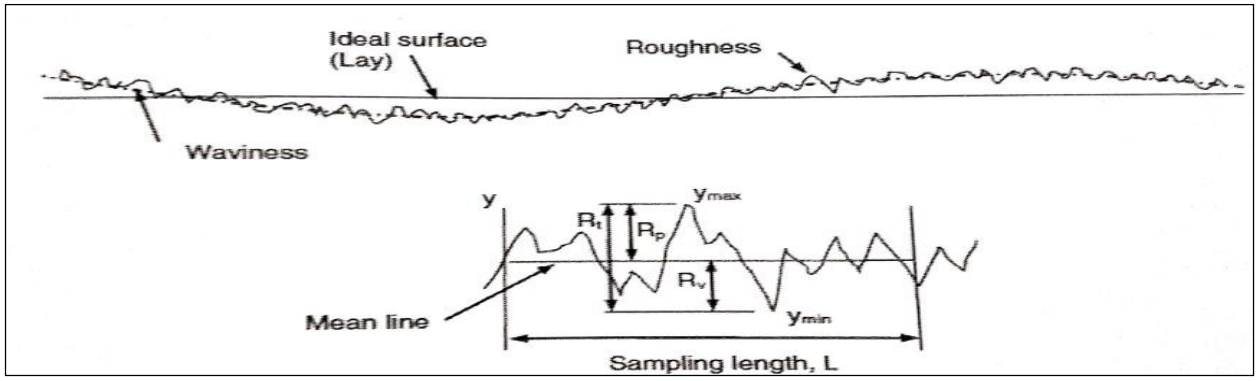

Fig- 1.19 Schematic representation of machined surface [52]

For a sampling length L, the surface variations are described as a function x, y = f (x). The mean line of the profile for this segment is determined as

$$\bar{y} = \frac{1}{L}\int_0^L y\, dx \qquad (1.36)$$

The maximum peak-to- valley height within the sampling length is determined by

$$R_t = y_{max} - y_{min} \qquad (1.37)$$

The maximum peak-to-mean height and valley-to-mean height are determined respectively, by

$$R_p = y_{max} - \bar{y} \qquad (1.38)$$

And $$R_v = \bar{y} - y_{min} \qquad (1.39)$$

The average of the numeric deviations from the mean line of the surface within the sample length, Ra is determined by

$$Ra = \frac{1}{L}\int_0^L | y - \bar{y} |\ dx \qquad (1.40)$$

Finally, the ten-point average, Rz is determined as the difference between the greatest peaks and the five lowest valleys within the sampling length.

$$Rz = \frac{1}{5}\left(\sum_1^5 y_i^p - \sum_1^5 y_i^V\right) \quad (1.41)$$

1.20 RESPONSE SURFACE METHODOLOGY

Response surface methodology (RSM) is a collection of mathematical and statistical techniques for empirical model building. By careful design of experiments, the objective is to optimize a response (output variable) which is influenced by several independent variables (input variables). An experiment is a series of tests, called runs, in which changes are made in the input variables in order to identify the reasons for changes in the output response. Originally, RSM was developed to model experimental responses (Box and Draper, 1987), and then migrated into the modeling of numerical experiments. The difference is in the type of error generated by the response. In physical experiments, inaccuracy can be due, for example, to measurement errors while, in computer experiments, numerical noise is a result of incomplete convergence of iterative processes, round-off errors or the discrete representation of continuous physical phenomena (Giunta et al., 1996; van Campen et al., 1990, Toropov et al., 1996). In RSM, the errors are assumed to be random.

The application of RSM to design optimization is aimed at reducing the cost of expensive analysis methods (e.g. finite element method or CFD analysis) and their associated numerical noise. The problem can be approximated as described in Chapter 2 with smooth functions that improve the convergence of the optimization process because they reduce the effects of noise and they allow for the use of derivative-based algorithms. Venter et al. (1996) have discussed the advantages of using RSM for design optimization applications. For example, in the case of the optimization of the calcination of Roman cement described in Section 6.3, the engineer wants to find the levels of temperature (x1) and time (x2) that maximize the early age strength (y) of the cement. The early age strength is a function of the levels of temperature and time, as follows:

$$y = f(x1, x2) + \varepsilon \quad (1.42)$$

Where, ε represents the noise or error observed in the response y. The surface represented by f(x1, x2) is called a response surface. The response can be represented graphically, either in the three-dimensional space or as contour plots that help visualize the shape of the response surface. Contours are curves of constant response drawn in the xi, xj plane keeping all other variables fixed. Each contour corresponds to a particular height of the response surface, as shown in Fig-1.20.

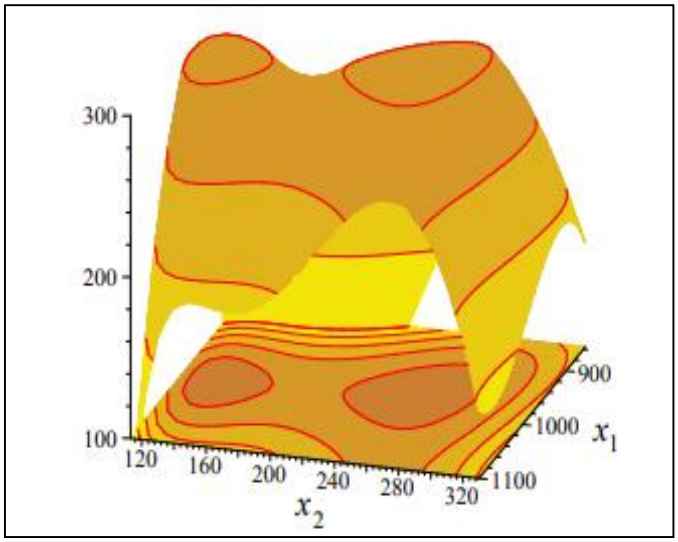

Fig- 1.20 Contour corresponds to a particular height of the response surface

(Three-dimensional response surface and the corresponding contour plot for the early age strength of Roman cement where x1 is the calcination temperature (°C) and x2 is the residence time (min)).

This chapter reviews the two basic concepts in RSM, first the choice of the approximate model and, second, the plan of experiments where the response has to be evaluated.

Approximate model function

Generally, the structure of the relationship between the response and the independent variables is unknown. The first step in RSM is to find a suitable approximation to the true relationship. The most common forms are low-order polynomials (first or second-order). In this thesis a new approach using genetic programming is suggested. The advantage is that the structure of the approximation is not assumed in advance, but is given as part of the solution, thus leading to a function structure of the best possible quality. In addition, the complexity of the function is not limited to a polynomial but can be generalized with the inclusion of any mathematical operator (e.g. trigonometric functions), depending on the engineering understanding of the problem. The regression coefficients included in the approximation model are called the tuning parameters and are estimated by minimizing the sum of squares of the errors (Box and Draper, 1987):

$$G(\boldsymbol{a}) = \sum_{p=1}^{P} \left\{ w_p \left(F_p - \widetilde{F}_p(\boldsymbol{a}) \right)^2 \right\} \rightarrow \min \tag{1.43}$$

Where w_p is a weight coefficient that characterizes the relative contribution of the information of the original function at the point p, p=1,...,P.

The construction of response surface models is an iterative process. Once an approximate model is obtained, the goodness-of-fit determines if the solution is satisfactory. If this is not the case, the approximation process is restarted and further experiments are made or the GP model is evolved with different parameters, as explained in Chapter 4. To reduce the number of analyses in computer simulations, sensitivity data may be used in the model fitting, although this information is not always available at low cost. If in addition to the values of the original function Fp = F(xp) their first order derivatives at point p

$$F_{p_i} = \frac{\partial}{\partial x_i} F_p \quad (i=1,\ldots,N,\ p=1,\ldots,P) \tag{1.44}$$

(i=1,…,N, p=1,…,P) are known, the problem (3.2) is replaced by the following one (Toropov et al., 1993):

$$G(\boldsymbol{a}) = \sum_{p=1}^{P} \left\{ w_p \left(\left(F_p - \tilde{F}_p(\boldsymbol{a}) \right)^2 + \gamma \frac{\sum_{i=1}^{N} \left(F_{p_i} - \tilde{F}_p(\boldsymbol{a})_{,i} \right)^2}{\sum_{i=1}^{N} {F_{p_i}}^2} \right) \right\} \rightarrow \min \tag{1.45}$$

Where, $\gamma > 0$ is the parameter characterizing a degree of inequality of the contribution of the response and the sensitivity data. In this thesis, γ is taken as 0.5, following recommendations by Toropov et al. (1993). Van Keulen et al. (2000) have presented a methodology for the construction of responses using both function values and derivatives on a weighted least-squares formulation. The authors conclude that the use of derivatives provides better accuracy and requires a reduced number of data

The response surface methodology analysis has been reviewed. RSM can be used for the approximation of both experimental and numerical responses. Two steps are necessary, the definition of an approximation function and the design of the plan of experiments. As concluded in Chapter 2, genetic programming is the method of choice to find a suitable approximation function and will be described in Chapter 4. A review of different designs for fitting response surfaces has been given. A desirable design of experiments should provide a distribution of points throughout the region of interest, which means to provide as much information as possible on the problem. This "space-filling" property is a characteristic of three plans: Latin hypercube sampling, Audze-Eglais and van Keulen. All three plans are independent of the mathematical model of the approximation. However, Latin hypercube sampling distributes the points randomly in the space, while Audze-Eglais uses a distribution based on maximum separation between points. The Audze-Eglais plan has been chosen in this thesis. It should be noted that if the model building is to be repeated within an iterative scheme (e.g. with mid-range approximations), van

Keulen's plan would become an attractive alternative as it adds points to an existing plan. This thesis is primarily focused on building global approximations.

Full factorial design

To construct an approximation model that can capture interactions between N design variables, a full factorial approach (Montgomery, 1997) may be necessary to investigate all possible combinations. A factorial experiment is an experimental strategy in which design variables are varied together, instead of one at a time. The lower and upper bounds of each of N design variables in the optimization problem needs to be defined. The allowable range is then discretized at different levels. If each of the variables is defined at only the lower and upper bounds (two levels), the experimental design is called 2N full factorial. Similarly, if the midpoints are included, the design is called 3N full factorial and shown in Fig-1.21.

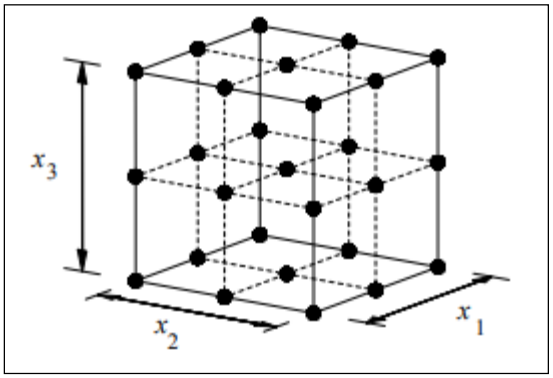

Fig- 1.21 3N full factorial

Factorial designs can be used for fitting second-order models. A second-order model can significantly improve the optimization process when a first-order model suffers lack of fit due to interaction between variables and surface curvature. A general second-order model is defined as

$$y = a_0 + \sum_{i=1}^{n} a_i x_i + \sum_{i=1}^{n} a_{ii} x_i^2 + \sum_{i=1}^{n}\sum_{\substack{i=1 \\ i<j}}^{n} a_{ij} x_i x_j \qquad (1.46)$$

Where, xi and xj are the design variables and a are the tuning parameters

The construction of a quadratic response surface model in N variables requires the study at three levels so that the tuning parameters can be estimated. Therefore, at least (N+1) (N+2) / 2 function evaluations are necessary. Generally, for a large number of variables, the number of experiments grows exponentially (3 N for a full factorial) and becomes impractical. A full factorial design typically is used for five or fewer variables. If the number of design variables becomes large, a fraction of a full factorial design can be used at the cost of estimating only a few combinations between variables. This is called fractional factorial design and is usually used

for screening important design variables. For a 3^N factorial design, a $(\frac{1}{3})^P$ fraction can be constructed, resulting in 3^{N-p} points. For example, for p=1 in a 3^3 design, the result is a one-third fraction, often called 3^{3-1} design, as shown in Fig- 1.22 (Montgomery, 1997)

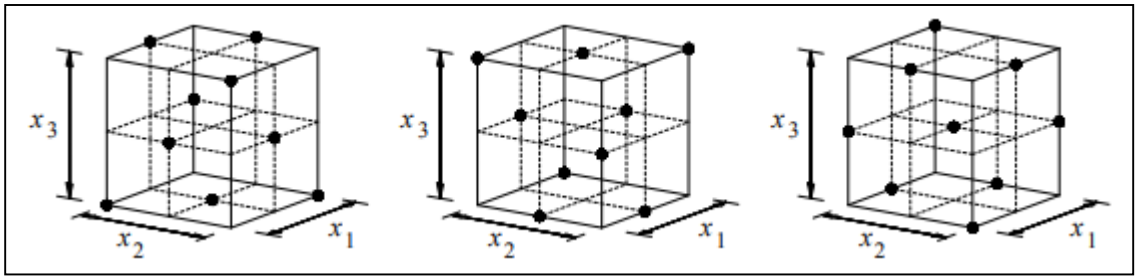

Fig- 1.22 Three one-third fractions of the 3^3 design

1.21 ANALYSIS OF VARIANCE (ANOVA)

The purpose of analysis of variance is to investigate which machining parameters significantly affect the responses. This process is carried out by computing the F-test value of the parameter with the standard F table value (F0.05) at the 5% significant level. The associated P-values are less than 0.05 for the models (i.e., α = 0.05, or 95% confidence level) indicate that the model terms are statistically significant. Percentage contribution of process parameters on response is determined from Seq SS values of ANOVA table. Percentage contribution is calculated using the following expression.

Percentage contribution of a term = $\frac{Seq\ SS\ for\ the\ term}{total\ Seq\ SS} \times 100$

SS = Sum of square deviation

Seq SS = Sequential sum of square deviation

F = Fisher's ratio, P = probability of significance

1.22 LITERATURE SURVEY

The purpose of this literature review is to provide previous information on the issues to be considered in this thesis and show the relevance of the present study. Composite materials are playing an important role in a broad range of application fields and replacing many traditional engineering materials.

Machining of polymers/ composites (***Evestine*** and ***Rogers*** [1]) is employed when the quantity of items does not satisfy for the cost for moulds, or when a product needs accurate dimensional accuracy, better surface finish. As high performance polymers have been increasingly used for a large number of industrial applications, the machining quality was become predominant factor for the development of new processes and materials. Nevertheless the knowledge about the polymers under machining is very limited, as well as the definition of suitable models for

predictions of cutting forces. In the scientific literature, machining of plastics is poorly treated. In the oldest reference, an experimental approach is preferred, assuming the plastics behave as metals.

Wang et al. [2] carried out an experimental study of orthogonal cutting mechanism in edge trimming of unidirectional graphite/ epoxy composite with polycrystalline diamond tools. They examined the effect of tool geometry and operating conditions from an analysis of chip formation, cutting force and machined surface topology.

Chen [3] demonstrated a study on effect of point, helix and chisel edge angles on thrust force and torque when drilling carbon fiber reinforced composite with high speed steel drills. They concluded that increase in the point angle increased the thrust force while torque was reduced. On the other hand, when helix and chisel edge angles were increased, the measure of both thrust force and torque were reduced.

Khashba [4] studied experimentally the influence of drilling and material variables on thrust force, torque and delamination of GFRP composites. They reported that for the same matrix type (polyester), although chopped composites had higher thrust force than woven composites, the former had lower push out delamination than latter composite, which contrary to the direct relationship between thrust force and delamination. In counterpoint, the torque of woven/polyester composites was higher than that for chopped/polyester composites

Khashba and Sonbaty [5] determined the effect of machining parameters (feed, speed and drill diameter) on the thrust force and machinabiity of woven glass fiber-reinforced epoxy composites. The machinability was characterized by delamination size at drilled entrance and ezit sides, Surface roughness and bearing strength of drilled holes. Correlation between thrust force and the machinibility parameters was performed. The high values of correlation coefficients between thrust force and machinibility parameters confirmed the importance of reducing the thrust force to improve the load carrying capacity of composite structure assembled by rivets or bolted joints.

Davim **et** ***al.*** [6] investigated the influence of cutting parameter on delamination factor and surface roughness in drilling glass fiber composites using cemented carbide (K10) drill. Feed rate had highest influence on delamination factor, while speed had highest effect on surface roughness for the composite materials.

El-sonbaty **et** ***al.*** [7] presented the influence of cutting speed, feed, drill size and fiber volume fraction on thrust force, torque and surface roughness in drilling process of chopped glass fiber reinforced epoxy composites. They reported that the cutting speed had insignificant effect on thrust force and surface roughness of epoxy resin. The drilled holes of GFRE composite with lower fiber volume fraction ratio at lower feed had greater roughness than that drilled at higher feed.

Hocheng et al. [8] made experiments of study the machinability of some reinforced thermoset and thermoplastics for drilling operation. They discussed the chip characteristics and the specific cutting energy to reveal the mechanism of material removal. They observed that the level for fiber loading and the deformation behaviour of matrix polymer determined the extent of plasticity in chip formation and the chip length. In further study they also observed that, drilling fiber reinforced-thermoplastics, the edge quality was generally fine except in the case of concentrated heat accumulation at tool tips, which was generated by high cutting speed and low feed rate.

An [9] reported that for the practical cutting of glass fiber, optimal cutting parameters should be taken into consideration to achieve less blade wear, good cutting quality, etc. During glass fiber cutting, the reduction of blade wear was a critical aspect. Long glass fibers were found to affect cutting quality significantly.

Caprino and Tagliaferri [10] carried out drilling tests on glass-polyester composites using standard HSS tools; drilling was interrupted at preset depths to study damage development during drilling. The specimens, polished by a metallographic technique, were examined by optical microscopy to identify any damage.

Davim and Mata [11] investigated the machinability in turning processes of glass fiber reinforced plastics (GFRPs) manufactured by hand lay-up. A statistical technique using orthogonal arrays and analysis of variance (ANOVA), were employed to know the influence of cutting parameters on specific cutting pressure and surface roughness. The machining parameters considered were cutting velocity and feed rate. The chosen array was the L_9 (2^4) with the nine rows corresponding to the number of test with two columns with three levels. They developed the plan of test to correlate the influence of the cutting velocity and the feed rate, with surface roughness and specific cutting pressure using two cutting tool materials (polycrystalline diamond tool and cemented carbide tool). They concluded that the polycrystalline diamond tool (PCD) presented smaller value of surface roughness and specific cutting pressure and the feed rate had the highest physical as well statistical influence on surface roughness and specific cutting pressure. A new machinability index had been proposed by them.

The investigation of ***Palanikumar*** [12] was focused on the multiple performances machining the investigation of characteristics of GFRP composites using carbide (K10) tool. Five parameters such as work piece fiber orientation, cutting speed, feed rate, depth of cut, and machining time were selected to minimize the surface roughness. It was found that the machining performance might be improved by including more number of parameter and levels.

Palanikumar [13] carried out investigation on the multiple performance optimizations of machining characteristics of glass fiber reinforced plastics composites by using non-dominated sorting Genetic Algorithm. Cutting speed, feed and depth of cut were selected to minimize the surface roughness, tool flank wear and maximize the metal removal rate. Polycrystalline diamond tool was used for turning operation.

Palanikumar et al. [14] used fuzzy logic for modelling and prediction of CFRP work piece. Three parameters such as depth of cut, feed rate and cutting speed were selected to minimize the surface roughness. Cubic boron nitride tool was used for turning process. It was found that fuzzy logic technique can be effectively used for prediction of surface roughness in machining of CFRP composites.

Konig [15] investigated the phenomenon of machining of FRP composites using different processes like drilling, routing, milling, water jet cutting and laser cutting. The machining of FRP was seemed to be different from that of metal working in many aspects because of the inhomogeneous material behaviour, dependence on fiber and matrix properties, fiber orientation and types of weave.

Palanikumar and Hussain [16] developed a surface roughness and cutting force prediction model for machining GFRP tubes using response surface methodology by using carbide tool (K_{20}), cubic boron nitride (CBN) and polycrystalline diamond tool. Four parameters such as cutting speed, feed, depth of cut and work piece (fiber orientation) were selected to minimize the roughness and cutting forces. It was found that polycrystalline diamond tool is better than the other tools.

Santhankrishnam [17] carried out face turning trials on glass fiber reinforced polymers (GFRP), carbon fiber reinforced polymers (CFRP) and Kevlar fiber reinforced polymers (KFRP) cylindrical tubes to study their machined surface for the possible application as friction surfaces. The surface roughness obtained and the observed morphology of the machined surfaces of fiber reinforced polymer (FRP) composites was compared. The mechanisms of material removal and tool wear were also discussed. The cutting forces encountered during machining of the composites also reported.

Davim and Mata [18] presented on optimization study of surface roughness in turning FRPs tubes manufacturing by filament winding and hand lay-up, using polycrystalline diamond tools. Optimal cutting parameters were identified to obtain a certain surface roughness (Ra and Rt/Rmax), corresponding to international dimensional precision (ISO) IT7 and IT8 in the FRP work pieces, using multiple regression analysis (MRA). Additionally, the optimal material removal rates identified.

Mohan [19] outlined the Taguchi optimization methodology, which is applied to optimize the cutting parameters in drilling of glass fiber reinforced composite (GFRC) material followed by analysis of variance (ANOVA); to study the effect of process parameters on machining process. The drilling parameters an specimens parameters evaluated were speed, feed rate, drill size and specimen thickness. A series of experiments were conducted to relate the cutting parameters and material parameters on cutting thrust and torque. An orthogonal array, signal-to-noise were employed to analyze the influence of these parameters on cutting force and torque during drilling. Analysis of Taguchi method indicated that among the all-significant parameters, speed and drill size were found to impose more significant influence on cutting thrust than the specimen thickness and feed rate.

Karnik [20] presented application of artificial neural network (ANN) model to study the machinability aspect of unreinforced polyetheretherketone (PEEK), reinforced polyetheretherketone with 30% of carbon fibers(PEEK CF30) and 30% of glass fibers (PEEK GF30) machining. A multilayer feed forward ANN was employed to study the effect of parameters such as tool material, work material, cutting speed and feed rate on two aspect machinibility namely power and specific cutting pressure. The input-output patterns required for training were obtained from the experiments planned through the full factorial design. The analysis reveals that minimum power result from combination of lower value of cutting speed and feed rate for all work-tool combinations. However, higher values of feed rate were required to achieve minimum specific cutting pressure. The investigation results exhibited that, K_{10} tool provide better machinability for PEEK and PEEK CF30 materials, while PCD tool was found preferable for PEEK GF30 material.

Kilickap [21] investigated the influence of the cutting parameters, such as cutting speed and feed rate, and point angle on delamination produced when drilling GFRP composite. The damage generated associated with drilling GFRP composites were observed, both at entrance and the exit during drilling. They obtained optimum cutting parameters for minimizing delamination at drilling GFRP composites. This paper presented the application of Taguchi method and analysis of variance (ANOVA) for minimization of delamination influenced by drilling parameters and drill point angle. The optimum drilling parameter combination was obtained by using the analysis of signal-to-noise ratio. The conclusion revealed that feed rate and cutting speed were the most influential factor on the delamination, respectively. The best results of delamination were obtained at lower cutting speeds and feed rates.

Kini and Chincholkar [22] studied the effect of varying machining parameters in turning on surface roughness and material removal rate (MRR) for ±30˚ filament wound glass fiber reinforced polymers in turning operations using coated tungsten carbide inserts under dry cutting conditions. They described the development of an empirical model for turning of GFRP utilizing factorial experiments. Second order predictive model covering speed, feed, depth of cut and tool nose radius was developed at 95% confidence intervals for surface roughness and material removal rate.

Bagci and Isik [23] carried out orthogonal cutting tests on unidirectional (GFRP), using cermets tools. During the test the process variables: depth of cut, feed rate and cutting speed were varied, whereas the cutting direction was held parallel to fiber orientation. Turning experiment were designed based on statistical three level full factorial experimental design. An artificial neural network (ANN) and response surface (RS) model were developed to predict surface roughness on turned part surface. In the development of predictive models, cutting parameters of cutting speed, depth of cut and feed rate were considered as model variables. The required data for predictive models were obtained by conducting a series of turning test and measuring the surface roughness data. Good agreement was observed between the predictive models results and the experimental, measurements. The ANN and RSM models for GFRPs turned part surfaces were compared with each other for accuracy and computational cost.

Jawali et al. [24] fabricated a series of short glass fiber-reinforced nylon 6 composites with different weight ratios of glass contents by melt mixing. The fabricated nylon 6 composites have been characterized for physical-mechanical properties such as specific gravity, tensile properties, and wear resistance. A marginal improvement in tensile strength and tensile modulus was observed with increase in high modulus fiber. Wear resistance was increased with the increased in rigid glass fiber content in the nylon matrix. The dimensional stability of the composite was found improved with the increase in the fiber content. The acoustic behaviour of the composites was measured using acoustic emission technique. The surface morphological behaviour of the composites was investigated by scanning electron microscopy (SEM).

Palanikumar and Davim [25] attempted to assess the factors influencing tool wear on the machining of GFRP composites. The factors considered were cutting speed, feed orientation angle, depth of cut and feed rate. A procedure was developed to assess and optimize the chosen factors to attain minimum tool wear by incorporating (i) response table and effect graph; (ii) normal probability plot; (iii) interaction graphs and (iv) analysis of variance (ANOVA) technique. The results indicated that cutting speed is a factor, which had greater influence on tool flank wear, followed by feed rate. Also the determined optimal conditions reduced the tool flank wear machining of GFRP composites within the ranges of the parameters studied.

Khairusshima et al. [26] studied the effect of chilled air on tool wear and work-piece quality during milling of glass fiber-reinforced plastics. In this study chilled air of -10˚c was applied to the cutting tool using a vortex tube, which is new in the machining of fibers, to minimize the heat generated during machining.

Balmungundan et al. [27] investigated the milling of friction stir processed glass fiber reinforced plastic plates. The friction stir processed plates were then subjected to milling with solid carbide K_6 end mill tool. Taguchi's L_9 orthogonal array was used for experimental design. The milling process parameters such as spindle speed, feed and depth of cut at three levels were optimized with multiple performance considerations of surface roughness and delamination factor. Multi optimization of machining parameters was done through desirability function analysis.

Panneerselvam et al. [28] used Taguchi method and grey relation analysis to optimize machining parameters on end milling of glass fiber reinforced plastics. The machining parameters were Tool condition (TC), number of flutes (z), cutting speed (v) and feed rate (f). The output responses were surface delamination, machining forces, cutting torque and surface roughness. Grey relation analysis was applied to convert the multiple quality characteristics to a single performance characteristic.

Rusinek [29] investigated the milling process of the epoxide-polymer matrix composite reinforced carbon fibers. They observed the effects of two control parameters, namely feed and rotational speed, on cutting forces. Experiments were conducted on a CNC machine with feed and rotational speed, on cutting forces. Experiments were conducted on a CNC machine with feed rate ranging from 200 to 720 mm/min and rotational speed from 2000 to 8000 rpm. The

experimental time series were analyzed by means of delay coordinates method in order to find suitable cutting regions and recognize the kind of behavior.

Davim [30] applied Taguchi method to find optimum process parameters for end millng of two GFRP materials (Viapal VUP 9731 and ATLAC 382-05). Materials were produced by hand lay-up, and made in two different matrices; unsaturated polyester and a propoxylatedbisphenol A-fumarated polyester. They had taken Taguchi's L9 orthogonal arrays, for designing the experiments wih two factors and three levels. They investigated the influence of cutting parameters (cutting velocity and feed rate) on the machining force in workpiece, delamination factor, surface roughness and international precision on two GFRP materials. Finally an ANOVA was performed to investigate the cutting characteristics of GFRP composite materials using cemented carbide ()K10 End mill.

Azmi [31] conducted end milling experiments under different experimental parameters and their levels according to the Taguchi design of experimental method. They used 3 factors 3 levels for this optimization technique and had done nine experiments. The process parameter varied had been name as feed rate, spindle speed, depth of cut. The responses were surface roughness, tool life and machining forces. Taguchi analysis combined with ANOVA was performed to quantify the effects of spindle speed, feed rate and depth of cut on those characteristics. Multiple regression analysis (MRA) was also employed to established parametric relationship between the experimental parameters and the machinability outputs. The most influencing factor in the process was feed rate, the spindle speed is the second one and depth of cut has negligible effect on the process.

Azmi [32] also applied the deve;lopment of an indirect approach in predicting and monitoring the wear on carbide tool during end milling using multiple regression analysis and neuro fuzzy modeling.

Parveen Raj [33] carried out end milling of GFRP plate for reduction of delamination and obtaining the good surface roughness. Their investigation dealt with the study and development of surface roughness and delamination prediction model for machining of GFRP plate using mathematical model and artificial neutral network (ANN) multi objective technique. The parameters were cutting speed; feed and depth of cut and tool material.

S.A. Tobias [34] proposed the first analytical expression for dynamic cutting force considering the incremental vibration of chip thickness, the of penetration and cutting speed. The investigations for determining the limit of stability in the machining process and identifying the condition leading to the onset of chatter had been made by many researchers such as ***Doi*** [35], ***J.A. Tlusty*** [36] and ***H.E***. ***Merritt*** [37].

Y. Kondo et al. [38] pointed out that the behavior of the self-excited vibration as governed by the multiple regenerative effects.

S. Saha et al. [39] discussed about the effect of cutting parameters on dynamic behavior of cylindrical grinding machine. They showed how some of the process parameters influenced vibration level during traverse cut grinding.

Chatter in grinding has been classified into two types [40, 41] based on based on the observations of the grinding wheel and work piece surface profile. The authors mentioned that in the first type, amplitude increased slowly and the pronounced waviness would develop on the periphery of grinding wheel. While in the second type of chatter amplitude growth rate was faster and pronounced waviness was found on the work piece circumference.

S. Malkin et al. [42] expressed that as with other machine tools grinding machine could be classified into two categories i.e. forced vibration and self-excited vibration. Forced vibrations are caused by periodic disturbances external to the grinding process. Such external source of disturbances may be affected by the factors affecting the spindle system such as out-of-balance shaft, bearing variable compliance, manufacturing errors and the method of assembly [43]. Sef excited vibraons, on the other hand, are generally associated with natural vibration modes of the machine tool structure, soueces of which may be a host of undesired caused-one important being uneven in-process grinding wheel wear [44].

Alfares et al. [44] Studied the effects of dynamic changes in the grinding force components due to changes in the grinding wheel flat area and work piece material on the vibration behavior of the grinding spindle. In this study the steady state dynamics and vibration behavior of the grinding machine spindle was simulated by a five degree of freedom model. This results indicated that the vibration behavior was different depending upon material being ground while using a grinding wheel with a fixed wear flat area increased, the level of vibration increased for all the degrees of freedom.

R.Aini et al. [43] and ***N. Akturk,*** [45] also investigated and modeled vibration of grinding spindle supported by a pair of angular contact ball bearings. In these models, the effect of several factors such as natural frequency of the shaft and bearing assembly, ball passage frequency, spindle speed variation, pre-load, misalignment and manufacturing defects influencing ball bearing vibration were considered and analyzed.

Y.S. Liao, and L.C. Shaing [46] presented models both for self-excited vibration and forced vibration caused by eccentricity of grinding wheel. These investigators find closed relationship between accuracy of the work piece and forced vibration on cylindrical plunge grinding operation. The results also indicated that exponentially lobes were developed on the circumference of work piece and the grinding wheel was under regenerative chatter, chatter frequency being always greater than the systems natural frequency.

Orynski [47] made a theoretical analysis of the dynamics of machine tool work piece system for cylindrical plunge grinding. The grinding machine they considered was equipped with hydrostatic bearing of grinding wheel spindle and hydrostatic slide ways. The proposed model

allowed quantitative investigation of grinding force characteristics and its influence on forced vibrations in grinding.

Drew [48] expressed that the poor results from conventional lathe may be traceable to harmful dynamic forces coupled to the work piece interface. A new system of sensors/ actuators would help detecting the causes and thereby leading a cure.

J.Y. Sheikh-Ahmad [49] developed a novel machining technique for polymers with capabilities to improve machining process. Many industrial applications are highly dependent on the actual geometry of the surface. The product performance on the bearing, cylindrical liners, and other mechanical contact problems are connected to the ability of the surface to retain oil. Conventional machining does not create this desirable surface and subsequent manufacturing processes are necessary to achieve the final surface.

Kobayashi [50] compiled several experimental observations in his book 'Machining of Plastics'. This text has been considered as a reference for long time in this field. Also the latest scientific reviews mention it to show the dependence of the cutting forces on process parameters.

During this thesis work some more books and MME/ M.Tech thesis [51-57] have been consulted.

1.23 SCOPE AND OBJECTIVE OF STUDY

The available literature indicates that few works have been attempted for milling of glass fiber reinforced polyester composite materials. Even, a mathematical model describing the milling of glass fiber reinforced polyester composite is yet to be developed. Moreover optimization of process parameters for multiple performance characteristics for this material is yet to be reported. Optimal process combinations of different process parameters are to be determined. The delamination is a major problem associated with the milling of chopped glass reinforced polyester composites. Surface roughness is also an important aspect of those composites. The milling by the optimal milling process parameters is most efficient, than the "trial and error" method, to achieve the optimum responses. For effective use of any machining process, it becomes necessary to find optimum process parameters to achieve improved quality as well as increased productivity.

The present works have been done to a large extent in the area of "machine toll vibration" or "dynamics of the machining process". Some experiments had been indeed done to find out vibration in milling for a particular phase of input parameters like feed, work speed, depth of cut etc (as these input parameters are restricted by the limitations associated with specific experimental set up, including limitation arising out of specifications of particular machine tool on which the study was done). If one cannot anticipate the vibration for varied levels of input parameters, suitable control will not be possible; on the other hand if anticipation is made, which has got some basis, then apart from close control of the process, good design of the machine tool

would also become possible. In automation or feedback control systems this anticipation proves to be very much fruitful. Very few studies have been made to predict vibration at different input conditions. Probably no previous work has been done in milling on this issue. The investigators studied on various aspects of dynamic behavior of machine tools,which include source of vibration, conditions leading to unset of chatter, mathematical analysis of the dynamic system etc. many of the studies were directed towards finding means for suppression or minimization of vibration. Some research works had developed analytical models for better understanding the behavior of the machine tools/ machining process under dynamic situations. The search is still being continued, which suggests that the knowledge regarding machine tool dynamics and methods leading to vibration have ample scope of further exploration and development The primary aim of the present work is to undertake a comprehensive study of side and face milling of chopped fiber glass reinforced polyester composite materials.

The present work is thus attended to predict the dynamic behavior of the conventional milling machine for any combination of input parameters. Experiments are planned as per Response Surface Method Full factorial design. The feed rate, rotational speed and depth of cut are chosen as process parameters. Delamination factor, surface roughness and cutter vibration are taken as the measure for performance. The optimization of single performance characteristichas been performed by RSM Full factorial methodology to achieve the goals. Mathematical modeling has been developed to relate the response(s) with input parameters. Response surface plots have also been made to show the interaction/ combined effects of the parameters on the selected responses. Further, analysis of variance has also been done to determine the relative significanceof machining parameters on the individual responses.

2. EXPERIMENTAL PLAN, SETUP AND PROCEDURE

The present study has been done through the following plan of experiments:

i) Checking and preparing the horizontal milling machine ready for performing the machining operation.

ii) Cutting GFRP sheet of 9 numbers, which are of dimensions 90 × 50 × 8 mm.

iii) Performing trial operation in milling machine to fix the values of the cutting parameters for the experiments.

iv) Conducting side and face milling on GFRP sheets using different levels of rotational speed, feed rate and depth of cut.

v) Observing and measuring the torque, surface roughness, delamination factor and cutter vibration through dynamometer, portable surface roughness tester, Olympus microscope, accelerometer and storage oscilloscope respectively.

2.1 EXPERIMENTAL PLAN

The three input parameters namely, rotational speeds, feed rate and depth of cut are considered. Torque (M_z), average surface roughness (Ra), delamination factor (F_d) and amplitude of acceleration (fa) are taken as performance parameters. The Response Surface Methodology based full factorial design is used. L_{27} (3^3) orthogonal array can be accommodate three factors each at three levels. Each row of orthogonal array represents the experiment number which contains the corresponding combination of the process parameter value. Total 27 experiments are conducted on milling operation of glass fiber reinforced polymers (GFRP) composite and each experiment has been repeated one time. The factors and their levels are listed in Table 2.1. The L_{27} design matrix is tabulated in Table 2.2.

Table 2.1 Factors and levels selected for milling operation of GRFP composites

Factors	Notation	Level 1	Level 2	Level 3
Feed rate (mm/min)	f	10	15	24
Rotational speed (rpm)	N	135	190	270
Depth of cut (mm)	d	1	1.5	2

Table 2.2 L_{27} design matrix

Run Order	Speed (rpm)	Feed (mm/min)	Depth of cut (mm)
1	270	10	1.5
2	270	10	2.0
3	190	10	2.0
4	270	15	2.0
5	135	10	1.0
6	190	15	2.0
7	135	24	1.0
8	135	10	2.0
9	270	15	1.5
10	190	24	1.0
11	190	10	1.0
12	190	15	1.5
13	270	24	1.0
14	135	24	1.5
15	190	24	1.5
16	190	10	1.5
17	190	24	2.0
18	135	24	2.0
19	135	15	1.5
20	270	10	1.0
21	270	24	2.0
22	135	15	1.0
23	135	10	1.5
24	270	15	1.0
25	270	24	1.5
26	190	15	1.0
27	135	15	2.0

2.2 EXPERIMENTAL SETUP, WORK MATERIALS AND INSTRUMENTS

The photographic view of milling machine is shown in Fig- 2.1 and pictorial view of experimental set up for the present work is shown in Fig- 2.2.

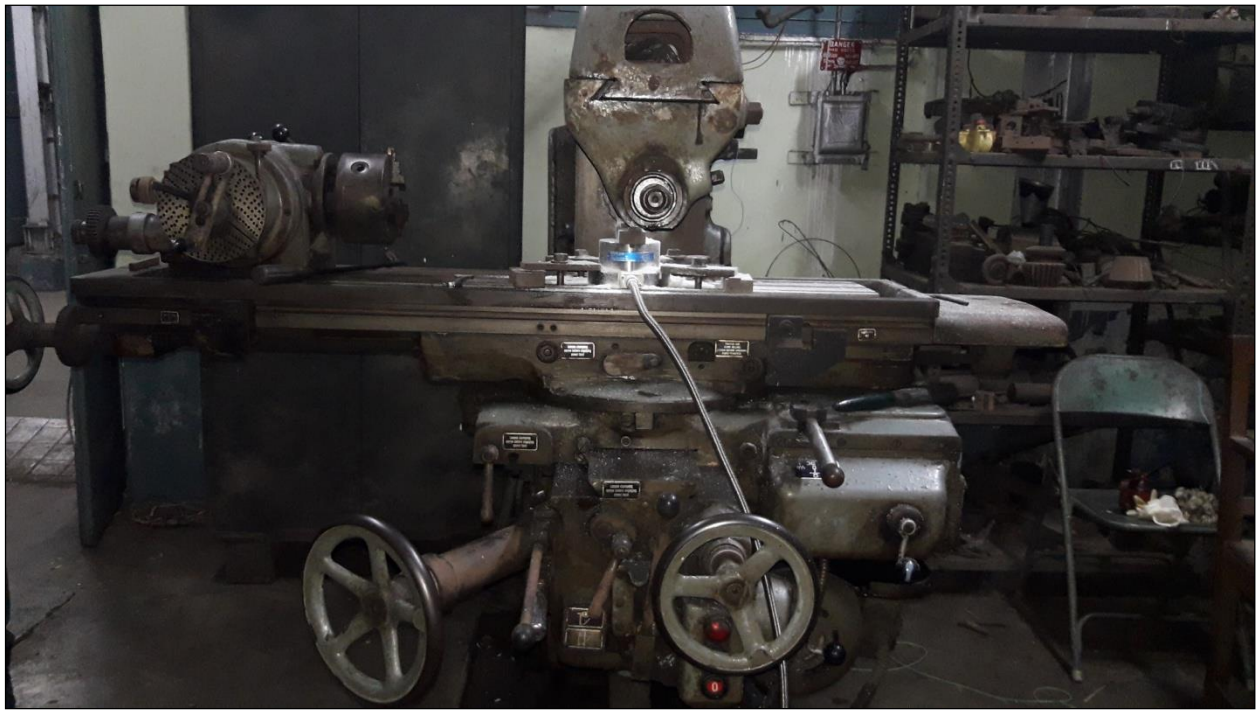

Fig- 2.1 Photographic View of Milling Machine

2.3 MACHINE AND INSTRUMENTS

(a) **HORIZONTAL MILLING MACHINE**

Manufacturer: Hindustan Machine Tools Ltd., Bangalore, India
Maximum rotational speed: 635 rpm
Rotational speed range: 34 – 635 rpm
Variable feed range: 6 – 190 mm/min
Variable depth of cut range: 0.05 – 5 mm
Serial No. – 3442

(b) **HSS SIDE AND FACE MILLING CUTTER**:

(i) Size: 75 mm × 12 mm × 25 mm bore
(ii) Manufacturer: Addison & Co. Ltd., India

Fig-2.2 Experimental set-up

(c) **4 - COMPONENT DYNAMOMETER:**

A four-component dynamometer (Kistler make) is used for measuring a torque Mz and the three orthogonal components of cutting force (Fx, Fy, Fz). The dynamometer has a great rigidity and consequently a high natural frequency. Its high resolution enables the smallest dynamic changes in large forces and torques to be measured. It is a compact and robust multi-component force measuring instrument which is suitable for cutting force measurements when milling. The dynamometer consists of a four component sensor fitted under high preload between a base plate and a top plate. The four components are measured practically without displacement. It must be taken into account that combined and eccentric loads may reduce the measuring ranges. The sensor is mounted ground-isolated. Therefore ground loop problems are largely eliminated. The dynamometer is rustproof and protected against penetration of splash water and cooling agents. Together with the connecting cable Type 1677A5/1679A5 it corresponds to the protection class IP 67. The picture of the dynamometer is shown in Fig- 2.3. In Table- 2.1 technical data of the dynamometer is mentioned. In Fig- 2.4, measuring system for 4 - component measurement M_Z, Fx, Fy and Fz is shown.

Application examples: (i) Measuring feed force, deflective force and moment when drilling, thread cutting etc. (ii) Cutting force measurements while milling and grinding (iii) Cutting force measurements while turning (iv) Testing torque wrenches (v) Testing springs (torsion) (vi) Measurements on small thrust bearings, friction clutches etc. (vii) Measuring starting torques on fractional horsepower and stepping motors (viii) Ergonomic measurements.

A typical measuring chain with DAQ system Type 5697A1 is showing in Fig- 2.5.

The dynamometer may be mounted with screws or claws on any clean, face-ground supporting surface, such as the table of a machine tool for example. Uneven supporting surface may set up internal stresses, which will impose severe additional loads on the sensor and may also increase

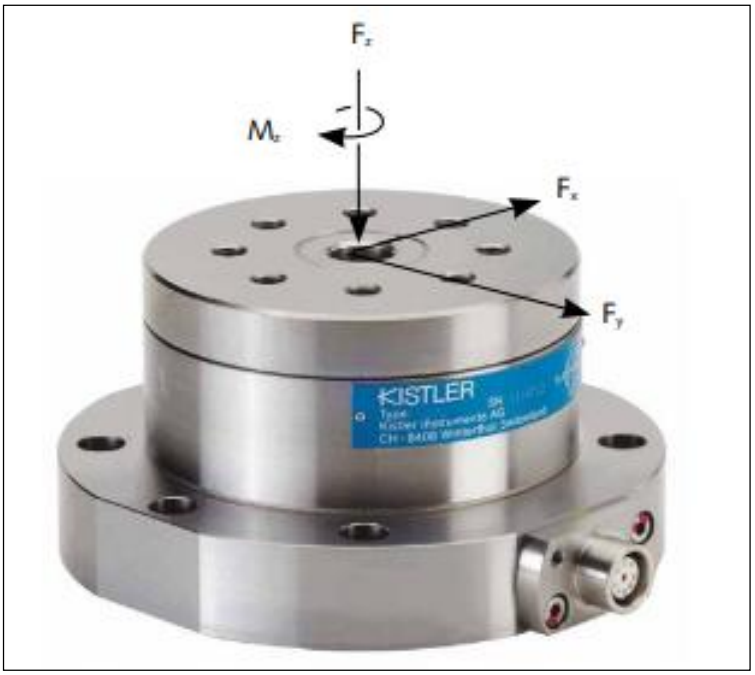

Fig- 2.3 A 4- Component Dynamometer

Table 2.3 Technical Data

Measuring range	Fx, Fy	kN	-5…….5[1]
	Fx	kN	-5……..20[2]
	Mz	N-m	-200….200
Calibrated measuring range 100%	Fx, Fy	kN	0…….5
	Fz	kN	0……..20
	Mz	N-m	0……..200
			0……-200
10%	Fx, Fy	kN	0……0.5
	Fz	kN	0……2
	Mz	N-m	0…….20
			0……..-20
Overall	Fx, Fy	kN	-6/6
	Fz	kN	-6/24
	Mz	N-m	-240/240
Max. bending	Mx, My	N-m	-400…….400

moment			
Threshold	Fx, Fy	N	<0.01
	Fz	N	<0.02
	Mz	mN-m	<0.2
Sensitivity	Fx, Fy	ϱC/N	-7.8
	Fz	ϱC/N	-3.5
	Mz	ϱC/N-m	-160
Linearity, all ranges		% FSO	≤±1
Hysteresis, all ranges		% FSO	≤1

Cross-talk. For mounting the force-introducing components, such as lathe tools and work-pieces, eight M8 mm threaded holes in the cover plate are available. The supporting surfaces for the force-introducing parts must be face-ground to obtain good mechanical coupling to the cover plate. For satisfactory mounting of lathe tools up to 20x20 mm shank cross section, the tool holder Type 9404 may be used. Charge amplifier channels are also needed to build a complete measuring system (e.g. Type 5080A...). These convert the measurement signal into an electrical voltage. The measured value is exactly proportional to the force acting.

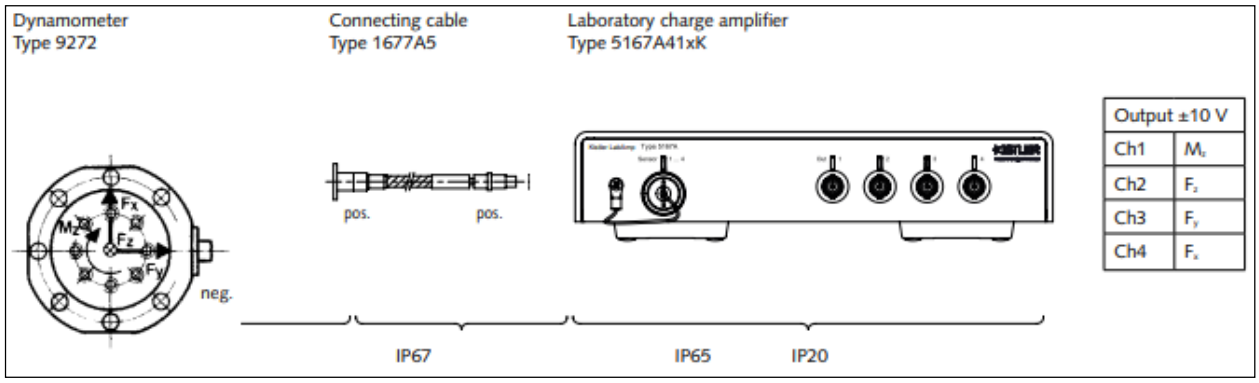

Fig-2.4 Measuring system for 4-component measurement MZ, FX, FY, F

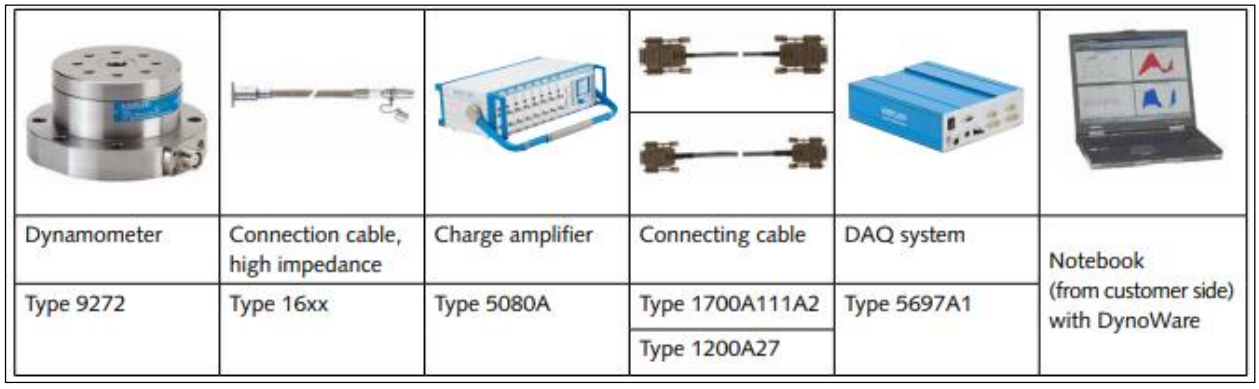

Fig-2.5 Typical measuring chain with DAQ system Type 5697A1

Vibration Measurement

(d) **ACCELEROMETER:**
Make: Syscon Instruments Private Limited, Bangalore.
Model No: 353B31
Serial No- 33899

(e) **STORAGE OSCILLOSCOPE:**
Make: Larsen and Tubro
Model- OS 1450
Serial No- CY 60 303

The storage type oscilloscope is shown in Fig- 2.6.
Display-
CRT: 8 × 10 cm rectangular mono accelerometer.
EHT- 2 KV

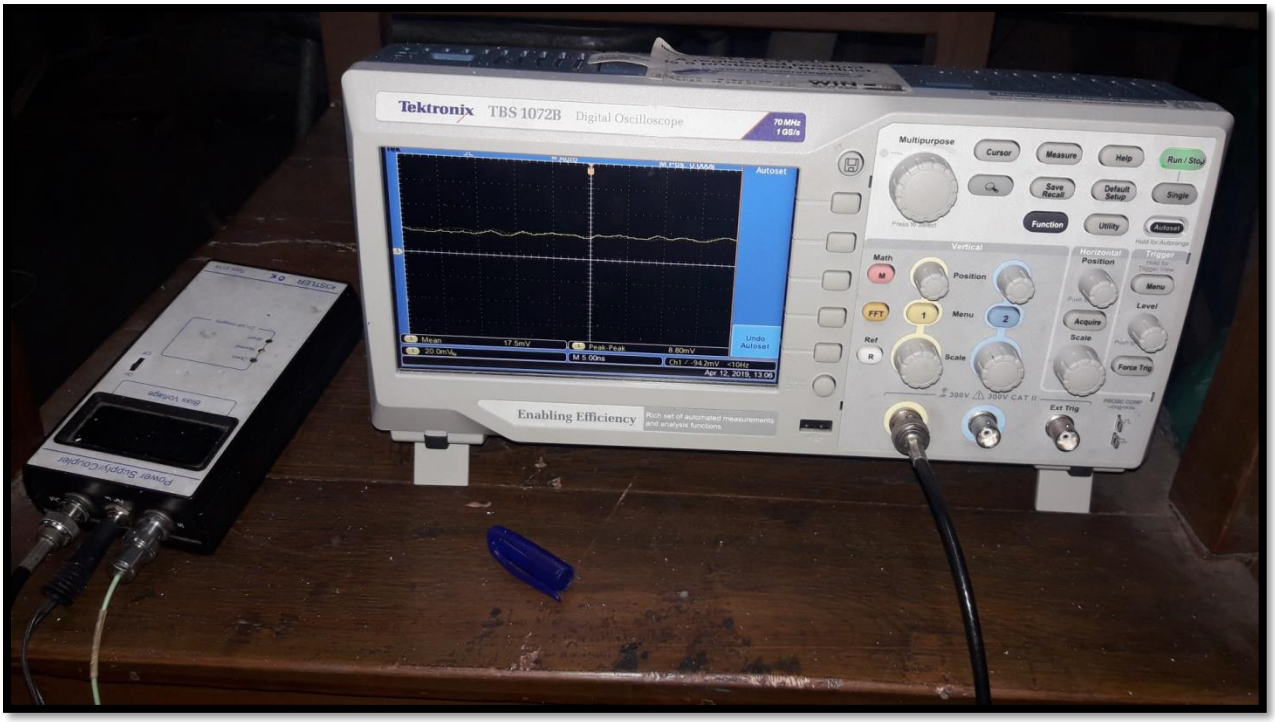

Fig- 2.6 Storage Oscilloscope with Vibrationmeter

Vertical deflection-
Two independent input channels CH1 and CH2.
Bandwidth- -3 dbd.c. to 20 MHz (2 Hz to 20 MHz on a.c.)
Sensitivity- 2 mV/ div to 10 V/ div in 1-2-5 sequence.
Accuracy- ± 3% in ×1 cal& ± 5% in ×2 cal.

Horizontal deflection:
Bandwidth: (-3 db) d.c. to 2 MHz with less than 3 degree phase shift at 50 KHz.
Normal mode swipe rate: 0.5 μs/div to 0.2 sec/div 18 ranges in 1-2-5 sequence.
Accuracy : ± 3% (to 200ns/div)

Display modes:
Single trace: CH1 or CH2
Dual trance: In normal, chopped or alternate modes selected by the mode switch.
The chop frequency is 500 KHz.
Add: CH1 & CH2 added to give the algebraic sum of the two channel inputs (normal mode only)
X-Y: CH1 gives X- deflection and CH2 gives Y- deflection
Test voltage: 16 Volts peak-to-peak, Triangular wave.

Digital facilities:
Store size: 1024 × 6 bits per channel
Vertical resolution: 1in 256 approximate, 28.5 samples/ div.
Horizontal resolution: 1 in 1024 approximate, 100 samples/div.
Dot joining: Linear interpolation between samples.
Wave storage: Upto 20 waveforms can be stored in back up memory and can be recalled onto screen when required.

(f) **VIBRATION METER**:
Make: Syscon Instruments private Limited, Bangalore.
Model No- 12DM-2C
Serial No- 7177
The measurement of vibration is calculated in m/s^2.

(g) **SURFACEROUGHNESS MEASUREMENT**

Surface roughness indicates the state of a machined surface. The instruments for measuring surface roughness can be broadly divided into contact and non-contact types.
(I) **Contact type**: With this type, the tip of the stylus directly touches the surface of the sample. As the stylus traces across the sample, it rises and falls together with the roughness on the sample surface. The movement in the stylus is picked up and used to measure surface roughness.
(II) **Non-contact type**: The leading method of this type is light. Light emitted from the instrument is reflected and read, to measure without touching the sample. Various noncontact systems include the focus deflection type, the confocal microscope type, and the interferometer type. As these systems never harm the sample, can measure soft and viscous materials.
However, contact method is used in the present experiment.

The **Surftest SJ-201P,** shown in Fig- 2.7**,** is a shop-floor type surface roughness measuring instrument, which traces the surfaces of various machine parts, calculates surface roughness

based on roughness standards, and displays the results. In Fig- 2.8 the configuration of standard SJ-201P is being shown.

SJ-201P surface roughness measurement principle:

A pick-up (here in after all referred to as the "Stylus") attached to the detector unit of the SJ-201P will trace the minute irregularities of the work-piece surface. The vertical stylus displacement during the trace is processed and digitally in the liquid crystal display of the SJ-201P.

(i) **Display unit**: The calculation results (measured result) are displayed on the LCD. The drive or detector units are designed to be removable from the display unit. Depending on the shape of the work-piece, it may be easier to perform measurement without mounting the drive/detector unit to the display unit.
Serial No- 178-243-2 (50 × 50 mm)

(ii) **Drive unit**: Serial No- 178-230-2
(iii) **Detector unit**:
Serial No- 178-390 (measuring force 4 mN)
178-296 (measuring force 0.75 mN)

(iv) **Connection cable**:
Serial No- 12BAA303
Size- 1m

Fig- 2.7 Surftest SJ-201P

(v) **AC adapter**:
Serial No- 526688 for 100 V
526688A for 120 V
526688D for 230 V
526688E for 240 V
526688K for 220 V
526688DC for 220 V
(vi) **Battery**:
Alkaline: minimum 600 measurements of 10 mm measurement length
NiCd: minimum 200 measurements of 10 mm measurement length
Size: 6LR61 (USA/Japan), 6F22 (IEC). Fixed battery, external charger.
External charger (NiCd only) : 110/240 V. RTH No.- 112/1591 50/60 Hz.

(vii) **Calibration sample**:
Serial No- 353134.

Transverse unit: transverse speed is 1 mm/sec.

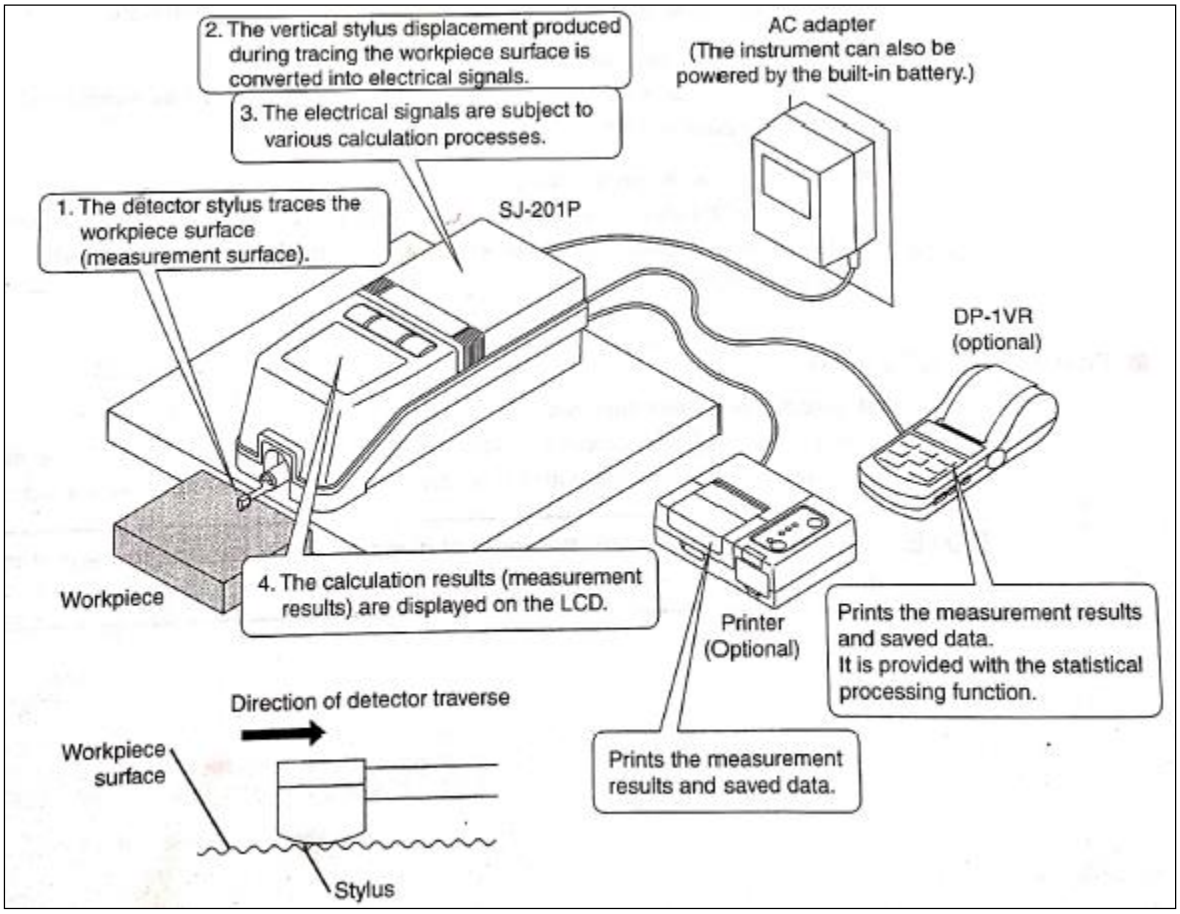

Fig- 2.8 Standard SJ-201P configurations

Measurement units: Metric/ inch preset by DIP-switch, deselect by menu.
Parameters: Ra, Rq, Rz (DIN), Ry and Sm.
Calculation time: 15 second for each double-stroke.

The detector stylus traces the work-piece surface (measurement surface). The vertical stylus displacement produced during tracing of the work-piece surface is converted into electrical signals. The electrical signals are subjected to various calculation processes. AC adapter can also be powered by the built-in battery. Printer prints the measurement results and saved data. DP-1VR prints the measurement results and saved the data. It is provided with the statistical processing function.

All the parameters Ra, Rq, Rz (DIN) and Sm have been noted during the measurement. However, in the present work only Ra value is taken into consideration for analysis and modeling.

(h) **OLYMPUS MICROSCOPE**:
Pictorial view of the microscope is presented in Fig- 2.9.
The delamination factor has been measured by using Olympus microscope. The specification of the microscope is given below:

Model name: OLYMPUS – BX53M
Serial No- 8M43096
Made in – T8, Tokyo, Japan.
Range – 5X to 100X.
Lens name- M Plan FL N- 5X/ 0.25BDP

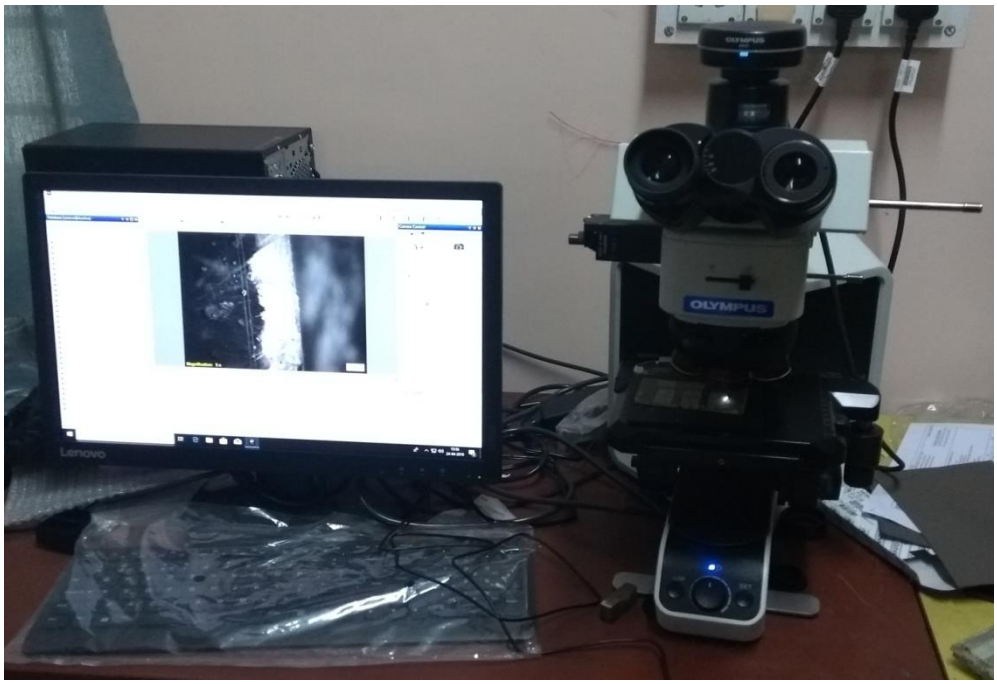

Fig- 2.9 Olympus microscope (BX53M)

2.4WORK PIRCE MATERIAL:

In the present work the GRFP composite with resin precipitate material has been considered as a work material. Hand lay-up technique is used for producing the composite. This is manufactured by VMT Glass Fiber Roofing Industries, India. The specification of the material is given below:
Volume fraction of the fiber glass: 0.33
Specific gravity: 1.6
GFRP Sample size: 90 mm × 50 mm
Tensile strength of the GFRP composite: 180 N/mm^2
Cross breaking strength: 200 N/mm^2
Compression strength of the GFRP composite: 200 N/mm^2
Shear strength of the material: 50 N/mm^2
Electrical strength (at 90°C in oil)
i) Plate wise: 6 kV/mm^2
ii) Edge wise: 30 kV/mm^2
Insulation resistance: 500 MΩ
Water absorption: 0.24% in 24 hrs at 250°C
Impact strength, edgewise: 30 kg/m^2
The chopped strand mat E-glass fiber is used as reinforced in polyester resin to prepare the laminate. The composition of the laminate is:
Matrix: Polyester
Hardener: Methyl Ethyl Ketone Peroxide.
Reinforcing: E-glass, chopped strand mat (450 g/mm^2)

2.5 EXPERIMENTAL PROCEDURE

For the purpose of the experiment a plate of dimension 300 mm × 300 mm × 8mm has been used. This plate is cut into 9 pieces of dimension 90 mm × 50 mm × 8 mm each. In each plate on each face three experiments have been conducted. Since no research has been done on side and face milling of GFRP, the values of input parameters for the milling process have been fixed with the help of few trial runs. Total 54 experiments have been performed for to repetition of each experiment two (2) times, thus full factorial arrays have been prepared by averaging values of the two experiments with same conditions. A plate after milling operation is shown in Fig-2.10.

2.5.1 MEASUREMENT OF FORCES AND TORQUE

In milling, the cutting tool rotates in a fixed position and the worktable travels slowly at desired feed rates. Generally, sensors or transducers are mounted on the slow moving part. In milling, the work-piece is clamped on the dynamometer. Unlike in turning and drilling, in milling the cutting or loading point keeps on shifting with respect to the work-piece and dynamometer. In strain gauge type milling dynamometer, the top plate holding the work-piece is schematically

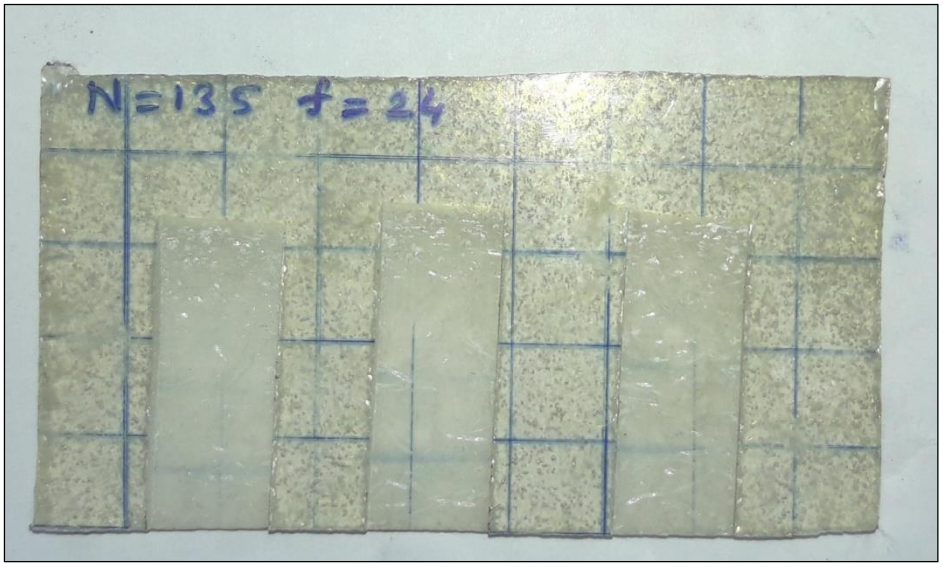

Fig- 2.10 Plate after milling operation

mounted on four identical O-rings or octagonal rings. The strain gauges mounted on each octagonal ring enable measurement of part of Fz and part of Fx or Fy. Altogether, sixteen gauges mounted on these four rings are used to measure the total force Fz. For measuring Fx and Fy, two separate sets of eight strain gauges are mounted on the diagonally opposite rings. However, three individual Wheatstone bridges are formed with the respective gauges for each Fz, Fx, and Fy mounted and use of such a milling dynamometer.

Piezoelectric type 2-D and 3-D milling dynamometers have also come up and are being used. Though costly, they are used for accurate, precise and reliable measurement of milling forces including their dynamic characteristics in plain milling, end milling and also face milling. In Fig-2.11 the measuring forces (F_x, Fy, Fz) and Torque (Mz) have been shown.

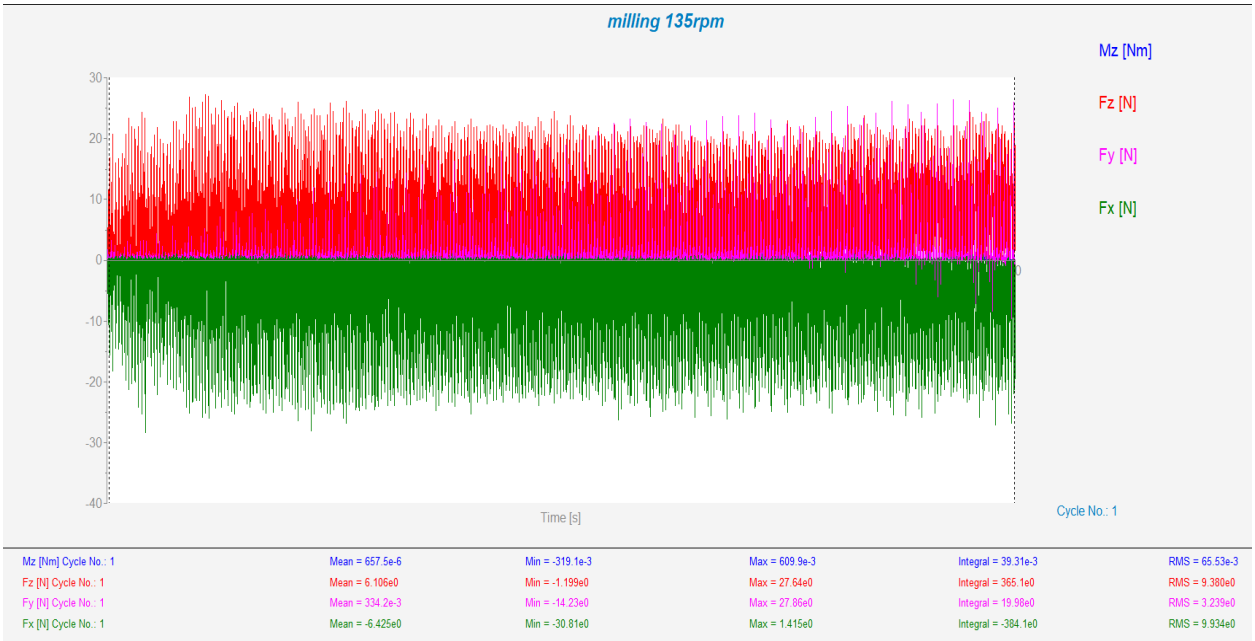

Fig- 2.11 Measurement of Forces and Torque

2.5.2 MEASUREMENT OF CUTTER VIBRATION

Vibration is sensed by the accelerometer mounted on the desired locations (i.e. the bearing housing near the cutter) of the conventional milling machine. The accelerometer converts the vibration into the electrical signal, which is then fed to the vibration meter and storage oscilloscope.

Idle run vibrations of the milling machine have been observed first. For this purpose, the milling machine has been made to rotate at constant speed with the work-piece idle and vibration signals have been read out from the vibration meter in terms of acceleration of vibration. Similarly readings have been taken when the cutter is removing materials from the work-piece. Vibration is measured only in vertical direction of the cutter at the bearing housing of the milling machine. Vibration signals corresponding to the experiments have been noted through the vibration meter in terms of ms^{-2}. The observations are taken in acceleration mode because of low frequency response and low sensitivity of the displacement and velocity mode.

The results of all the sets of experiments have been presented in the tables and analyzed by RSM to predict vibration for different combinations of input parameters. In Fig- 2.12 the measurement of milling cutter vibration is shown.

2.5.3 MEASUREMENT OF SURFACE ROUGHNESS

After milling, surface roughness has been measured for all the 54 slots by using Surftest which has been mentioned earlier. Measurements of surface roughness parameters, namely the average surface roughness value (Ra) is made over the milling surface using SJ-201P Surftest. The surface finish of the work material has been measured with 10 mm sampling length. The average value of surface roughness parameter Ra for each experiment has been obtained directly from the surface profile software integrated with the machine. For each test five (5) measurements are made and average is taken as the process response. The photographic view of Surftest is shown in Fig- 2.7

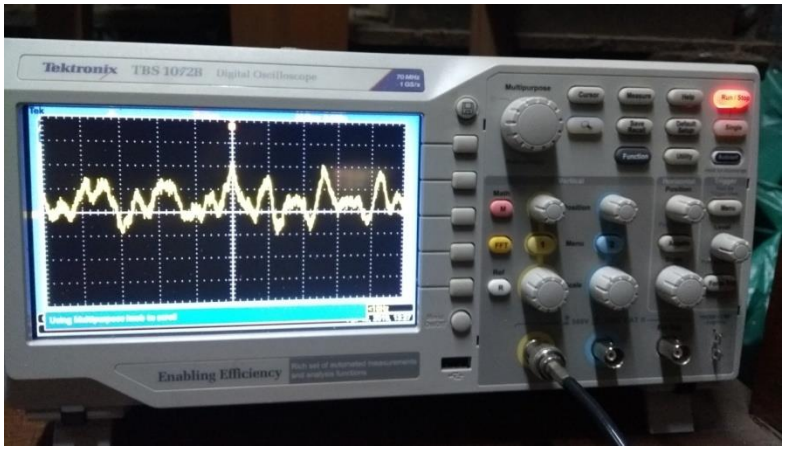

Fig- 2.12 Measurement of Milling cutter vibration

2.5.4 MEASUREMENT OF DELAMINATION FACTOR

In Fig- 2.14 the delamination of the composite material under microscope has shown. The damage around the slot has been measured with Olympus microscope with 5X magnification. For each test three (3) measurements are made and the average of three values of Delamination factor (Fd) is taken as the process response. The damage caused on the GFRP composite material is measured perpendicular to the feed rate. The composite material is positioned and fixed on the XY stage glass of the microscope by initial observation, the positions for maximum width of the damaged zone (Wmax) has been noted. Then by moving the XY stage glass by turning the micrometer head with a digital counter, the cross hair is aligned with the outside of the damaged zone. The difference reading of the micrometer gives the value of W_{max}. After measuring the maximum width of damage suffered by the material, the damage, normally assigned by Delamination factor (Fd) is determined. The delamination factor is the ratio between maximum width of the damaged zone and width of the cutter i.e. Fd = $\frac{W_{max}}{W}$ (Fig- 2.13)

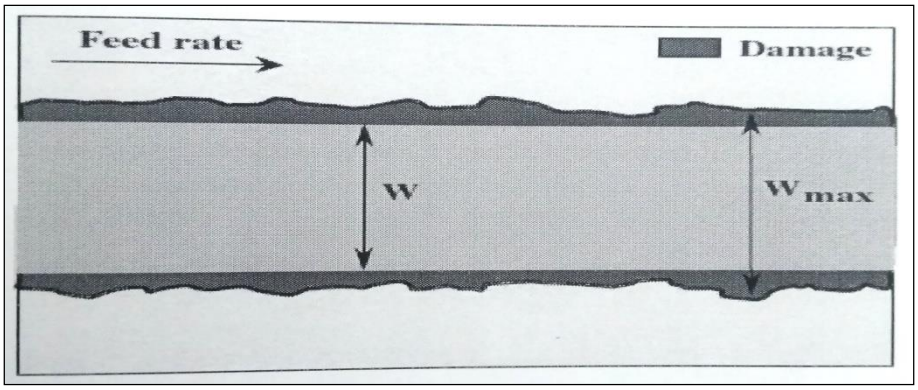

Fig- 2.13 Scheme of measurement of the delamination factor

Fig- 2.14 Delamination under microscope.

The results of the experiments, their discussion and analyses are given in the next chapter (i.e. Chapter- 3).

3. RESULTS, ANALYSIS AND MATHEMETICAL MODELLING

In the previous chapter details of experimental plan, set up and procedure have been discussed. In this chapter results are presented, discussed and analyzed. Analysis has been done for single objective and multi-objective optimization of side and face milling of glass fiber reinforced polymers. Also, the observed data have been analyzed using mathematical modeling, optimization and response surface plots.

3.1 RESULTS OF VARIOUS FORCES

Table - 3.1 Force parallel to cutter axis (F_X)

Exp. no.	N (rpm)	f (mm/min)	d (mm)	F_x max (N)	F_x min (N)	F_x mean (N)	Repetition (N)
1	135	10	1.0	2.237	-65.440	-5.018	-5.043
2	135	10	1.5	3.874	-122.900	-10.470	-10.520
3	135	10	2.0	1.380	-182.400	-7.646	-7.684
4	135	15	1.0	2.858	-68.660	-13.260	-13.320
5	135	15	1.5	12.760	-166.100	-6.509	-6.541
6	135	15	2.0	3.296	-246.400	-22.300	-22.410
7	135	24	1.0	4.501	-4.501	-4.501	-4.523
8	135	24	1.5	15.38	-70.830	-10.630	-10.680
9	135	24	2.0	3.082	-100.900	-26.720	-26.850
10	190	10	1.0	7.852	-18.290	-48.580	-48.820
11	190	10	1.5	1.899	-57.100	-8.635	-8.678
12	190	10	2.0	0.778	-16.900	-23.200	-23.316
13	190	15	1.0	3.860	-60.810	-9.410	-9.457
14	190	15	1.5	11.450	-98.980	-3.582	-3.599
15	190	15	2.0	9.157	-66.730	-7.095	-7.130
16	190	24	1.0	17.450	-44.810	4.140	4.160
17	190	24	1.5	19.880	-92.680	-0.125	-0.127
18	190	24	2.0	3.697	-116.600	-16.640	-16.720
19	270	10	1.0	2.816	-27.340	-4.445	-4.467
20	270	10	1.5	1.415	-30.810	-6.425	-6.457
21	270	10	2.0	5.773	-49.390	-4.483	-4.505
22	270	15	1.0	7.330	-39.630	-2.168	-2.178
23	270	15	1.5	2.339	-35.560	-8.590	-8.632
24	270	15	2.0	8.235	-32.840	-3.005	-3.020
25	270	24	1.0	3.590	-46.380	-7.533	-7.570
26	270	24	1.5	6.755	-143.300	-8.146	-8.186
27	270	24	2.0	7.265	-49.500	-8.054	-8.094

The measured values of F_x is shown in Table- 3.1. From the results of F_x, it is found that the F_x varies from 4.14 N to -48.58 N. The maximum value of F_x is 4.14 N at the speed of 190 rpm, feed of 10 mm/min and depth of cut 1 mm respectively. The minimum value of F_x is -48.58 N with respect to speed of 190 rpm, feed of 24 mm/min and depth of cut 1 mm. In the second experiment, from the results of F_x, it is observed that the F_x varies from 4.16 N to –48.82 N. The maximum value of F_x is 4.16 N for speed= 190 rpm, feed= 10 mm/min and depth of cut= 1 mm respectively. The minimum value of F_x is -48.82 N with respect to speed of 190 rpm, feed of 24 mm/min and depth of cut 1 mm. This force is responsible for delamination of the composite and has also affected the surface roughness of the machined area. The maximum difference in result between two sets of experiment is 3.96% (<5%). Thus, both the experiments are validated.

Table - 3.2 Force in the feed direction (F_y)

Exp. no.	N (rpm)	f (mm/min)	d (mm)	F_y max (N)	$F_y$min (N)	F_y mean (N)	Repetition (N)
1	135	10	1.0	20.69	-16.46	-0.212	-0.213
2	135	10	1.5	29.65	-33.14	-0.418	-0.419
3	135	10	2.0	31.04	-34.51	-0.262	-0.263
4	135	15	1.0	27.24	-23.25	-0.312	-0.313
5	135	15	1.5	31.49	-36.84	-1.858	-1.864
6	135	15	2.0	39.75	-45.62	-1.301	-1.300
7	135	24	1.0	33.74	-32.81	-1.153	-1.156
8	135	24	1.5	43.43	-39.93	-0.184	-0.185
9	135	24	2.0	40.53	-55.29	-1.910	-1.916
10	190	10	1.0	22.98	-11.96	-0.112	-0.113
11	190	10	1.5	35.08	-26.65	-0.192	-0.193
12	190	10	2.0	0.034	-29.43	-7.849	-7.873
13	190	15	1.0	18.84	-22.12	-0.126	-0.126
14	190	15	1.5	23.20	-23.54	-0.403	-0.404
15	190	15	2.0	25.41	-26.42	-0.902	-0.904
16	190	24	1.0	18.88	-18.25	-0.788	-0.790
17	190	24	1.5	29.04	-28.17	-0.988	-0.991
18	190	24	2.0	37.28	-35.23	-0.278	-0.279
19	270	10	1.0	10.29	-11.15	-0.380	-0.381
20	270	10	1.5	27.86	-14.23	-0.334	-0.335
21	270	10	2.0	30.00	-25.58	0.168	0.161
22	270	15	1.0	13.50	-12.60	-0.796	-0.798
23	270	15	1.5	12.59	-16.08	-0.563	-0.564
24	270	15	2.0	18.83	-16.11	0.211	0.210
25	270	24	1.0	14.95	-13.33	-0.233	-0.234
26	270	24	1.5	21.99	-20.80	-0.192	-0.191
27	270	24	2.0	20.84	-31.02	-0.665	-0.667

Table - 3.2 shows the results of F_y. From Table 3.2, it is found that, the F_y varies from 0.112 N to 7.849 N. The maximum value has been obtained for the speed of 190 rpm, feed of 10 mm/min and depth of cut 2 mm respectively. While minimum value is at the speed of 190 rpm, feed of 24 mm/min and depth of cut 1 mm. In the second Experiment from the results of F_y measurement, it has been seen that the F_y varies from 0.113 N to 7.873 N. The maximum value of F_y is 7.873 N has been obtained for the parametric setting of the speed= 190 rpm, feed= 10 mm/min and depth of cut= 2 mm respectively. In the same way, the minimum value of F_y is 0.113 N has been obtained for the speed= 190 rpm, feed= 24 mm/min and depth of cut= 1mm. This force (F_y) plays important role for obtaining delamination and surface finish of GFRP. The maximum difference in results between two set of experiments is 4.02%. Hence, both the experiments are validated.

Table - 3.3 Force perpendicular to the cutter axis (F_z)

Exp. no.	N (rpm)	f (mm/min)	d (mm)	F_z max (N)	F_z min (N)	F_z mean (N)	Repetition (N)
1	135	10	1.0	94.26	-3.475	8.540	8.530
2	135	10	1.5	58.88	-2.114	12.070	12.110
3	135	10	2.0	37.37	-9.199	8.914	8.914
4	135	15	1.0	85.92	-3.866	18.270	18.340
5	135	15	1.5	51.05	-13.700	8.658	8.660
6	135	15	2.0	52.93	-28.700	16.620	16.710
7	135	24	1.0	78.05	-28.200	-0.184	-0.175
8	135	24	1.5	90.63	-17.990	12.000	12.900
9	135	24	2.0	12.80	-4.373	25.790	25.840
10	190	10	1.0	67.90	-10.920	-0.210	-0.180
11	190	10	1.5	58.18	-2.572	8.336	8.339
12	190	10	2.0	62.55	-1.051	20.930	21.100
13	190	15	1.0	70.28	-4.277	11.360	11.400
14	190	15	1.5	34.74	-11.850	2.483	2.534
15	190	15	2.0	37.13	-7.874	6.925	7.190
16	190	24	1.0	54.78	-21.300	-3.922	-3.764
17	190	24	1.5	36.25	-17.870	-0.831	0.902
18	190	24	2.0	48.72	-2.838	15.270	15.423
19	270	10	1.0	30.42	-3.261	5.284	5.298
20	270	10	1.5	27.64	-1.199	6.106	6.210
21	270	10	2.0	30.08	-4.634	3.175	3.240
22	270	15	1.0	52.36	-9.292	1.756	1.800
23	270	15	1.5	35.39	-2.084	9.514	9.645
24	270	15	2.0	25.68	-7.965	2.862	2.967
25	270	24	1.0	44.52	-4.368	8.576	8.325
26	270	24	1.5	35.26	-7.329	7.843	7.848
27	270	24	2.0	43.92	-6.797	6.263	6.109

The results of F_z have been presented in Table - 3.3. From the results of F_z, it can be concluded that, the value F_z varies from 0.184 N to 25.79 N. The maximum and minimum values have been obtained at the speed of 135 rpm, feed of 24 mm/min and depth of cut 2 mm; the speed of 135 rpm, feed of 24 mm/min and depth of cut 1 mm respectively. From the second Experiments, it is found that the F_z varies from 25.84 N to 0.175 N. The maximum and minimum values of F_z have been achieved for the parametric setting of the speed of 135 rpm, feed of 24 mm/min and depth of cut 2 mm; speed of 135 rpm, feed of 24 mm/min and depth of cut 1 mm respectively. This force is responsible for deteriorating surface roughness of the machined area. The maximum difference in results between two set of experiments is 2.93%. So, both the experiments have been validated.

3.2 MEASUREMENT OF TORQUE (M_z)

The recorded result from measuring instrument for M_z is shown in Table - 3.4.

Table - 3.4 Results of torque during milling

Exp. no.	N (rpm)	f (mm/min)	d (mm)	M_Z max (N-m)	M_Z min (N-m)	M_Z mean (N-mm)	Repetition (N-mm)
1	135	10	1.0	5.232	-0.267	-86.93	-87.19
2	135	10	1.5	0.613	-0.822	-55.88	-56.04
3	135	10	2.0	4.424	-0.167	172.10	172.61
4	135	15	1.0	0.264	-1.802	-342.10	-343.12
5	135	15	1.5	0.858	-0.936	-35.80	-35.90
6	135	15	2.0	5.803	-0.483	259.60	260.37
7	135	24	1.0	0.674	-1.655	-4.810	-4.82
8	135	24	1.5	0.744	-0.635	17.37	17.42
9	135	24	2.0	2.234	-0.495	624.40	626.27
10	190	10	1.0	0.445	-1.269	-18.66	-18.71
11	190	10	1.5	0.732	-0.656	-17.55	-17.60
12	190	10	2.0	0.891	-0.051	327.70	328.68
13	190	15	1.0	0.231	-1.707	-272.60	-273.41
14	190	15	1.5	0.576	-0.618	10.17	10.20
15	190	15	2.0	1.402	-0.483	135.40	135.80
16	190	24	1.0	0.688	-1.269	91.86	92.14
17	190	24	1.5	0.706	-0.711	-21.08	-21.14
18	190	24	2.0	2.728	-0.196	410.30	411.53
19	270	10	1.0	0.136	-0.713	-118.30	-118.66
20	270	10	1.5	0.609	-0.319	657.50	659.47
21	270	10	2.0	1.246	-0.117	109.50	109.83
22	270	15	1.0	0.187	-1.108	-62.56	-62.75
23	270	15	1.5	0.180	-0.384	-41.79	-41.92

24	270	15	2.0	0.646	-0.276	50.77	50.92
25	270	24	1.0	0.149	-1.277	-219.60	-220.26
26	270	24	1.5	0.470	-0.551	-33.36	-33.46
27	270	24	2.0	1.026	-0.153	151.20	151.65

From the results of M_z measurement, it has been observed that the M_z varies from 4.81 N-mm to 657.5 N-mm. The maximum value and minimum value of M_z is at the parametric setting of the speed= 270 rpm, feed= 10 mm/min and depth of cut= 1.5 mm; speed=135 rpm, feed= 24 mm/min and depth of cut= 1mm respectively. In the second experiment from the results of M_z measurement, recorded data shows that the M_z varies from 4.82 N-mm to 659.47 N-mm. The maximum value of M_z is 659.47 N-mm at the speed of 270 rpm, feed of 10 mm/min and depth of cut 1.5 mm respectively while the minimum value of M_z is 4.82 N-mm is at the speed of 135 rpm, feed of 24 mm/min and depth of cut 1mm. The torque represents directly the power consumption during machining. The maximum difference in results between two sets of experiments is 3.54%. So, both the experiments are validated.

3.3MEASUREMENT OF MILLING CUTTER VIBRATION

Table- 3.5 Results of milling cutter vibration (Acceleration f_a (m/s^2))

Exp. no.	N (rpm)	f (mm/min)	d (mm)	Peak f_a (m/s^2)	Avg. f_a (m/s^2)	Repetition (m/s^2)
1	135	10	1.0	28.0	24.0	24.2
2	135	10	1.5	35.0	31.0	32.6
3	135	10	2.0	32.0	29.0	28.8
4	135	15	1.0	46.0	45.0	44.0
5	135	15	1.5	41.0	39.0	38.0
6	135	15	2.0	39.0	38.0	37.0
7	135	24	1.0	42.0	37.0	35.0
8	135	24	1.5	40.0	38.0	34.7
9	135	24	2.0	38.0	37.4	36.2
10	190	10	1.0	32.0	31.0	30.8
11	190	10	1.5	35.0	33.4	32.0
12	190	10	2.0	31.0	28.6	29.0
13	190	15	1.0	28.0	26.4	25.8
14	190	15	1.5	29.8	26.3	27.0
15	190	15	2.0	28.0	26.6	28.1
16	190	24	1.0	37.2	33.6	34.0
17	190	24	1.5	24.0	22.4	22.4
18	190	24	2.0	30.0	28.4	28.6
19	270	10	1.0	45.0	42.0	41.8
20	270	10	1.5	43.0	42.8	43.0
21	270	10	2.0	36.0	33.0	34.0

22	270	15	1.0	25.0	22.8	23.0
23	270	15	1.5	27.0	23.8	24.1
24	270	15	2.0	25.0	23.8	24.0
25	270	24	1.0	38.7	37.0	38.0
26	270	24	1.5	26.5	21.2	21.3
27	270	24	2.0	27.2	23.8	24.2

The result obtained from the measurement of f_a has been shown in Table - 3.5. The measured data of f_a shows that the f_a varies from 22.4 m/s^2 to 45 m/s^2. The maximum value of f_a has been found at the speed of 135 rpm, feed of 15 mm/min and depth of cut 1 mm while the minimum value is at the speed of 190 rpm, feed of 24 mm/min and depth of cut 1.5 mm. In the second experiment of f_a measurement, it can be seen that the f_a varies from 22.4 m/s^2 to 44 m/s^2. The maximum value of f_a is 44 m/s^2 with parametric setting of the speed= 135 rpm, feed= 15 mm/min and depth of cut= 1 mm; and the minimum value of f_a is 22.4 m/s^2 with parametric setting of the speed= 190 rpm, feed= 24 mm/min and depth of cut= 1.5 mm. The torque represents directly the power consumption during machining. The maximum difference in result between two sets of experiments is 2.07%. So, both the experiments are validated.

3.4 MEASUREMENT OF SURFACE ROUGHNESS (Ra)

Table - 3.6 Results of surface roughness (R_a (μm))

Exp. no.	N (rpm)	f (mm/min)	d (mm)	Avg. R_a (μm)	Repetition (μm)
1	135	10	1.0	1.224	1.223
2	135	10	1.5	0.803	0.804
3	135	10	2.0	0.628	0.629
4	135	15	1.0	0.075	0.073
5	135	15	1.5	0.086	0.089
6	135	15	2.0	0.703	0.705
7	135	24	1.0	0.735	0.731
8	135	24	1.5	0.656	0.659
9	135	24	2.0	0.024	0.025
10	190	10	1.0	0.982	0.986
11	190	10	1.5	0.884	0.886
12	190	10	2.0	1.226	1.250
13	190	15	1.0	0.035	0.038
14	190	15	1.5	0.050	0.039
15	190	15	2.0	0.668	0.669
16	190	24	1.0	1.110	1.142
17	190	24	1.5	0.878	0.880
18	190	24	2.0	1.278	1.282
19	270	10	1.0	1.034	1.038

20	270	10	1.5	1.190	1.186
21	270	10	2.0	1.242	1.139
22	270	15	1.0	1.172	1.170
23	270	15	1.5	0.158	0.162
24	270	15	2.0	0.700	0.689
25	270	24	1.0	1.343	1.347
26	270	24	1.5	1.194	1.179
27	270	24	2.0	1.210	1.240

The recorded data of R_a has been presented in Table - 3.6. The recorded of R_a shows that the R_a varies from 0.024 μm to 1.343 μm. The maximum and minimum value of R_a has been observed at the speed of 190 rpm, feed of 24 mm/min and depth of cut 2 mm.; and at the speed of 135 rpm, feed of 24 mm/min and depth of cut 2 mm respectively. In the second experiment from the results of R_a measurement, it is found that the R_a varies from 0.025 μm to 1.347 μm. The maximum value of R_a is 1.347 μm has been obtained at the speed of 135 rpm, feed of 24 mm/min and depth of cut 2 mm respectively. The minimum value of R_a is 0.025 μm has been observed at the speed of 135 rpm, feed of 24 mm/min and depth of cut 2 mm. The maximum difference in results between two sets of experiments is 4.03%. So, both the experiments are validated.

3.5MEASUREMENT DELAMINATION FACTOR (F_d)

Table - 3.7 Results of Delamination factor (F_d)

Exp. no.	N (rpm)	f (mm/min)	d (mm)	Avg. F_d	Repetition
1	135	10	1.0	1.03675	1.038824
2	135	10	1.5	1.034362	1.036431
3	135	10	2.0	1.030283	1.032344
4	135	15	1.0	1.023022	1.025068
5	135	15	1.5	1.020072	1.022112
6	135	15	2.0	1.02545	1.027501
7	135	24	1.0	1.024102	1.02615
8	135	24	1.5	1.019057	1.021095
9	135	24	2.0	1.019003	1.021041
10	190	10	1.0	1.027162	1.029216
11	190	10	1.5	1.03194	1.034004
12	190	10	2.0	1.032745	1.03481
13	190	15	1.0	1.030493	1.032554
14	190	15	1.5	1.022548	1.024593
15	190	15	2.0	1.023837	1.025885
16	190	24	1.0	1.027053	1.029107
17	190	24	1.5	1.027393	1.029448

18	190	24	2.0	1.02288	1.024926
19	270	10	1.0	1.030868	1.03293
20	270	10	1.5	1.034410	1.036479
21	270	10	2.0	1.033873	1.035941
22	270	15	1.0	1.029052	1.03111
23	270	15	1.5	1.028893	1.030951
24	270	15	2.0	1.026958	1.029012
25	270	24	1.0	1.024013	1.026061
26	270	24	1.5	1.022982	1.025028
27	270	24	2.0	1.017558	1.019593

Table- 3.7 shows the value of F_d. From the results of F_d, it is found that F_d varies from 1.07558 to 1.03675. The maximum and minimum value for F_d have been obtained with respect to the speed of 135 rpm, feed of 10 mm/min and depth of cut 1 mm; the speed of 270 rpm, feed of 24 mm/min and depth of cut 2 mm respectively. From the second experiment, the values of F_d varies from 1.019593 to 1.038824. The maximum value of F_d is 1.038824 with respect to the speed of 135 rpm, feed of 10 mm/min and depth of cut 1 mm respectively. Whereas, the minimum value of F_d is 1.19593 with respect to speed of 270 rpm, feed of 24 mm/min and depth of cut 2 mm. The maximum difference in results between two sets of experiments is 4.56%. Thus, both the experiments have been validated.

As all the results of the first set of experiment is within 5% of the corresponding values of the second set of experiment, so only the data from the first set of experiment is considered for the further analyses (graphical and surface plots). Graphical plots and surface plots for experiment set no– 2 are given in the Appendix-B.

3.6 MAIN EFFECT PLOTS AND INTERACTION PLOTS

The main effect plots for the Torque are presented in Fig- 3.1 and Fig- 3.2. It can be concluded from the plots that the value of torque first decreases then increases with increasing value of the rotational speed. With increase in the value of the feed rate, the torque decreases but at the higher feed rate it increases at nearly the same rate at which it was decreasing. The most influencing factor on the torque is depth of cut. With increase in depth of cut, the torque decreases slightly but with higher depth of cut it increases abruptly. From the plots, optimal combination of input parameters for minimization of torque is obtained at low value of the mean of torque. Obtained optimal condition is: rotational speed = 190 rpm, feed rate = 15 mm/min and depth of cut = 1.5 mm.

EFFECT OF PROCESS PARAMETERS ON TORQUE (T)

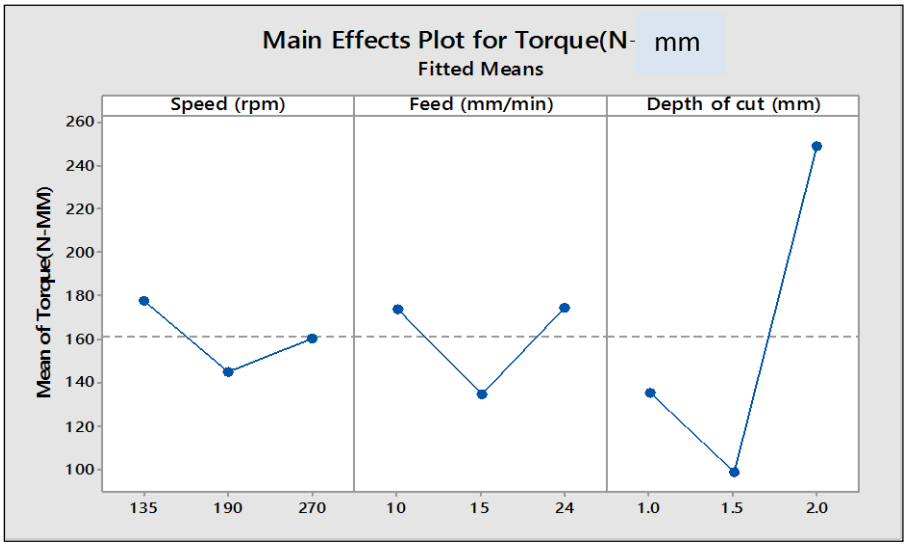

Fig- 3.1 Main effect plot for Torque

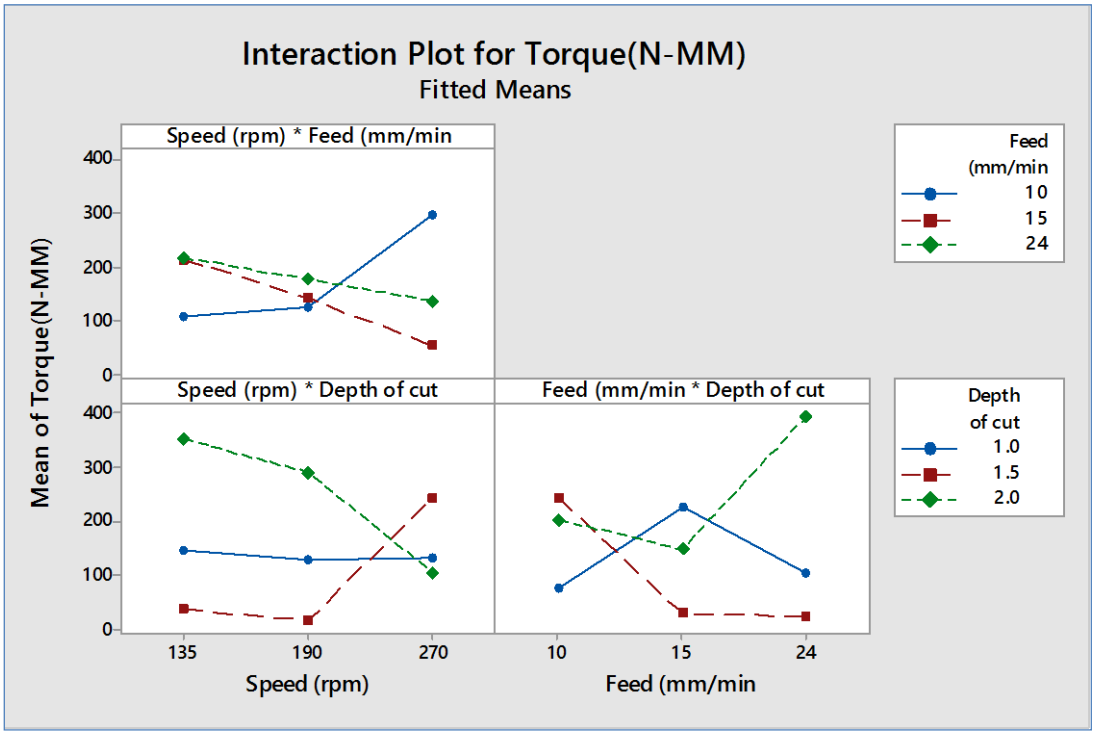

Fig- 3.2 Interaction plot for Torque

EFFECT OF PROCESS PARAMETERS ON CUTTER VIBRATION (f_a)

The effect of process parameters on the cutter vibration are depicted in Fig- 3.3 and Fig- 3.4. The most influencing factor on the cutter vibration is rotational speed of cutter. It is found from these plots that with increase in rotational speed initially the cutter vibration decreases abruptly but at higher speed it increases at lower rate. With increasing the feed rate the cutter vibration

decreases but at higher feed rate it increase at a much lower rate. With increase in depth of cut the Cutter vibration decreases but the rate of decrement slows down at higher depth of cut. From the plots, optimal combination of input parameters for minimization of Cutter vibration is obtained at low value of the responses. Obtained optimal condition is: rotational speed = 190 rpm, feed rate = 15 mm/min and depth of cut = 2 mm.

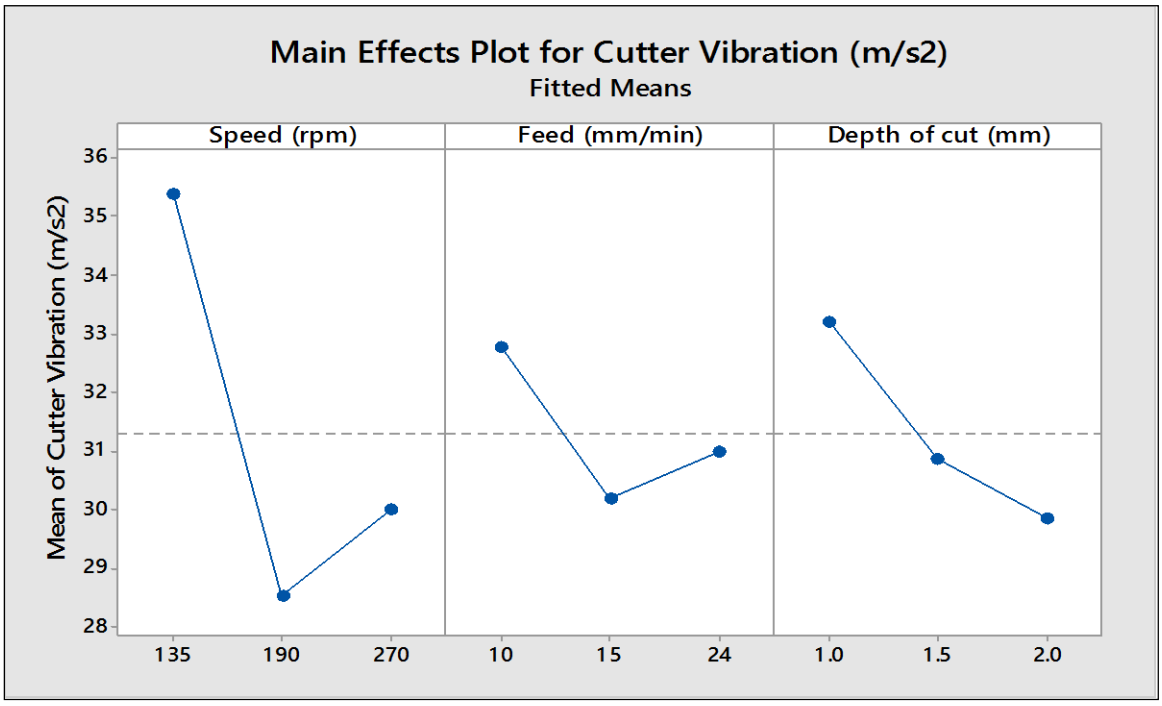

Fig- 3.3 Main effect plots for milling cutter vibration

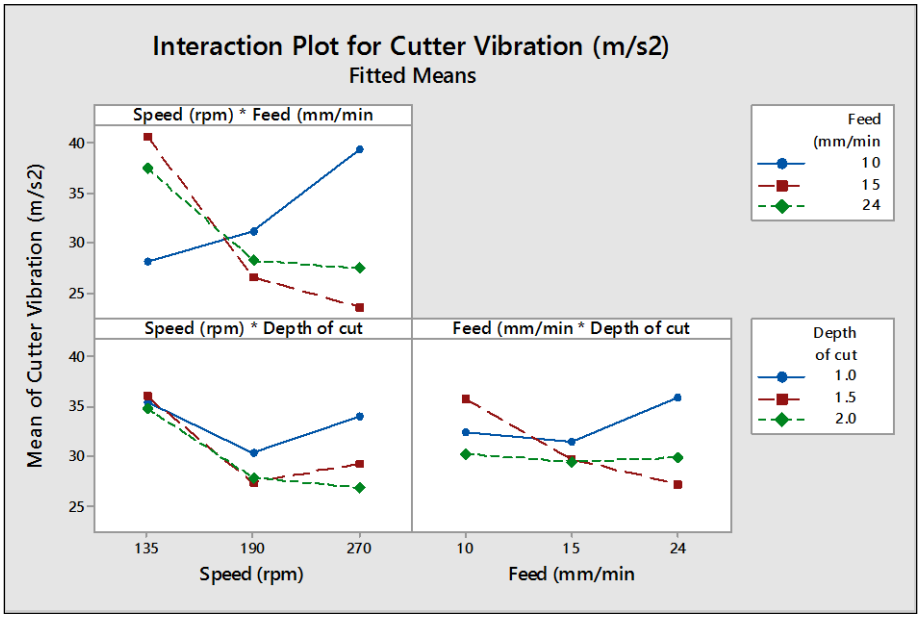

Fig- 3.4 Interaction plots for milling cutter vibration

EFFECTS OF PROCESS PARAMETERS ON SURFACE ROUGHNESS (Ra)

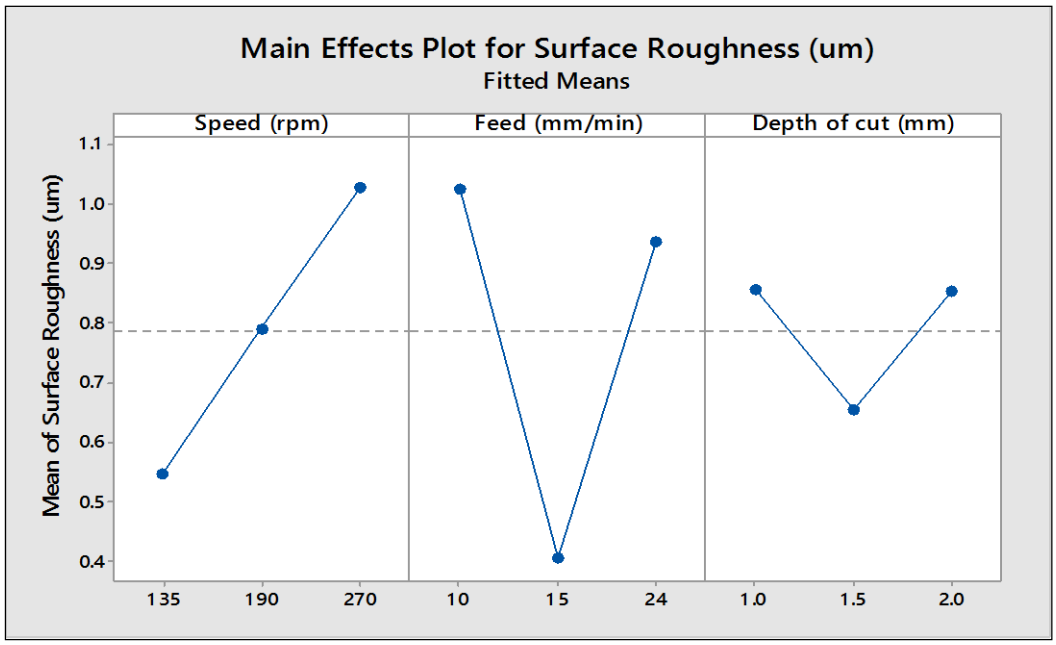

Fig- 3.5 Main effect plots for Surface Roughness

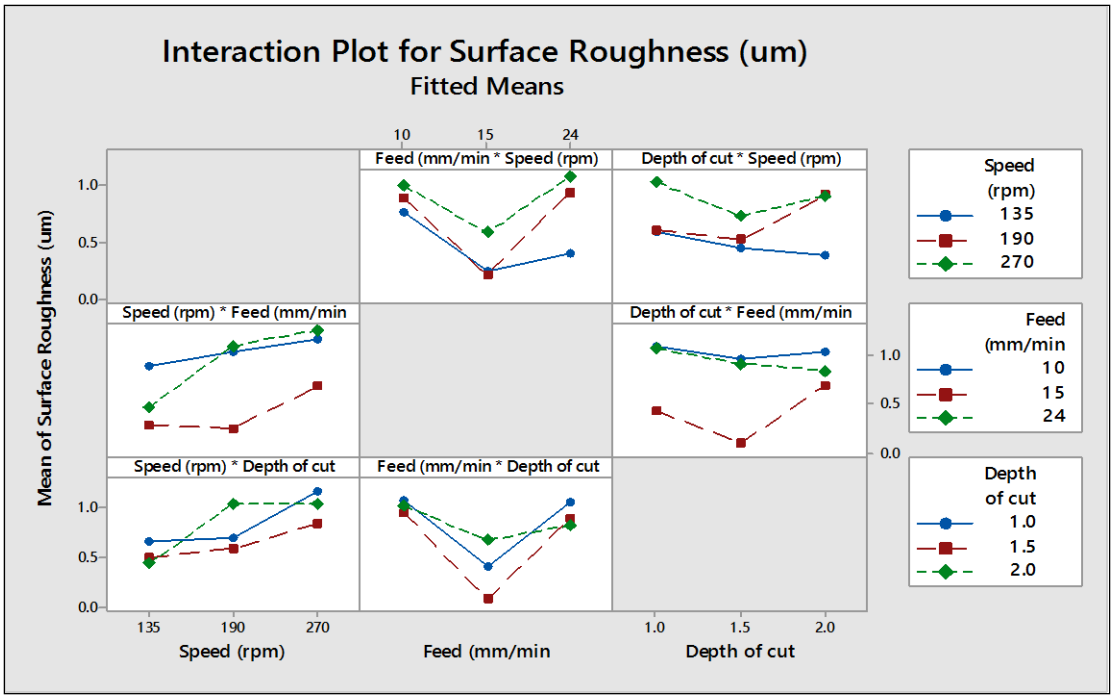

Fig- 3.6 Interaction Plot for Surface Roughness

The effect of process parameters on the surface roughness are depicted in Fig- 3.5 and Fig- 3.6. It is found from these plots that, with increase in rotational speed the surface roughness increases. The most influencing factor on the surface roughness is feed rate. With increasing the feed rate the surface roughness decreases abruptly and at higher feed rate it increase. With increase in depth of cut the surface roughness decreases but it increases at higher depth of cut. From the plots, optimal combination of input parameters for minimization of surface roughness is obtained at low value of the responses. Obtained optimal condition is: rotational speed = 135 rpm, feed rate = 15 mm/min and depth of cut = 1.5 mm.

EFFECTS OF PROCESS PARAMETERS ON DELAMINATION FACTOR (F_d)

The effect of process parameters on the Delamination Factor are shown in Fig- 3.7 and Fig- 3.8. It is found from these plots that, with increase in rotational speed the surface roughness increases continuously but at higher speed the increment of delemination factor is negligible. The most influencing factor on the delamination factor is feed rate. With increasing the feed rate and depth of cut the delamination factor decreases continuously. Obtained optimal condition is: rotational speed = 135 rpm, feed rate = 24 mm/min and depth of cut = 2 mm.

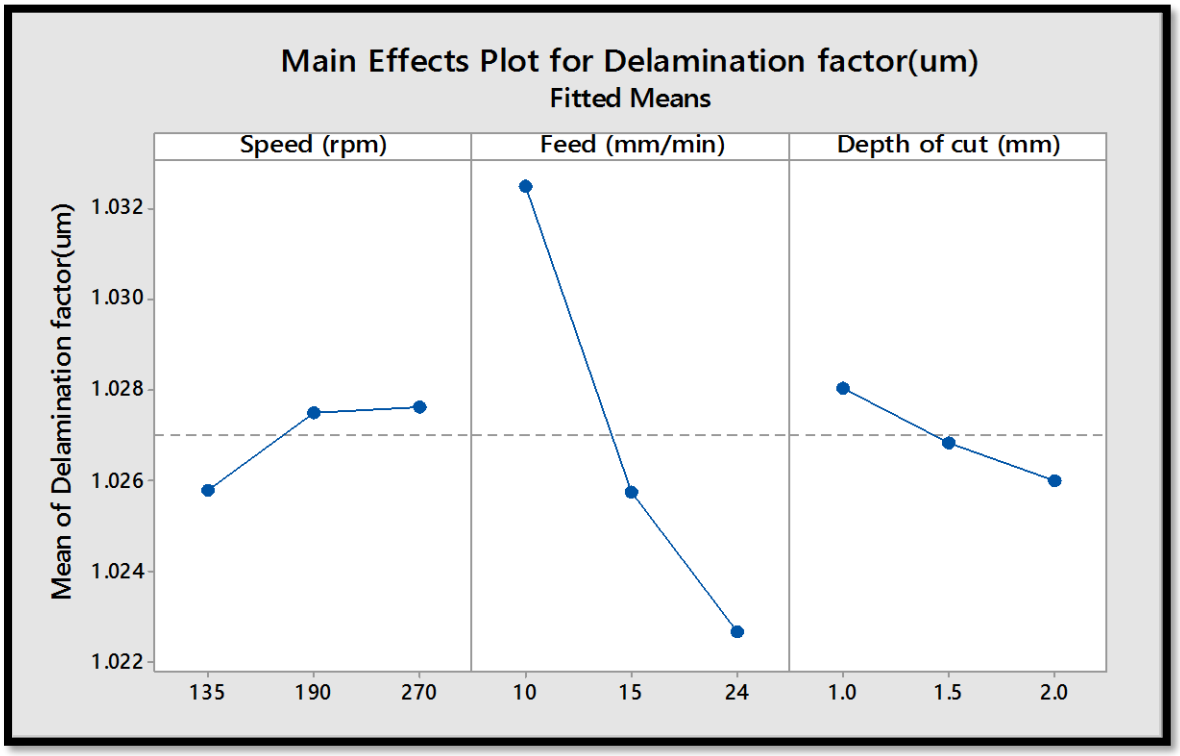

Fig- 3.7 Main effect plots for Delamination Factor

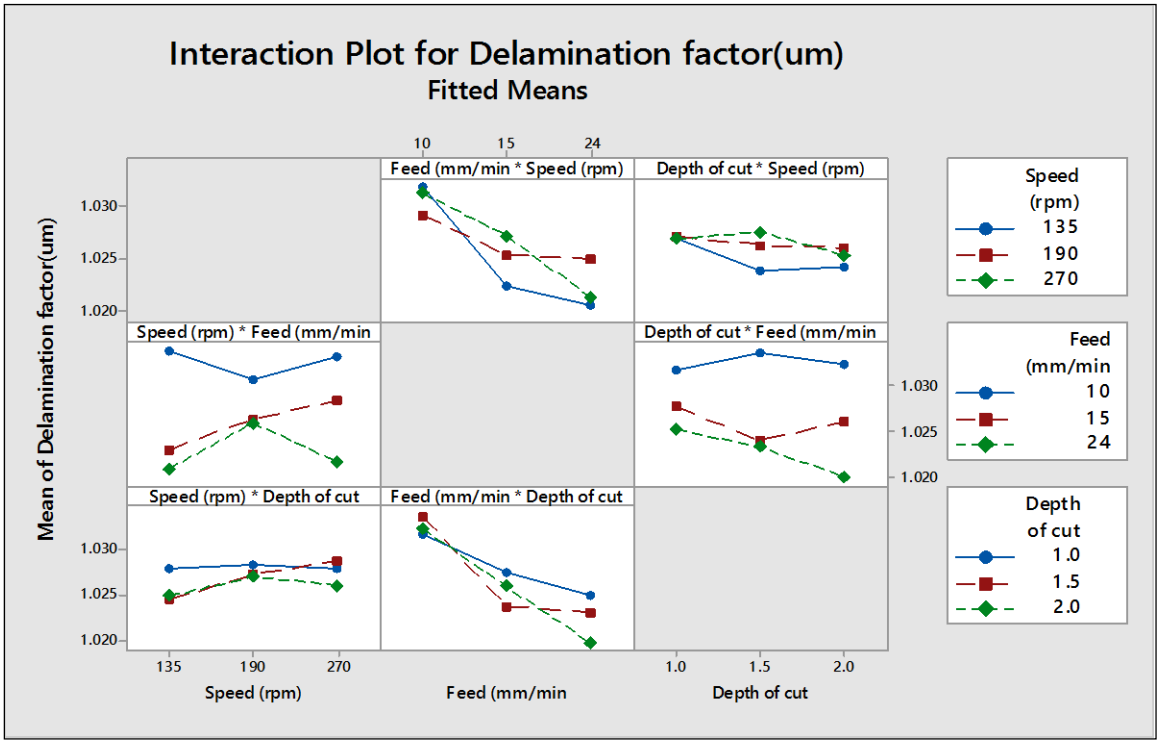

Fig- 3.8 Interaction Plot for Delamination factor

As the same curve is repeating during the repetition of experiment, so, we are taking the curves for the first experiments only.

3.7 MATHEMATICAL MODELING AND RESPONSE SURFACE PLOTS

In order to investigate the influence of process parameters on Torque, Cutter vibration, Surface roughness and Delamination factor, RSM based analysis is made and mathematical modeling is, thus, developed. The process (i.e. input) parameters are rotational speed (N), feed rate (f) and depth of cut (d). The responses are torque (T), milling cutter vibration (f_a), surface roughness (Ra) and Delamination factor (F_d). The model chosen linear with interaction which can be expressed as:

$$Y = \beta_0 + \sum_j^k X_j\beta_j + \sum_i \sum_{<j=2}^k \beta_{ij}X_iX_j + e_i \qquad (3.1)$$

Where, Y is response, Xi and Xj the independent factors, β0 the constant coefficient. Bj and βij the coefficient for linear and interaction effect and e_i is the error. Based on the observed data of Torque, Milling cutter vibration, Surface roughness and Delamination factor, given in Table (3.1, 3.2, 3.3 and 3.4) the values of different constants (i.e. all beta values) of Eqs. (3.2, 3.3, 3.4 and 3.5) are obtained for Torque (M_z), Milling cutter vibration (f_a), Surface roughness (Ra) and Delamination Factor (F_d) for experiment no – 1 and Eqs. (3.6, 3.7, 3.8 and 3.9) for experiment no - 2. The mathematical relationship for correlating the torque, cutter vibration, surface roughness and delamination factor with the selected process parameters has been established.

$M_z = 161.1 + 16.60\ N + 12.72\ f – 25.8\ d – 85.42\ N*f – 7.251\ N*d – 73.36\ f*d + 88.37\ N*f*d$ (3.2)

$f_a = 31.31 + 4.069\ N + 1.447\ f + 1.891\ d – 8.825\ N*f – 1.936\ N*d + 3.405\ f*d – 1.642\ N*f*d$ (3.3)

$R_a = 0.7885 – 0.2403\ N + 0.2352\ f + 0.0683\ d + 0.1016\ N*f + 0.06148\ N*d – 0.01196\ f*d + 0.2212\ N*f*d$ (3.4)

$F_d = 1.027 – 0.001188\ N + 0.005511\ f + 0.005511\ d + 0.0025\ N*f + 0.10001088\ N*d – 0.001975\ f*d + 0.002758\ N*f*d$ (3.5)

$M_z = 160.1 + 16.70\ N + 12.92\ f – 35.8\ d – 75.42\ N*f – 7.351\ N*d – 75.36\ f*d + 89.37\ N*f*d$ (3.6)

$f_a = 32.31 + 8.069\ N + 2.447\ f + 2.891\ d – 7.825\ N*f – 0.936\ N*d + 4.405\ f*d – 1.842\ N*f*d$ (3.7)

$R_a = 0.7985 – 0.2503\ N + 0.2342\ f + 0.0783\ d + 0.0016\ N*f + 0.06148\ N*d – 0.03196\ f*d + 0.2312\ N*f*d$ (3.8)

$F_d = 1.025 – 0.001888\ N + 0.006511\ f + 0.002511\ d + 0.0015\ N*f + 0.10009088\ N*d – 0.002075\ f*d + 0.001958\ N*f*d$ (3.9)

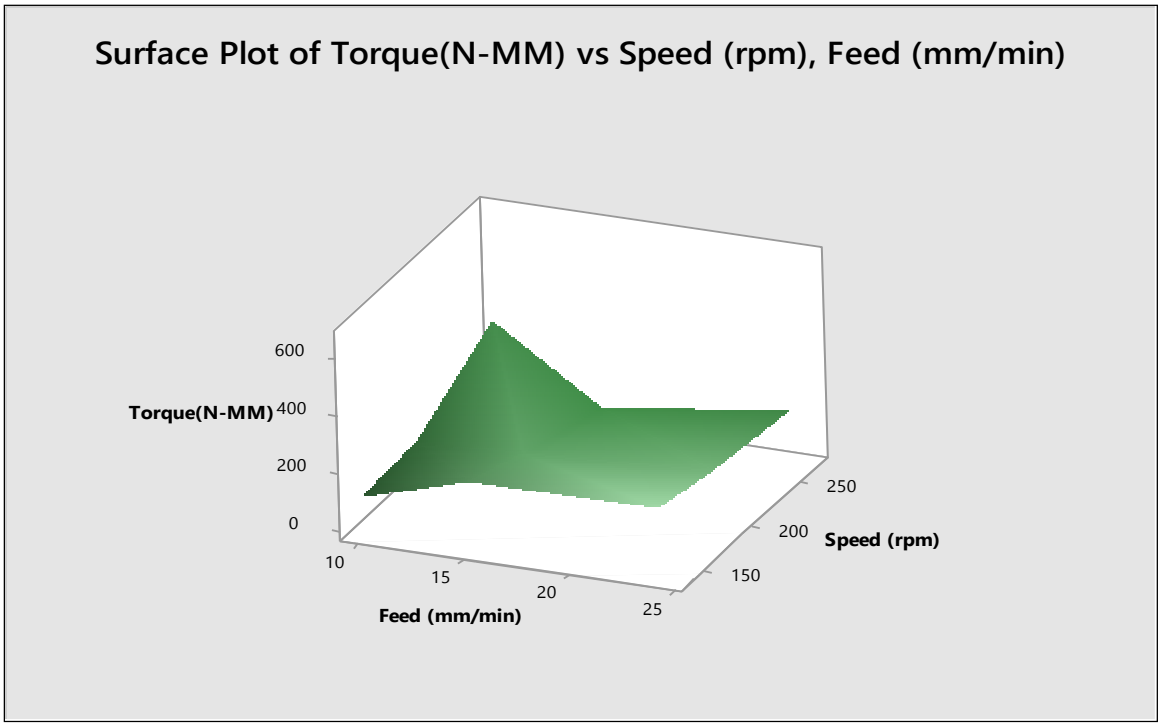

Fig- 3.9 Response surface showing combined effect of rotational speed and feed rate on Torque

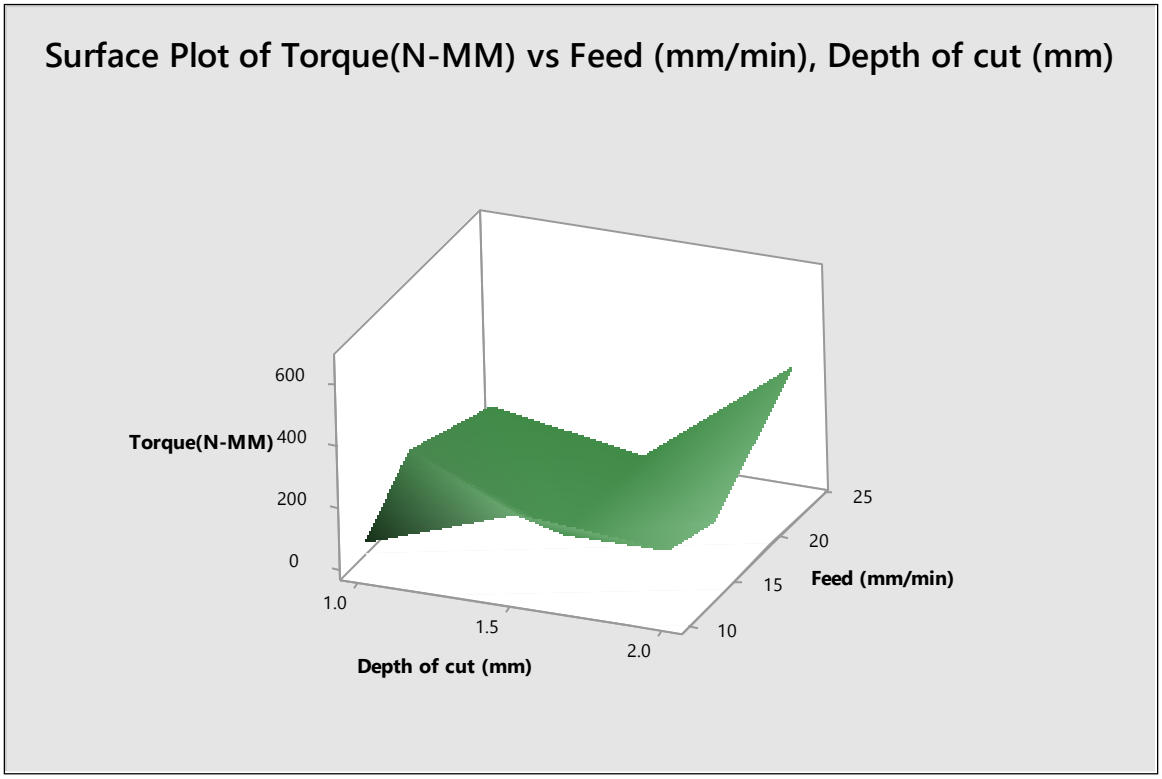

Fig– 3.10 Response surface showing combined effect of feed rate and depth of cut on Torque

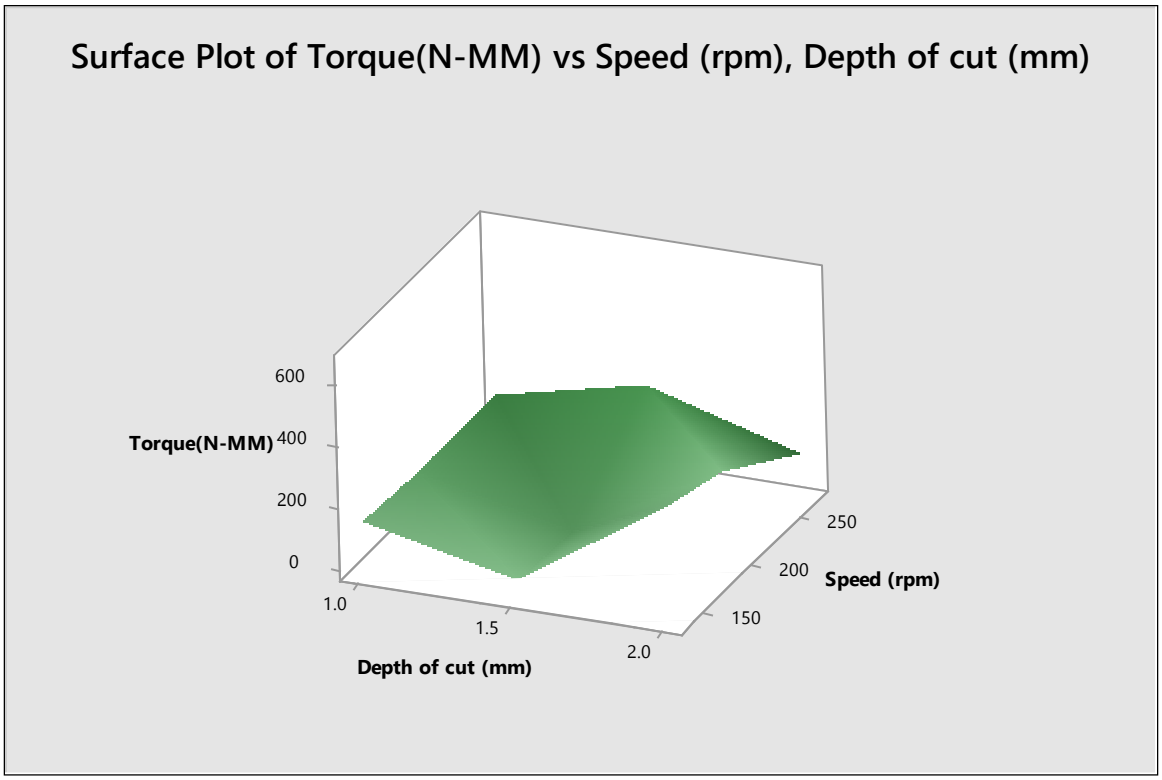

Fig- 3.11 Response surface showing combined effect of speed and depth of cut on Torque

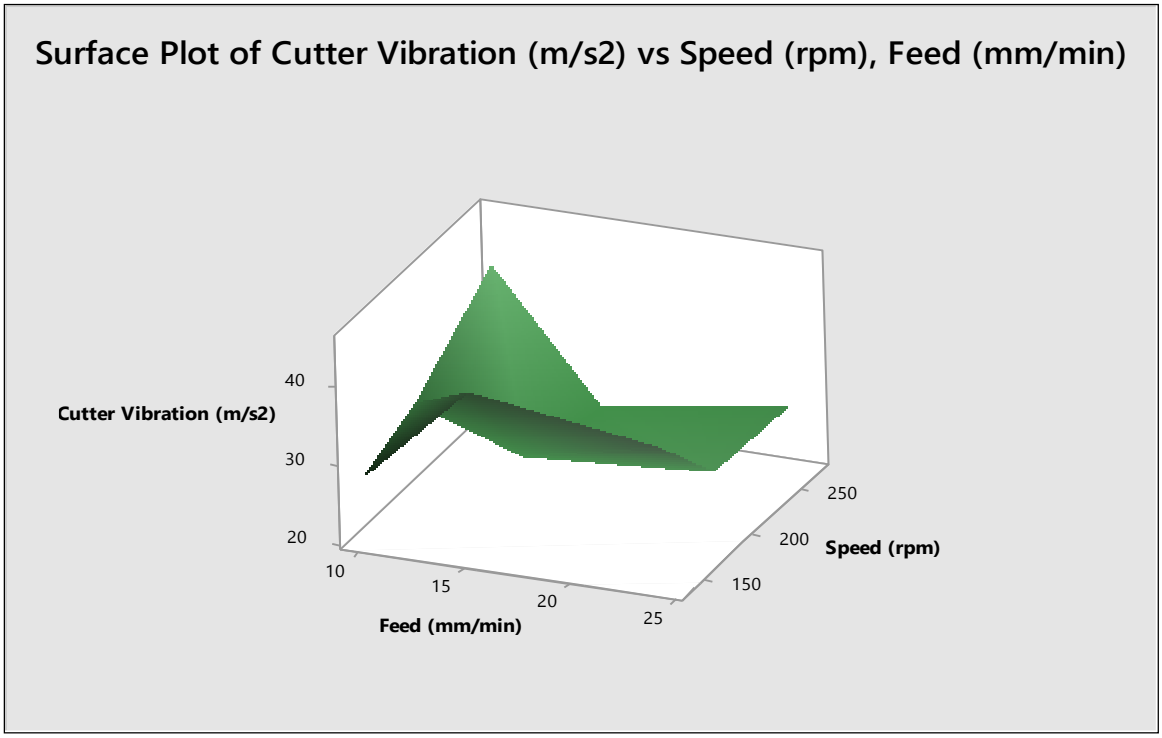

Fig– 3.12 Response surface showing combined effect of rotational speed and feed rate on milling cutter vibration

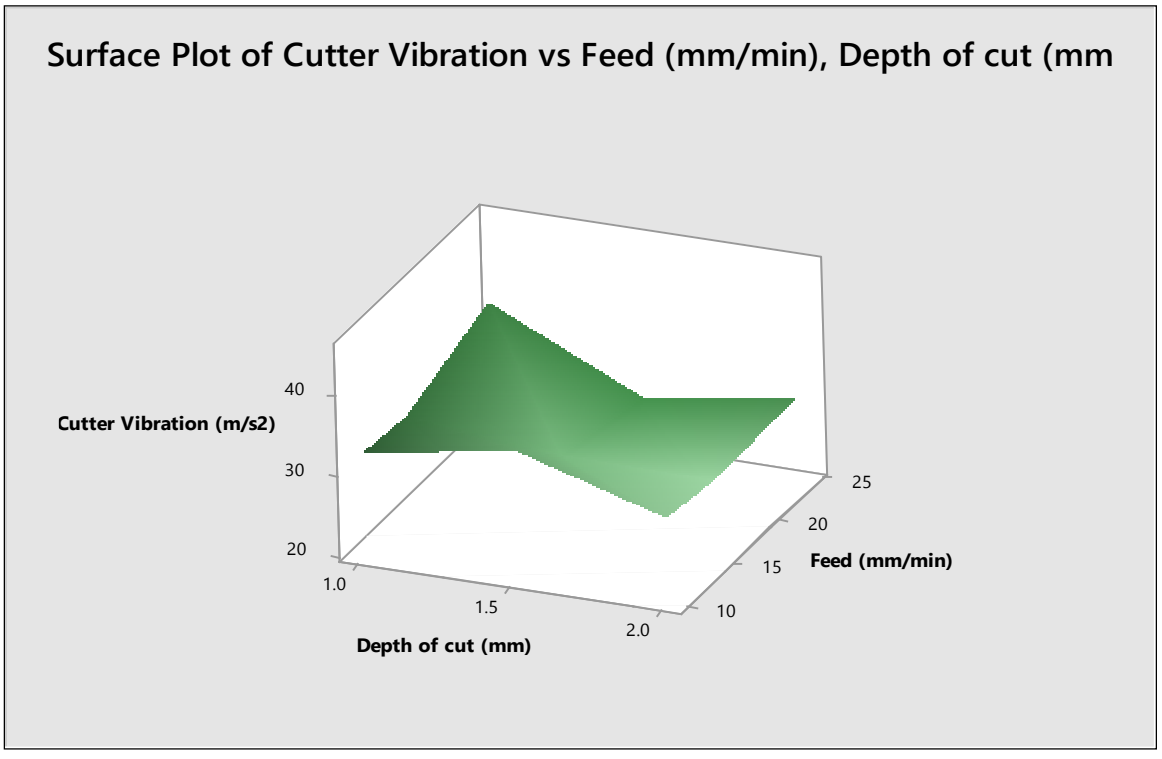

Fig – 3.13 Response surface showing combined effect of Depth of cut and feed rate on milling cutter vibration

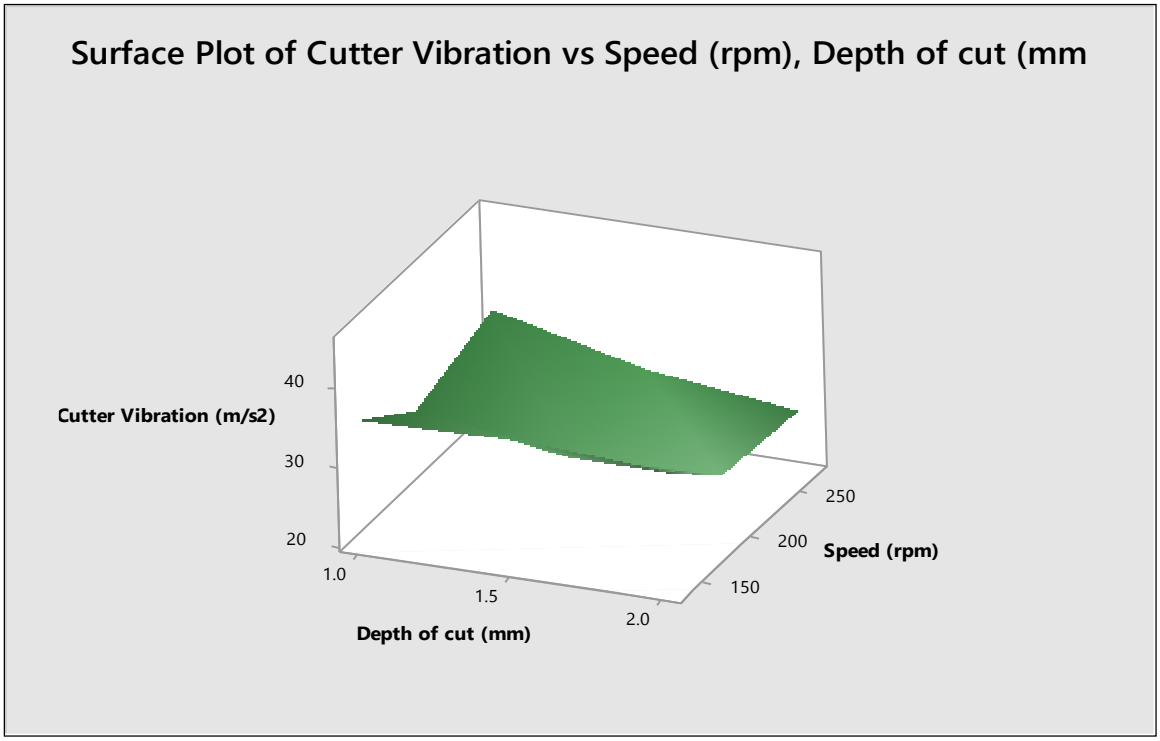

Fig – 3.14 Response surface showing combined effect of rotational speed and Depth of cut on milling cutter vibration

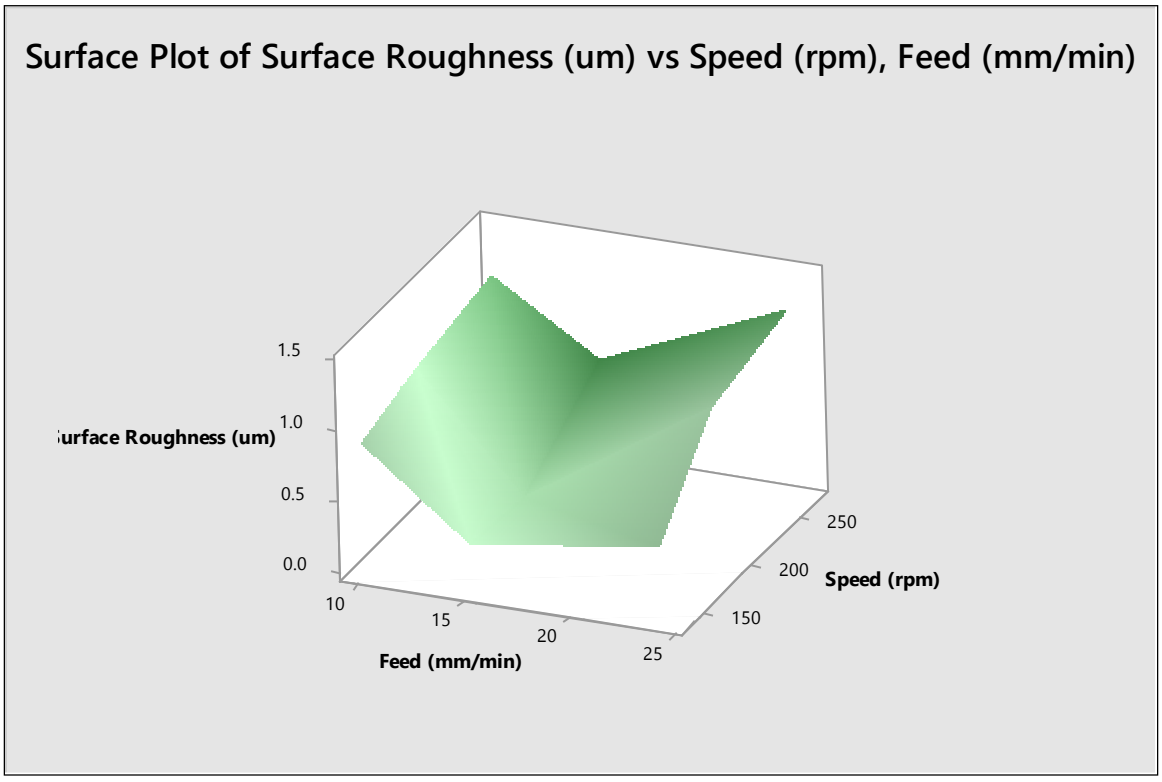

Fig – 3.15 Response surface showing combined effect of rotational speed and feed rate on Surface Roughness

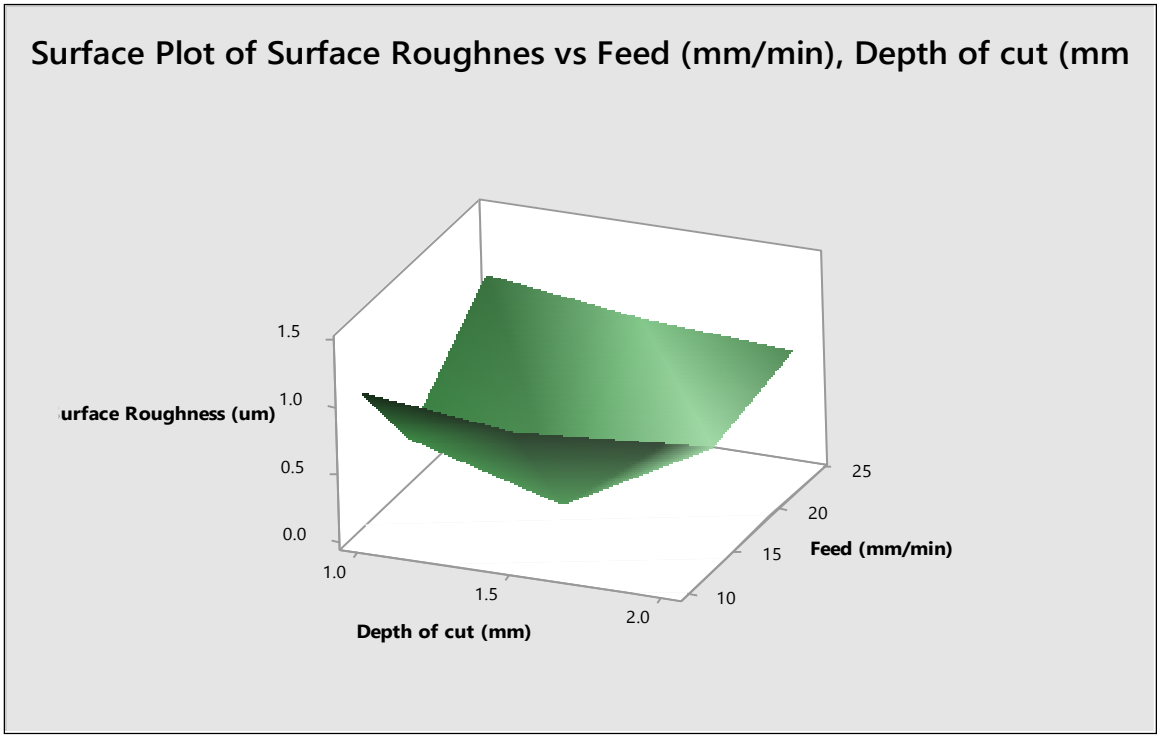

Fig – 3.16 Response surface showing combined effect of Depth of cut and feed rate on Surface Roughness

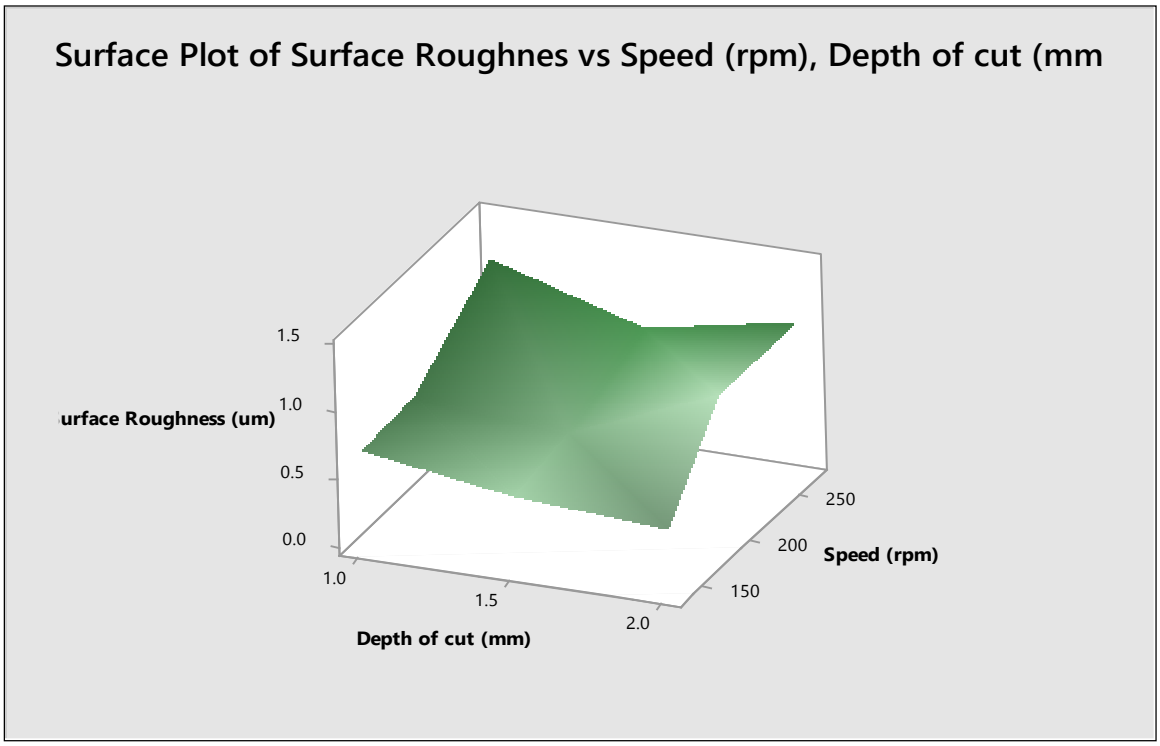

Fig – 3.17 Response surface showing combined effect of rotational speed and depth of cut on Surface Roughness

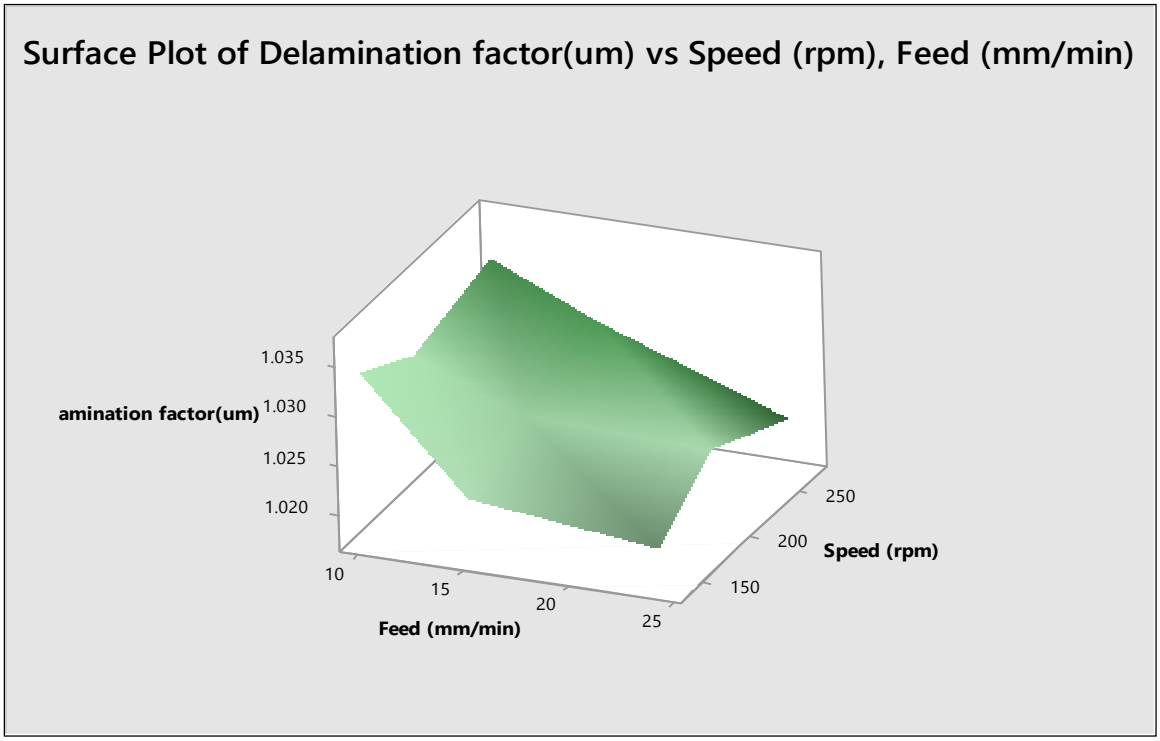

Fig – 3.18 Response surface showing combined effect of rotational speed and feed rate on Delamination Factor

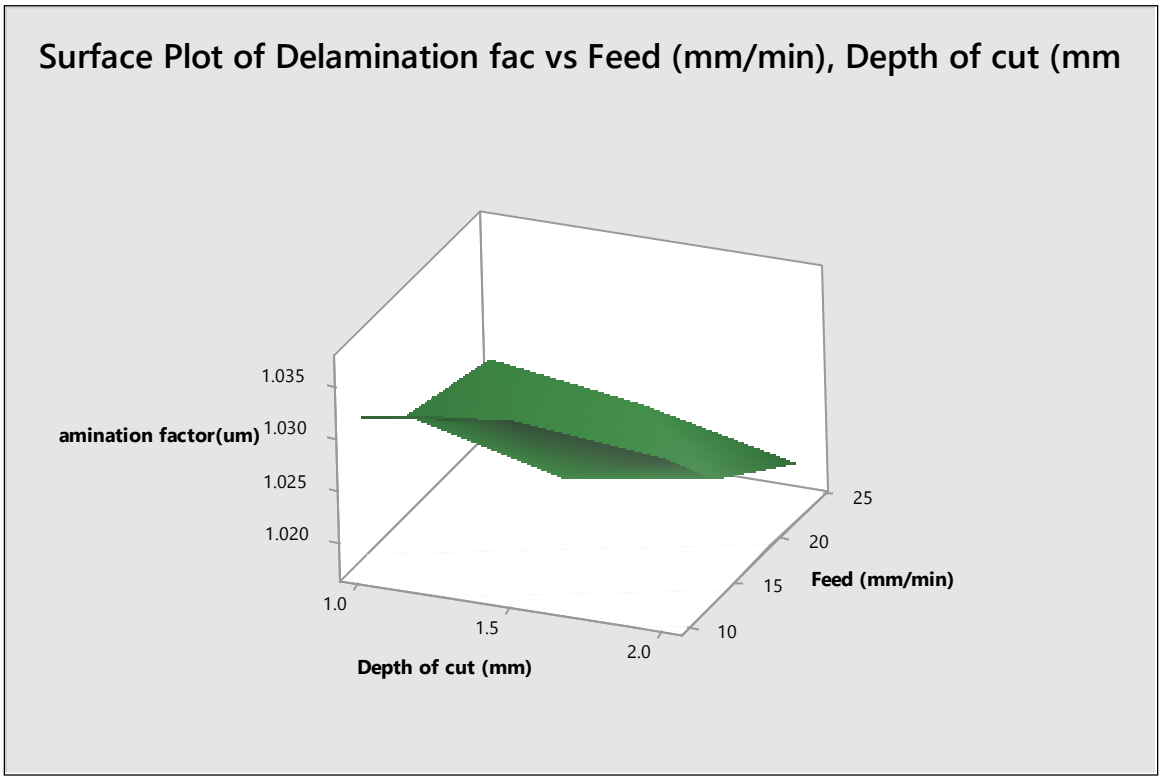

Fig – 3.19 Response surface showing combined effect of depth of cut and feed rate on Delamination Factor

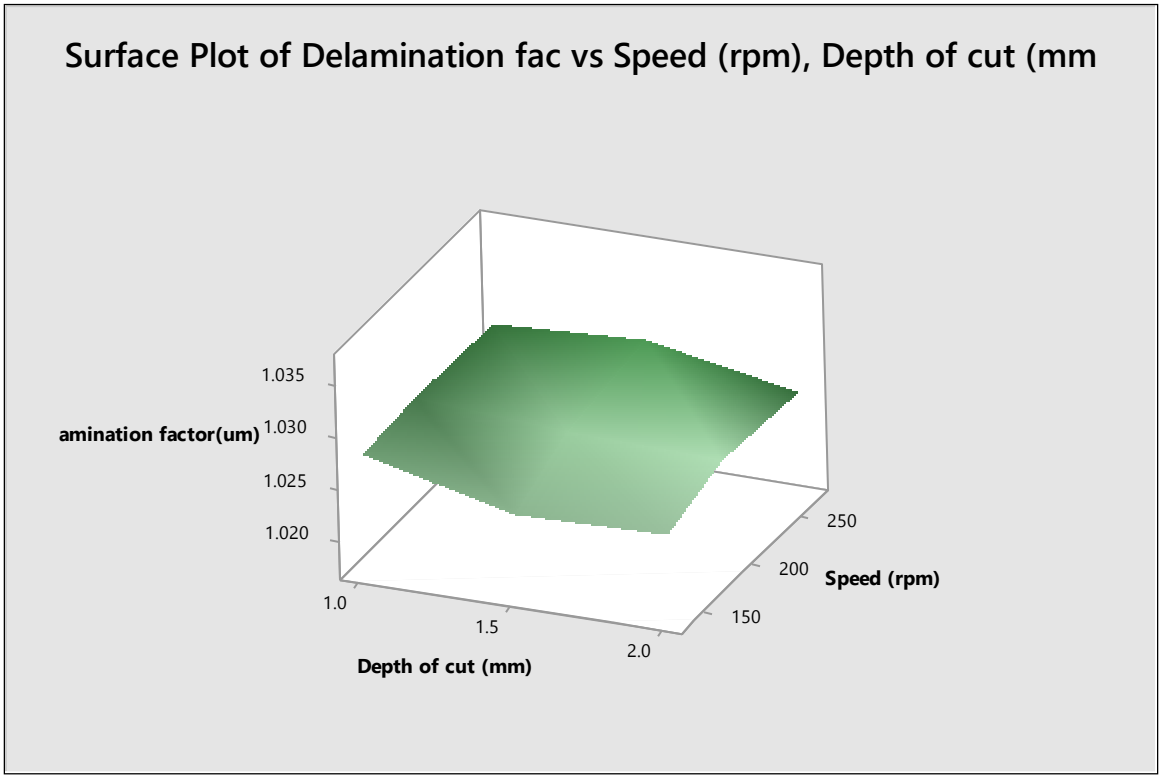

Fig – 3.20 Response surface showing combined effect of rotational speed and depth of cut on Delamination Factor

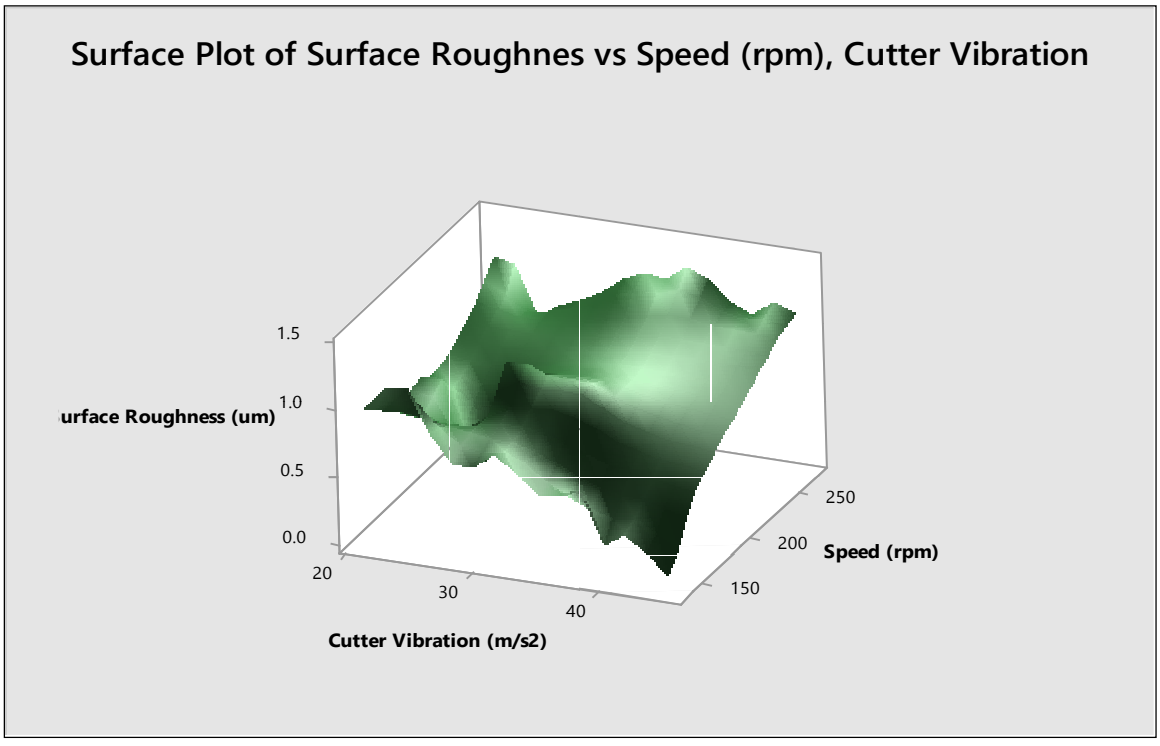

Fig – 3.21 Response surface showing combined effect of Cutter vibration and Rotational speed on Surface Roughness

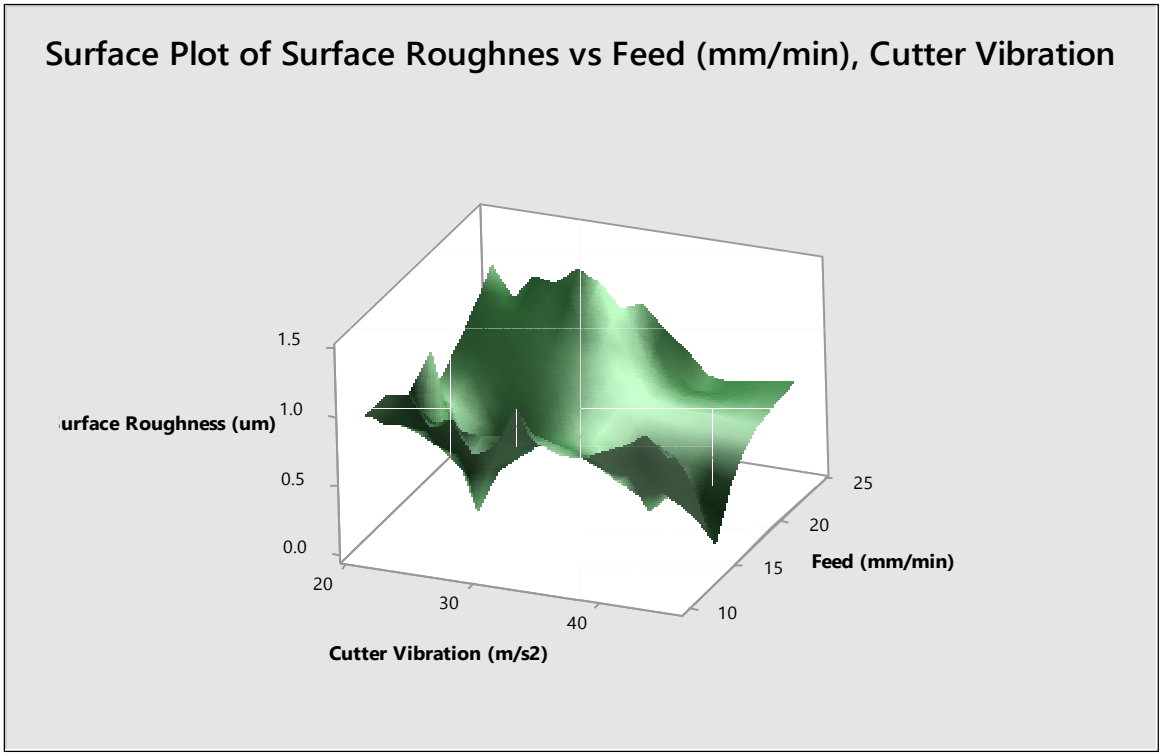

Fig – 3.22 Response surface showing combined effect of Cutter vibration and Feed rate on Surface Roughness

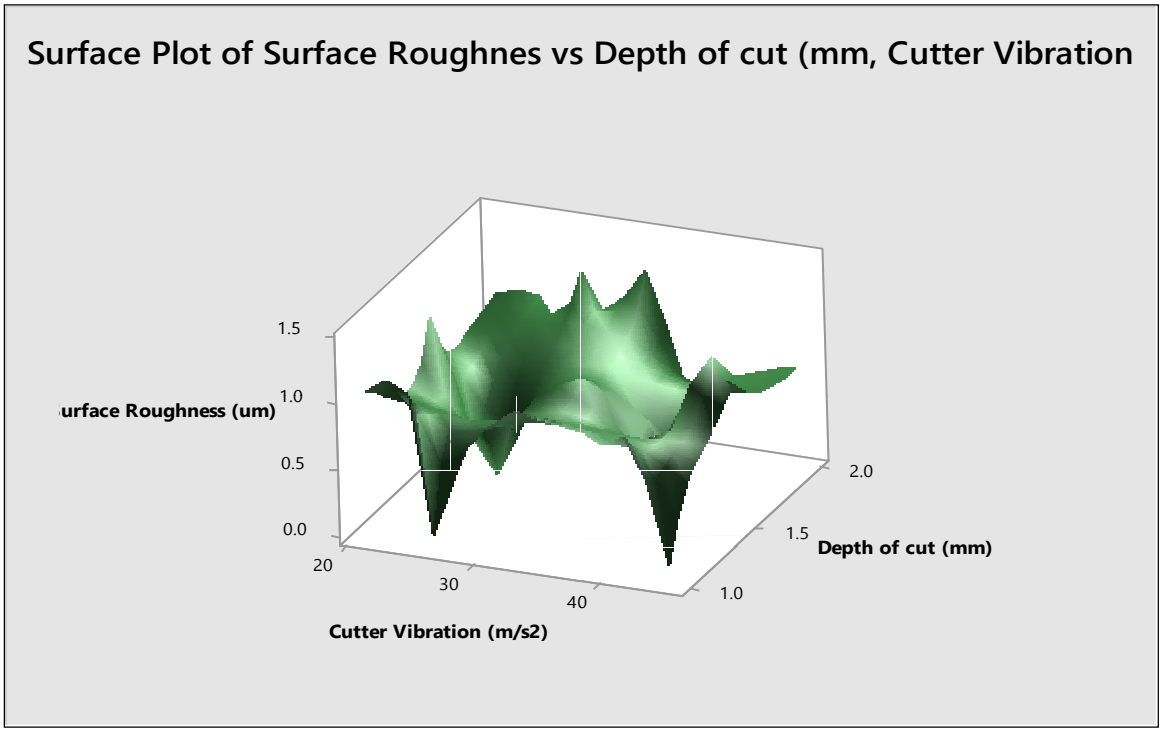

Fig – 3.23 Response surface showing combined effect of Cutter vibration and Depth of cut on Surface Roughness

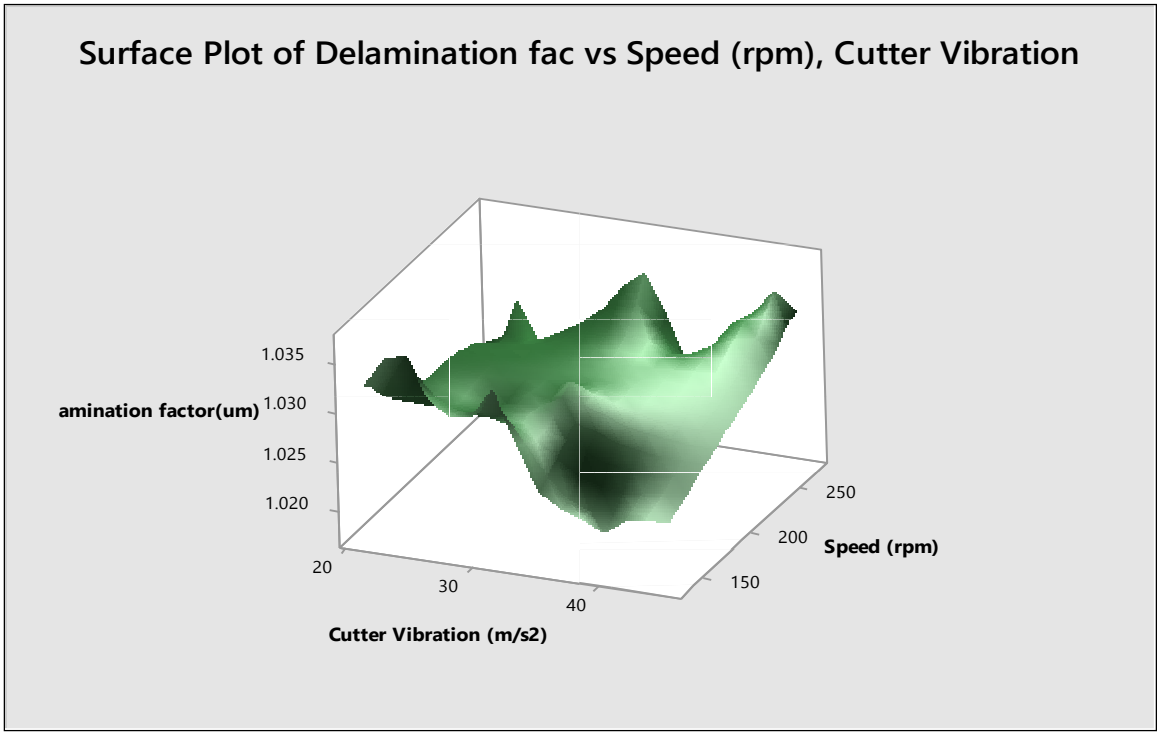

Fig – 3.24 Response surface showing combined effect of Cutter vibration and Rotational speed on Delamination Factor

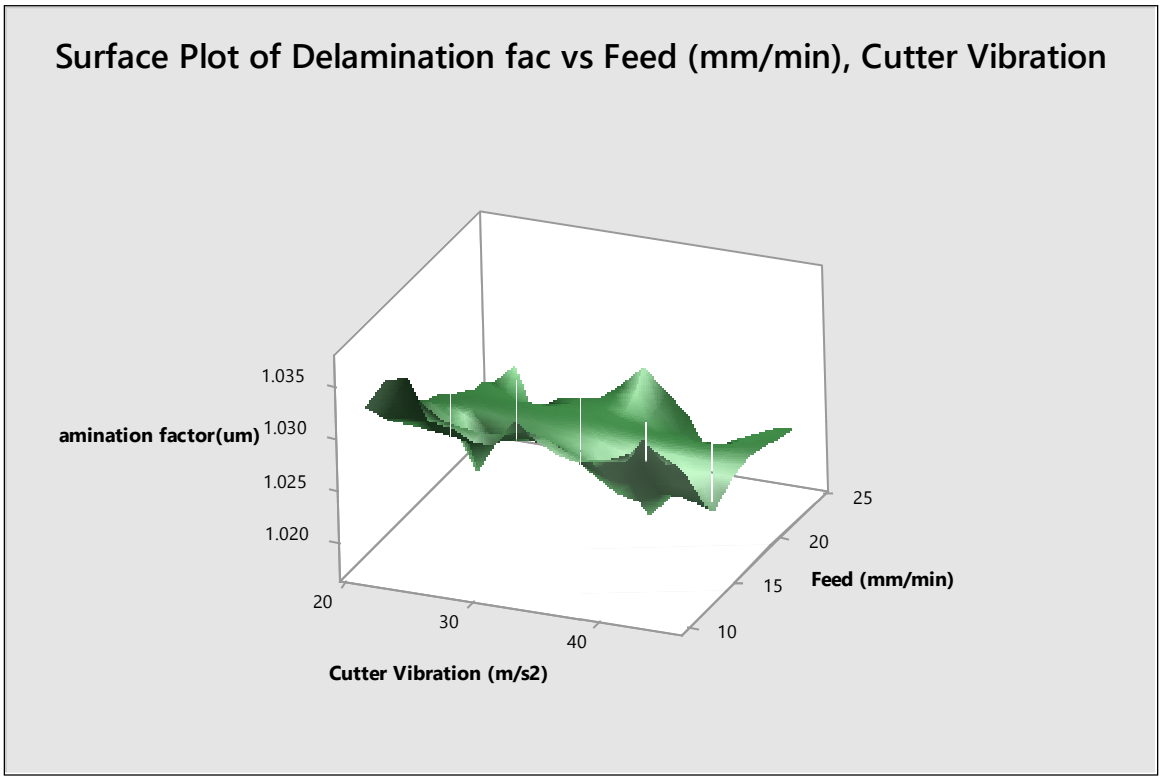

Fig – 3.25 Response surface showing combined effect of Cutter vibration and Feed rate on Delamination Factor

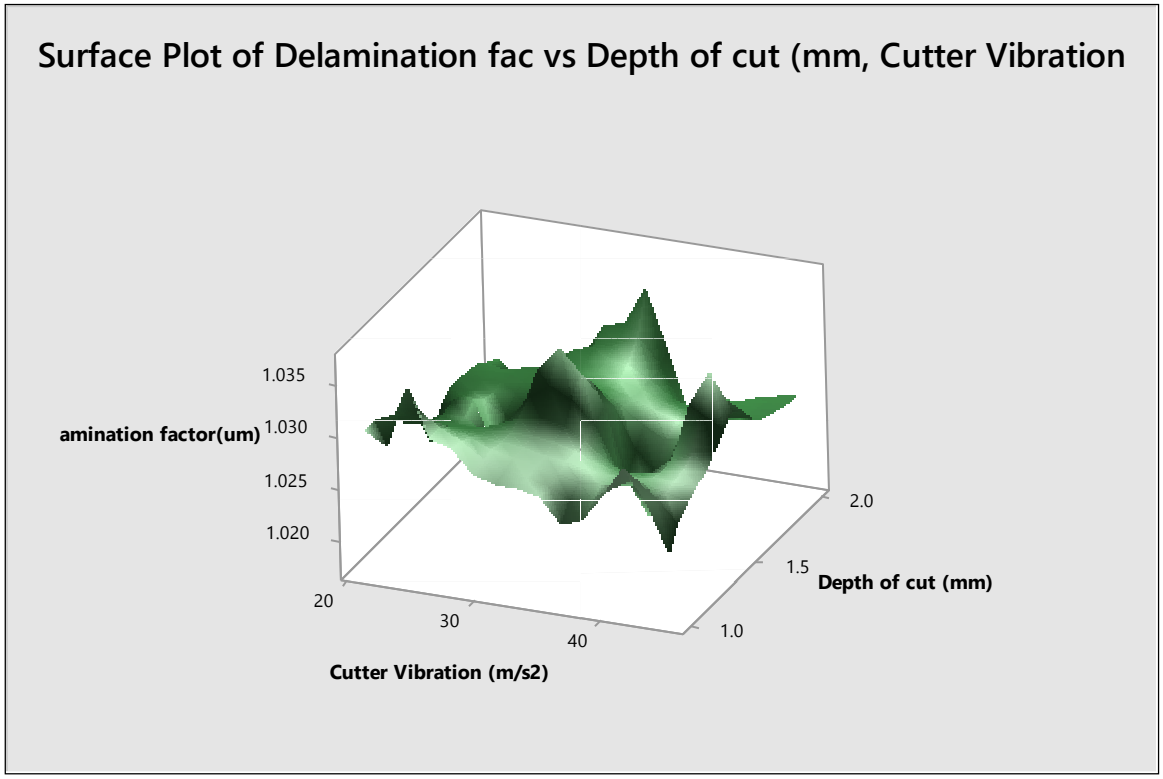

Fig – 3.26 Response surface showing combined effect of Cutter vibration and Depth of cut on Delamination Factor

3.8 ANALYSIS OF EXPERIMENTAL DATA

In the previous topic results of the experiments/ measurements/tests have been reported and discussed. In this chapter, analysis of the observed data is presented. Analysis has been done for single objective optimization through side and face milling of glass fiber reinforced polymer. Response surface methodology's full factorial concept has been used for minimizing the torque, cutter vibration, surface roughness and delamination factor i.e. separately. For the purpose of determining the optimum parametric condition for minimization of torque, cutter vibration, surface roughness and delamination factor have been done simultaneously analysis of variance (ANOVA) has been also done to determine the relative significance of machining parameters on individual responses.

3.8.1 SINGLR OBJECTIVE OPTIMIZATION FOR TORQUE, CUTTER VIBRATION, SURFACE ROUGHNESS AND DELAMINATION FACTOR BY USING RSM

For optimization of process parameters in side and face milling RSM Full factorial has been adopted. The RSM tool from MINITAB17 software has been used for this purpose. The experimental results with one repetition of each experiment as per RSM Full Factorial (L_{27}) orthogonal arrays are listed in Table (3.4, 3.5, 3.6 & 3.7). The responses (M_Z, fa, Ra and F_d) are taken from Table (3.4, 3.5, 3.6 and 3.7).

Factorial Analysis

From Tables 3.4, 3.5, 3.6 & 3.7 the experimental values of M_Z, Fa, Ra &Fd can be studied. For minimum Torque (optimum value) the process parameters N, f and d are optimal at level 2, 2 & 2 respectively as these level acquire lowest values as shown in Fig- 3.1 and also it may be obtained from Table No- 3.4. Similarly, for cutter vibration considering Table No- 3.5and Fig- 3.3, N, f & d are optimal at level 2, 2, 3. In case of surface roughness the considering Table No- 3.6 and Fig- 3.5, the optimal surface roughness is at the level 1, 2, 2. For delamination factor considering the Table No- 3.7 and Fig- 3.7 the optimal values are at 1, 3, 3.

Utilizing equations (3.2), (3.3), (3.4) and (3.5) response surface plots are made. The response surface plots are shown in Fig- 3.9 – 3.11 (for the response: Torque), Fig- 3.12 – 3.14 (for the response: cutter vibration), Fig- 3.15 – 3.17 (for the response: surface roughness) and Fig- 3.18 – 3.20 (for the response: delamination factor). In each of the surface plots, two process parameters are varying while the third and fourth parameters are kept constant at some selected level i.e. low level/ medium level/ high level. These 3-D plots are very useful to identify the combined effect of any two process parameters on the response variables (Torque, Cutter vibration, Surface roughness and Delamination factor) while the second and third input parameters are held constant. In other words one can predict the response under given parametric setting of any two factors (like rotational speed-feed rate, rotational speed-depth of cut etc.).

Further, interaction effects can also be evaluated from these plots. Curvature or bend in the surface plots indicates that interaction effect is significant. Comparatively plane surface suggest no or lesser interaction effects. Further an idea about the change in response value for the change in input parameters can be developed, by examining the surface plots.

Fig- 3.9 presents the response surface plot for torque for varying rotational speed and feed. It is found from the plot that, with increasing rotational speed torque decreases and after optimum value it again increases. It is also found that with increasing feed rate torque decreases but after the optimum input it again increases. Fig-3.10 represents the surface plot for torque for varying feed and depth of cut. It is found that with increasing depth of cut the value of torques decreases but after the optimum value the output response increases abruptly. Fig- 3.11 is showing the surface roughness plot for varying rotational speed and depth of cut on output response torque.

Fig- 3.12 presents the response surface plot for milling cutter vibration for varying rotational speed and feed. It is found from the plot that, with increasing rotational speed cutter vibration decreases and after optimum value it again increases. It is also found that with increasing feed rate cutter vibration decreases but after the optimum input it again increases. Fig-3.13 represents the surface plot for cutter vibration for varying feed and depth of cut. It is found that with increasing depth of cut the value of cutter vibration decreases continuously. Fig- 3.14 is showing the surface roughness plot for varying rotational speed and depth of cut on output response cutter vibration.

Fig- 3.15 presents the response surface plot for Surface roughness for varying rotational speed and feed. It is found from the plot that, with increasing rotational speed surface roughness

continuously increases. It is also found that with increasing feed rate surface roughness decreases but after the optimum input it again increases. Fig-3.16 represents the surface plot for surface roughness for varying feed and depth of cut. It is found that with increasing depth of cut the value of surface roughness decreases but after the optimum value the output response increases abruptly. Fig- 3.17 is showing the surface roughness plot for varying rotational speed and depth of cut on output response torque.

Fig- 3.18 presents the response surface plot for delamination factor for varying rotational speed and feed. It is found from the plot that, with increasing rotational speed delamination factor increases and after optimum value it again increases slightly. It is also found that with increasing feed rate delamination factor decreases continuously. Fig-3.19 represents the surface plot for delamination factor for varying feed and depth of cut. It is found that with increasing depth of cut the value of delamination factor decreases continuously. Fig- 3.20 is showing the surface roughness plot for varying rotational speed and depth of cut on output response delamination factor.

Fig- 3.21- 2.23 represents a surface plot on surface roughness for combined effect of cutter vibration and rotational speed (Fig- 3.21), feed (Fig- 3.22) and depth of cut (Fig- 3.23). It is found from the plots that with increasing cutter vibration surface roughness first decreases and then it increases abruptly for some time and then again it decreases.

Fig- 3.24 – 3.26 represents the surface plots for delamination factor with varying cutter vibration and speed (Fig-3.24), feed (Fig- 3.25) and depth of cut (Fig- 3.26). It is found from the plots that like surface roughness with increasing cutter vibration first delamination factor decreases and then it increases for some time and again with increasing cutter vibration it decreases and then again it rises.

ANALYSIS OF VARIENCE (ANOVA) FOR TORQUE, CUTTER VIBRATION, SURFACE ROUGHNESS AND DELAMINATION FACTOR

The purpose of analysis of variance is to investigate which machining parameters significantly affect the responses. This process is carried out by computing the F-test value of the parameter with the standard F table value (F0.05) at the 5% significant level. The associated P-values are less than 0.05 for the models (i.e., $\alpha = 0.05$, or 95% confidence level) indicate that the model terms are statistically significant. Percentage contribution of process parameters on response is determined from Seq SS values of ANOVA table. Percentage contribution is calculated using the following expression.

Percentage contribution of a term = $\frac{Seq\ SS\ for\ the\ term}{total\ Seq\ SS} \times 100\ \%$

(A) **TORQUE DATA ANALYSIS BY ANOVA**

Table No - 3.8 Factor Information

Factor	Levels	1	2	3
Speed (rpm)	3	135	190	270
Feed (mm/min)	3	10	15	24
DOC (mm)	3	1	1.5	2

Table No - 3.9 Analysis of Variance for Torque

Source	DF	Seq SS	Adj SS	Adj MS	F	P	Percentage of contribution
Model	26	832476	832476	32018			
Linear	6	124616	124616	20769	10.4170	0.63246	100.0000
Speed	2	4795	4795	2398	0.5013	0.51799	2.5186
Feed	2	9513	9513	4756	36.7963	0. 11074	6.3130
Depth of Cut	2	110307	110307	55154	4.1681	0.00373	87.1983
2- way Interaction	12	525926	525926	43827	0.2024	0.05893	100.0000
Speed + Feed	4	110510	110510	27627	18.445	0.05736	21.0121
Speed+ DOC	4	191623	191623	47906	20.6375	0.00193	36.4356
Feed + DOC	4	223793	223793	55948	153.37	0.00041	42.5522
3-Way Interaction	8	181934	181934	22742	76.722	0.00021	100.0000
Speed + feed + doc	8	181934	181934	22742	76.722	0.00021	1

Model Summary: R-sq = 96.04%

From Table No- 3.9 it can be calculated that input parameter depth of cut is significant parameter on Torque (As its P value is less than 0.05). Feed value is also considerable effect on torque close to 0.05 and rotational speed has very less influence on torque. The percentage contribution of process parameters on Torque i.e. “Torque” is calculated by Eq. 3.2. Percentage contribution of process parameters on response is given. The percentage contributions of process parameters on Torque are listed in Table No- 3.9 and the corresponding pie-chart is shown in Fig- 3.27.

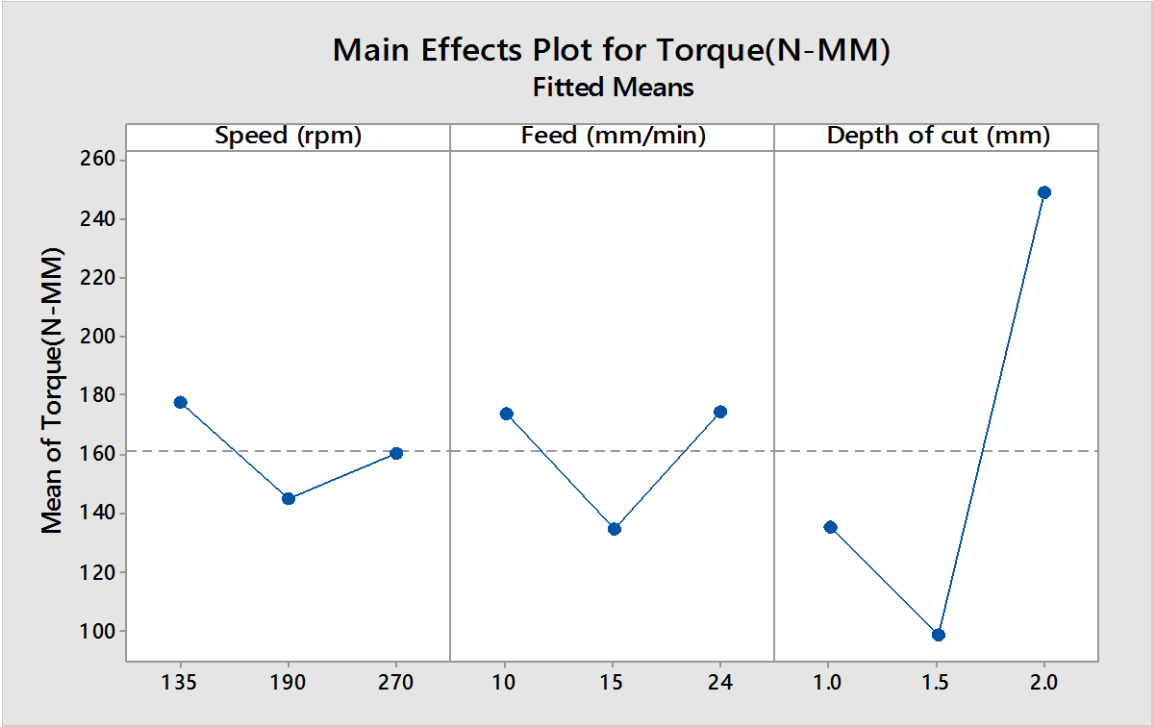

Fig- 3.1 Main effect plot of Torque vs Seed, feed & Depth of cut

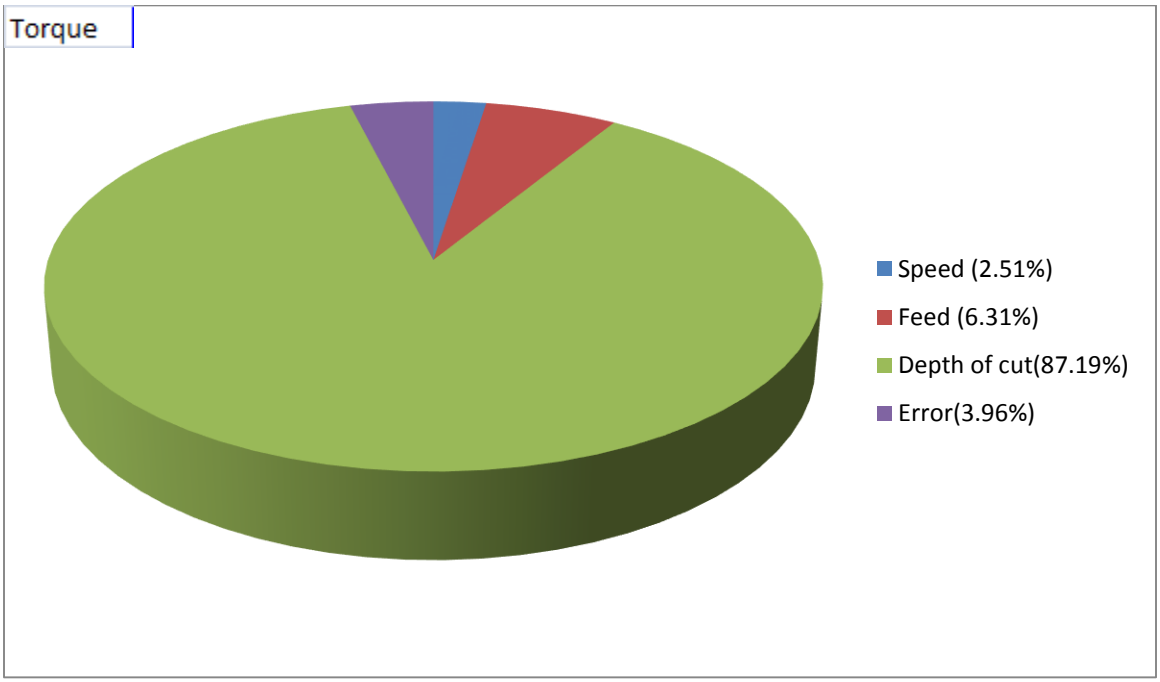

Fig- 3.27 Percentage contribution of factors on torque

(B) **CUTTER DATA ANALYSIS BY ANOVA**

Table No- 3.10 Analysis of Variance for milling cutter vibration

Source	DF	Seq SS	Adj SS	Adj MS	F	P	Percentage of contribution
Model	26	1265.76	1265.76	48.68			
Linear	6	317.80	317.80	12.22	9.4170	0.8886	100.00
Speed	2	233.62	233.62	8.98	0.5013	0.0035	73.42
Feed	2	31.04	31.04	1.19	36.7963	0.7898	9.77
Depth of Cut	2	53.14	53.14	2.04	4.1681	0.0953	16.72
2- way Interaction	12	818.14	818.14	31.47	0.2024	0.0893	100.00
Speed + Feed	4	668.09	668.09	25.69	12.445	0.0736	7.17
Speed+ DOC	4	41.58	41.58	1.59	20.6375	0.0193	12.27
Feed + DOC	4	118.47	118.47	4.55	153.37	0.0041	1.63
3-Way Interaction	8	119.82	119.82	4.60	76.722	0.0021	100.00
Speed + feed +DOC	8	119.82	119.82	4.60	76.722	0.0021	1
Error	6.47						

Model Summary: R-sq = 93.53%

From Table No- 3.10 it can be calculated that input parameter cutter speed is significant parameter on cutter vibration (As its P value is less than 0.05). Depth of cut value is also considerable effect on torque close to 0.05 and rotational speed has very less influence on cutter vibration. The percentage contribution of process parameters on cutter vibration i.e. “Cutter Vibration” is calculated by Eq. 3.3. Percentage contribution of process parameters on response is given. The percentage contributions of process parameters on Cutter vibration are listed in Table No- 3.10 and the corresponding pie-chart is shown in Fig- 3.28.

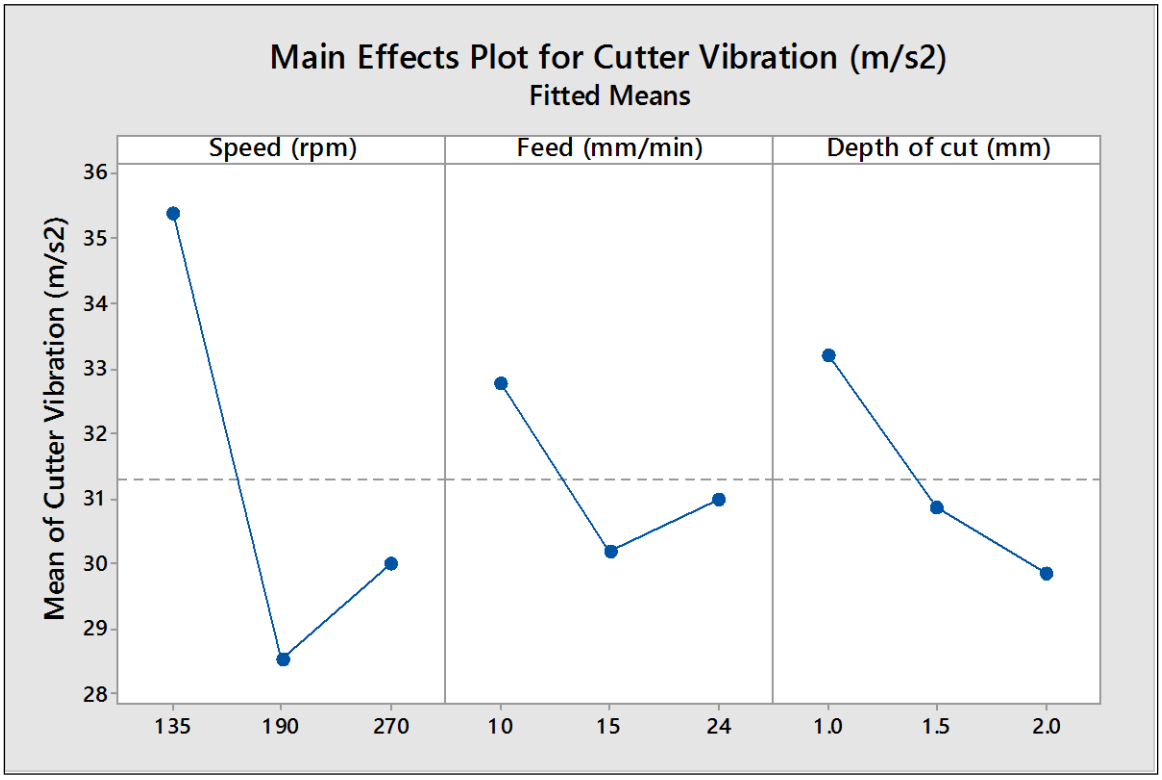

Fig- 3.3 Main effect plot of cutter vibration Vs speed, feed & depth of cut

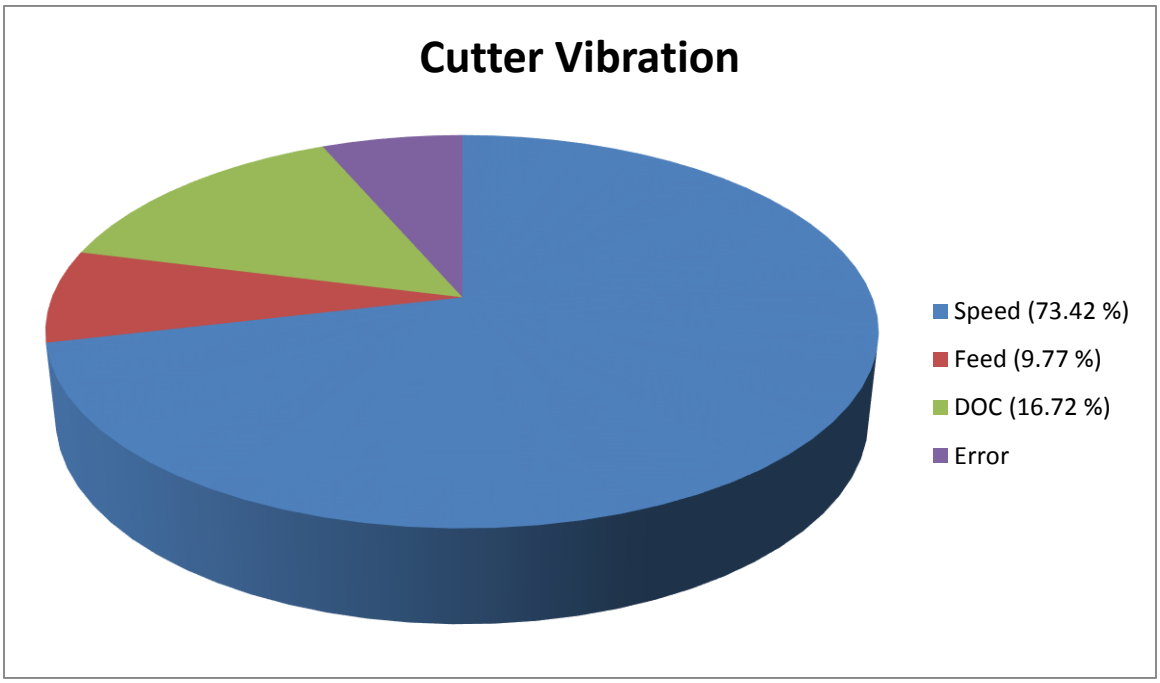

Fig- 3.28 Percentage contribution of factors on milling cutter vibration

(C) **Surface roughness data Analysis by ANOVA**

Table No- 3.11 Analysis of Variance for Surface Roughness

Source	DF	Seq SS	Adj SS	Adj MS	F	P	Percentage of contribution
Model	26	5.177	5.177	0.199			
Linear	6	3.287	3.287	0.126	0.146		100.00
Speed	2	1.032	1.032	0.040	0.492	0.0678	31.40
Feed	2	2.016	2.016	0.077	0.293	0.0036	61.33
Depth of Cut	2	0.239	0.239	0.006	0.028	0.136	7.27
2- way Interaction	12	1.166	1.166	0.044	0.422	0.089	100.00
Speed + Feed	4	0.423	0.423	0.016	0.536	0.002	19.25
Speed+ DOC	4	0.352	0.352	0.013	0.006	0.007	2.28
Feed + DOC	4	0.391	0.391	0.015	0.531	0.004	4.45
3-Way Interaction	8	0.723	0.723	0.027	0.498	0.001	100.00
Speed + feed +DOC	8	0.723	0.723	0.027	0.498	0.001	1
Error	3.48						

Model Summary: R-sq = 96.52%

From Table No- 3.11 it can be calculated that input parameter Feed is significant parameter on Surface Roughness (As its P value is less than 0.05). Cutter speed value is also considerable effect on surface roughness close to 0.05 and depth of cut has very less influence on cutter vibration. The percentage contribution of process parameters on cutter vibration i.e. “Surface Roughness” is calculated by Eq. 3.4. Percentage contribution of process parameters on response is given. The percentage of contributions of process parameters on Surface roughness are listed in Table No- 3.11 and the corresponding pie-chart is shown in Fig- 3.29.

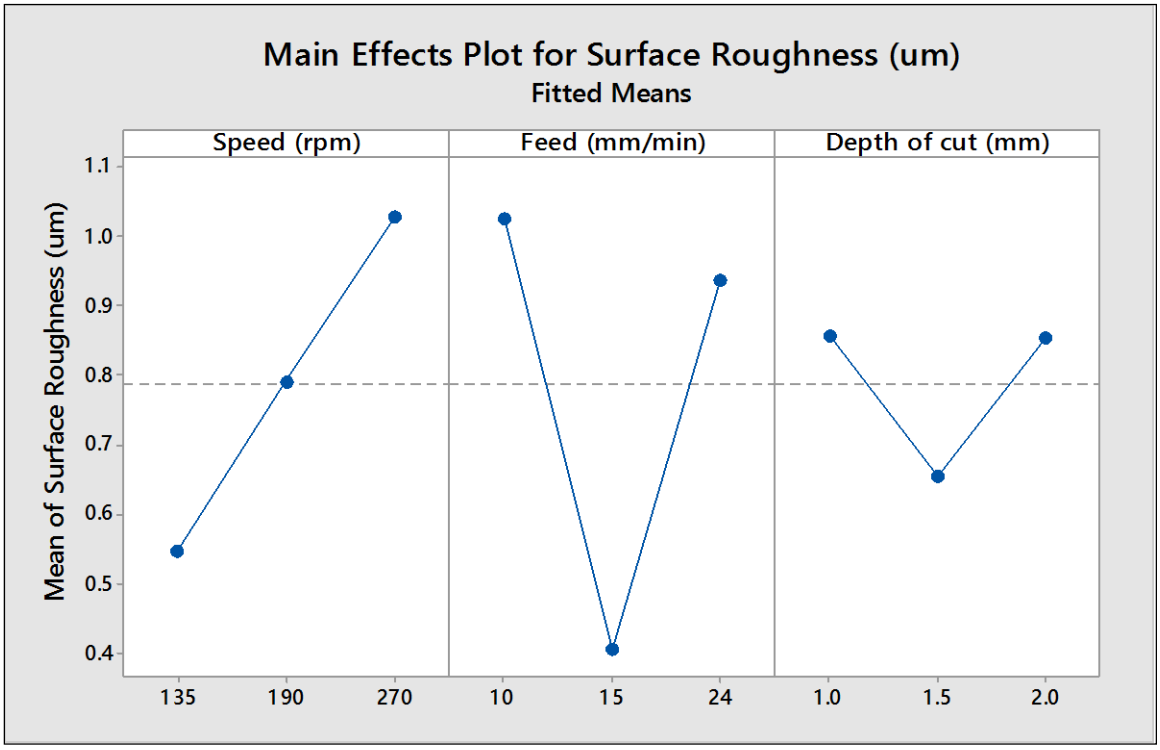

Fig- 3.5 Main effect plot of Surface Roughness Vs Seed, feed & Depth of cut

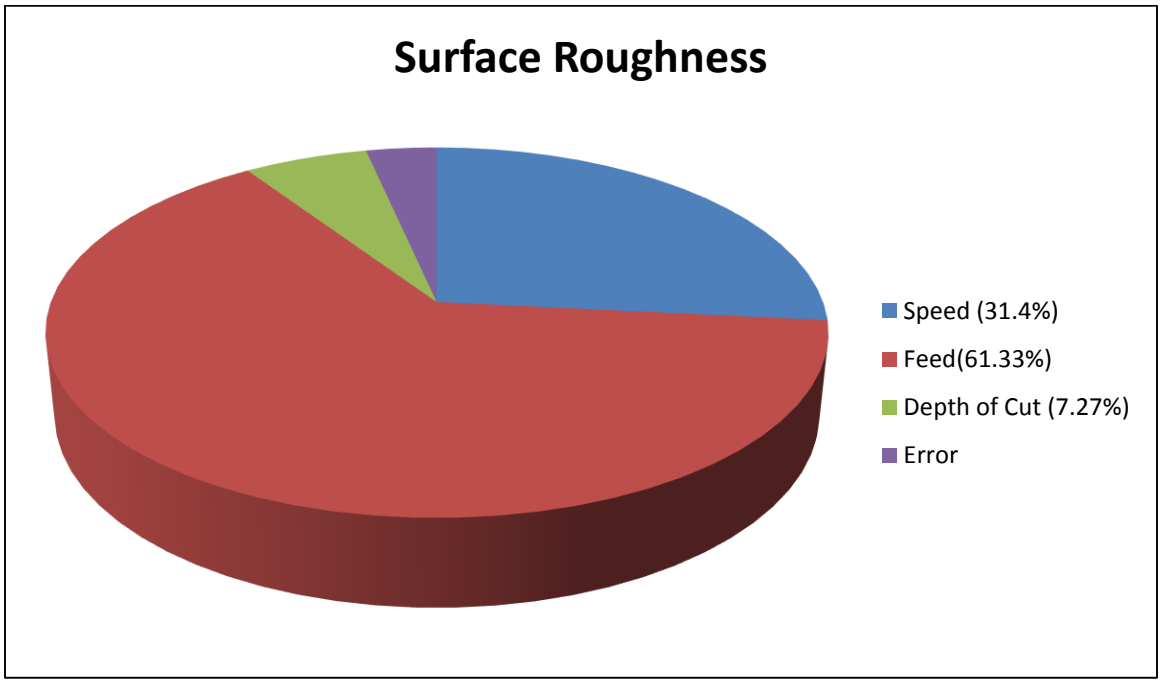

Fig- 3.29 Percentage Contribution of factors on Surface Roughness

(D) **Delamination Factor Analysis by ANOVA**

Table No- 3.12 Analysis of Variance for Delamination Factor

Source	DF	Seq SS	Adj SS	Adj MS	F	P	Percentage of contribution
Model	26	0.00071	0.00001	0.00199			
Linear	6	0.00049	0.00001	0.00126	0.146		100.00
Speed	2	0.00002	0.00001	0.00040	0.492	0.1789	4.08
Feed	2	0.00045	0.00001	0.00077	0.293	0.0004	91.83
Depth of Cut	2	0.00002	0.00001	0.00006	0.028	0.1890	4.08
2- way Interaction	12	0.00015	0.00001	0.00044	0.422	0.0089	100.00
Speed + Feed	4	0.00009	0.00001	0.00016	0.536	0.0002	3.75
Speed+ DOC	4	0.00001	0.00001	0.00013	0.006	0.0007	0.16
Feed + DOC	4	0.00005	0.00001	0.00015	0.531	0.0004	3.75
3-Way Interaction	8	0.00007	0.00001	0.00027	0.498	0.0001	100.00
Speed + feed +DOC	8	0.00007	0.00001	0.00027	0.498	0.0001	1
Error	2.45						

Model Summary: R-sq = 97.55%

From Table No- 3.12 it can be calculated that input parameter Feed is significant parameter on Delamination Factor (As its P value is less than 0.05). Cutter speed and depth of cut have very less influence on cutter vibration. The percentage contribution of process parameters on delamination factor i.e. “Delamination Factor” is calculated by Eq. 3.5. Percentage contribution of process parameters on response is given. The percentage of contributions of process parameters on Delamination Factor is listed in Table No- 3.12 and the corresponding pie-chart is shown in Fig- 3.30.

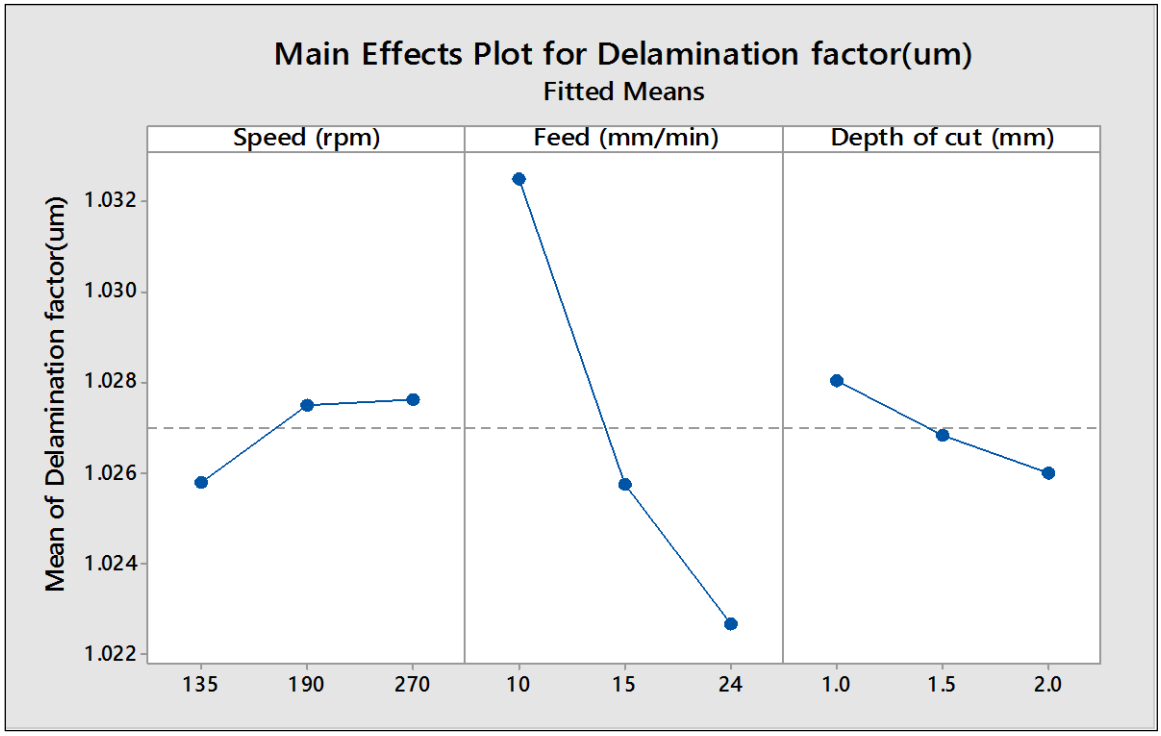

Fig- 3.7 Main effect plot for Delamination Factor

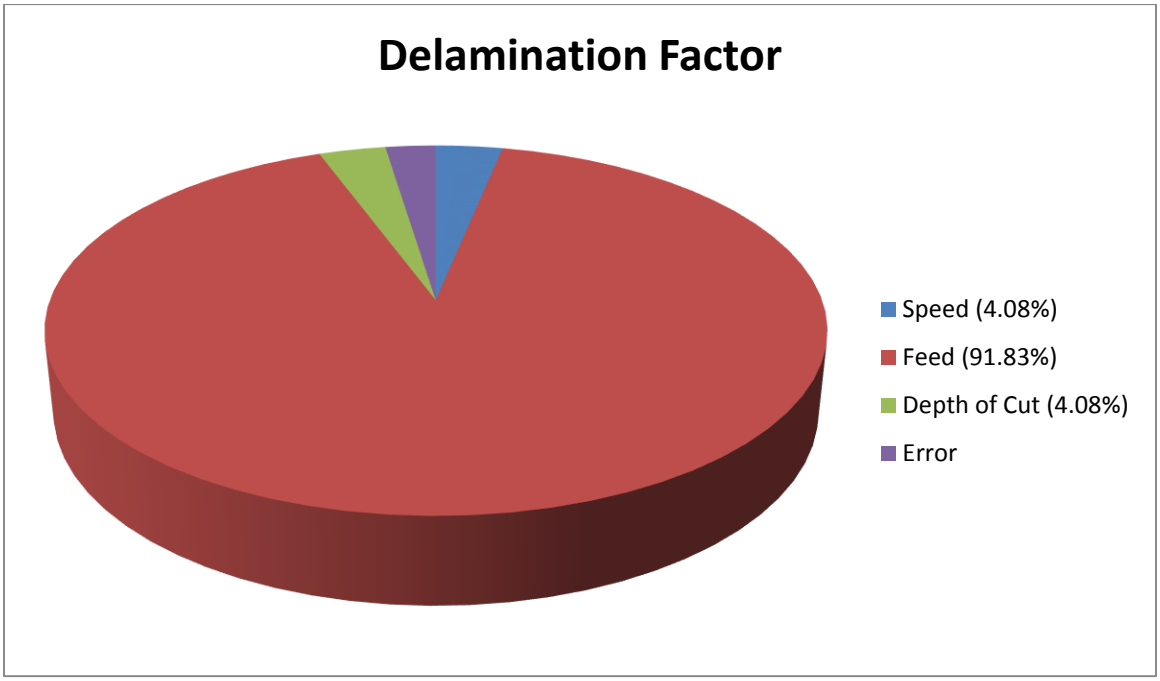

Fig- 3.30 Percentage Contribution of factors on Delamination Factor

3.9 CONFORMATORY TEST

Under the optimum combination of the process parameters the predicted value of η, denoted by η_{opt} is calculated for different responses as follows. For Torque (M_z),

$$\eta_{opt} = \eta_m + (\eta_{mN2} - \eta_m) + (\eta_{mf2} - \eta_m) + (\eta_{md2} - \eta_m) \quad (3.10)$$

For Milling Cutter Vibration (f_a),

$$\eta_{opt} = \eta_m + (\eta_{mN2} - \eta_m) + (\eta_{mf2} - \eta_m) + (\eta_{md3} - \eta_m) \quad (3.11)$$

For Surface Roughness (μm),

$$\eta_{opt} = \eta_m + (\eta_{mN1} - \eta_m) + (\eta_{mf2} - \eta_m) + (\eta_{md2} - \eta_m) \quad (3.12)$$

For delamination factor (F_d),

$$\eta_{opt} = \eta_m + (\eta_{mN1} - \eta_m) + (\eta_{mf3} - \eta_m) + (\eta_{md3} - \eta_m) \quad (3.13)$$

where, η_m is the mean of all values corresponding to speed , feed and depth of cut and η_{mN2} is the optimum values of speed after analysis through ANOVA and so on. The corresponding predicted value of Mz, fa, Ra and Fd at optimum level can be calculated from,

$$y_{opt}^2 = 10^{0.1 \times \eta_{opt}} \quad (3.14)$$

Using this eq. (3.14) the predicted values are calculated and founded as Mz = 10.17 N-mm, f_a = 28 m/s^2, Ra = 0.086 μm and F_d = 1.019003. Results of conformation tests are for Mz= 10.28 N-mm, f_a= 28.5 m/s^2, Ra= 0.092 μm and F_d = 1.02005.

CHAPTER – 4

4. CONCLUSIONS AND FUTURE SCOPE OF WORK

4.1 CONCLUSIONS

In the present work, milling of glass fiber reinforced polymer has been done under different machining conditions, by through side and face milling. Based on the observations and analysis made in the study, following conclusions are drawn:

- Effects of rotational speed, feed rate and depth of cut on torque, milling cutter vibration, surface roughness and delamination factor have been identified and analyzed.
- The value of torque decreases with increasing rotational speed, feed and depth of cut up to the optimum level but after the optimal value it again raises.
- ANOVA indicates that depth of cut is the most significant factor which influences the torque. Other factors are not significant for torque.
- The value of cutter vibration decreases with increasing rotational speed, feed and up to the optimum level but after the optimal value it again rises.The value of cutter vibration continuously decreases with increasing depth of cut.
- ANOVA indicates that speed is the only significant factor which influences the cutter vibration. Other factors are not significant for cutter vibration.
- The value of surface roughness decreases with increasing feed and depth of cut up to the optimum level but after the optimal value it again raises. The value of surface roughness continuously increases with increasing rotational speed.
- ANOVA indicates that feed is the most significant factor which influences the surface roughness. Other factors are not significant for surface roughness.
- The value of delamination factor increases with the rotational speed but for feed and depth of cut its value continuously decreases with increasing the feed and depth of cut.
- ANOVA indicates that feed is the only significant factor which influences the delamination factor. Other factors are not significant for delamination factor.
- In single objective optimization, it is found that the optimum parametric condition for minimum torque is: N2 f2 d2 (i.e. rotational speed at 190 rpm, feed at 15 mm/min and depth of cut at 1.5 mm); for minimum cutter vibration is: N2 f2 d3 (i.e. rotational speed at 190 rpm, feed at 15 mm/min and depth of cut at 2 mm); for minimum surface roughness is: N1 f2 d2 (i.e. rotational speed at 135 rpm, feed at 15 mm/min and depth of cut at 1.5 mm); for minimum delamination factor is: N1 f3 d3 (i.e. rotational speed at 135 rpm, feed at 24 mm/min and depth of cut at 2 mm). Single objective optimization has been carried out by RSM Full Factorial Method.
- From ANOVA, it is found that for torque, significant factor is depth of cut and the contribution of individual parameters for torque is: N 2.51%, f 6.31%, d 87.19%. The model summary is: R-sq: 96.04%.

- For cutter vibration, significant factor is rotational speed and the contribution of individual parameters for cutter vibration is: N 73.42%, f 9.77%, d 16.72%. The model summary is: R-sq: 93.53%.
- For Surface roughness, significant factor is feed and the contribution of individual parameters for surface roughness is: N 31.4%, f 61.33%, d 7.27%. The model summary is: R-sq: 96.52%.
- For delamination factor, significant factor is feed and the contribution of individual parameters for torque is: N 4.08 %, f 91.83 %, d 4.08 %. The model summary is: R-sq: 97.55 %.
- Mathematical modelling is done and relationship between (a) torque and process parameter (b) cutter vibration and process parameter (c) surface roughness and process parameter and (d) delamination factor and process parameter are developed.
- The developed models are utilized to generate response surface plots for (a) torque (b) cutter vibration (c) surface roughness and (d) delamination factor.
- Response plots may be used to predict the response value (s) [i.e. torque/ cutter vibration/ surface roughness/ delamination factor] at some given combination of any two parameters, while the third parameter and forth parameter are hold constant level.

4.2 FUTURE SCOPE OF WORK

- The accuracy of the developed model can be improved by including more number of factors and levels.
- The investigation of delamination, in milling different types of GFRP like roving and epoxy resin can be used.
- Other different types of optimization techniques such as generic, simultaneous annealing etc. can be process optimization in this experiment.

REFERENCES

1. **G.C. Evestine and T.G. Rogers** (1971), 'A Theory of Machining of Fiber-Reinforced Materials', Journal of Composite Materials, **5**, 94-106.

2. **D.H. Wang, M. Ramulu and D. Arola** (1995), 'Orthogonal Cutting Mechanisms of Graphite/ Epoxy Composite part: 1 unidirectional laminates', International Journal of Machine Tools and Manufacture, **35**, 1623-1638.

3. **W.C. Chen** (1997), 'Some Experimental Investigation in the Drilling of Carbon Fiber Reinforced Plastics (CFRP) Composite Laminates', International journal of machine tools and manufacture, **37**(8), 1097-1108.

4. **U.A. Khashaba** (2004), 'Delamination in drilling GFR- Thermoset Composite', Journal of Composite Structures, **63**, 313-327.

5. **U.A. Khashaba and I.A. El-Sonbaty** (2010), 'Machinability Analysis in Drilling Woven GFR/epoxy Composites: Part I- Effect of Machining Parameters', Journal of Composite Structures, **41**, 391-400.

6. **J.P. Davim, P. Reis and A.C. Conceicao** (2004) 'Drilling Fiber Reinforced Plastics (FRPs) manufactured by hand lay-up: influence of matrix (Viapal VUP 9731 and ATLAC 382-05)', Journal of Material Process Technology, **155-156**, 1828-1823.

7. **I.A. El- Sonbaty, U.A. Khashaba and T. Machaly** (2004), 'Factors affecting the Machinability of GFR/ Epoxy Composites', Journal of Composite Structures, **63**, 329-338.

8. **H. Hocheng, H.Y Pwu. and K.C. Yao** (1993), 'On Drilling Characteristics of Fiber Reinforced Thermoset and Thermoplastics', Materials and Manufacturing Processes, **8**, 653-682.

9. **S.O. An** (2004) 'A study on the cutting characteristics of glass fiber reinforced plastics with respect to tool materials and geometries', Journal of Materials Processing Technology, **68**(1), 60-67.

10. **G. Caprino and V. Tagliaferri** (1995), 'Damage Development in Drill Glass Fiber Reinforced Plastics', International Journal of Machine Tool Manufacture, **35**(6), 817-829.

11. **J.P. Davim and F. Mata** (2007), 'New Machinability of GFRP plastics using Polycrystalline Diamond and Cemented Carbide (K15) Tools', Material and Design, **28**, 1050-1054.

12. **K. Palanikumar** (2006), 'Multiple Performance Optimization of Machining Parameters on the Machining of GFRP Composites using Carbide (K10) Tool', Materials and Manufacturing Process, **21**, 846-852.

13. **K. Palanikumar** (2009), 'Multiple performance Optimizations in Machining of GFRP Composites by a PCD Tool using non-dominated sorted Genetic Algorithm (NSGA-II)', Met. Mater. Int., **15** (2), 249-258.

14. **T. Rajashekharan and K. Palanikumar** (2011), 'Application of Fuzzy Logic for Modeling Surface Roughness in Turning CFRP Composites using CBN Tool', Production Engineering. Res, Deve, **5**, 191-199.

15. **W. Konig** (1985) 'Machining of Fiber Reinforced Plastics': Annals of CIRF, **34**, 537-548.

16. **S.A. Hussain, V. Pandurungadu and K. Palanikumar** (2011), 'Machinability of GFRP Composite Materials', International Journal of Engineering, Science and Technology, **3**(4), 103-118.

17. **G. Santhanakrishnam** (1988), 'Machinability Characteristics of Fiber Reinforced Plastics Composites', Journal of Mechanical Working Technology, **17**, 195-204.

18. **J.P. Davim and F. Mata** (2005), 'Optimization of Surface Roughness on Turning Fiber Reinforced Plastics (FRPs) with Diamond Cutting Tools', International journal of Advance Manufacturing Technology, **26**, 319-323.

19. **N.S. Mohan** (2005), 'Influence of Process Parameters on Cutting Force and Torque during Drilling GFRP', Composite Structures, **71**, 407-413.

20. **S.R. Karnik** (2008), 'Investigative study on Machinability aspects of Unreinforced and Reinforced PEEK Composite Machining using ANN model', Journal of Reinforced Plastics and Composites, **27**(7), 751-768.

21. **E. Kilickap** (2010), 'Optimization of Cutting Parameters on Delamination based on Taguchi method during Drilling of GFRP composites', Expert system with Applications, **37**, 6116-6122.

22. **M.V. Kini and A.M. Chinchokar** (2010), 'Effect of Machining Parameters on Surface roughness and Material Removal Rate in finish Turning of 300 GFRP', Materials and Design, **31**, 3590-3598.

23. **E. Bagci and B. Isik** (2006), 'Investigation of Surface Roughness in Turning unidirectional GFRP Composites by using Response Surface Methodology', Materials and Design, **31**, 10-17.

24. **N.D. Jawali and B. Siddeswarapa** (2006), 'Physic mechanical Properties, Machinability and Morphological behavior of short Glass Fiber-Reinforced Nylon 6 Composites', Journal of Reinforced Plastics and Composites, **25**(13), 1409-1418.

25. **K. Palanikumar and J.P. Davim** (2009), 'Assessment of some Influencing Tool Wear on the Machining of GFRP by Coating Cemented Carbide Tool', Journal of Materials Processing Technology, **209**, 511-519.

26. **M.K. Nor and Khairusshima** (2013), 'Effect of Chilled Air on Tool Wear and Work-piece during Milling of CFRP', **302**, 1113-1123.

27. **B. Balamugundan and L. Karthikeyan** (2012), 'Multi Characteristics Optimization during Milling of Friction Stir Processed GFRP', ICMOC, **32**, 1276-1285.

28. **K. Panneerselvam, K. Pardeep** (2012), 'Optimization of End Milling parameters for GFRP using Grey Relational Analysis', ICMOC, **38**, 3962-3968.

29. **R. Rusinek** (2010), 'Cutting process of Composite Materials: An experimental study', International Journal of Non-linear Mechanics, **45**, 458-462.

30. **J.P. Davim** (2004), 'A study on milling of glass fiber reinforced polymer manufactured by hand-lay up using statistical analysis (ANOVA)', Journal of Composite Structures, **64**, 493-500.

31. **A.I. Azmi** (2013), 'Machinability study of Glass Fiber Reinforced Polymer Composites During End Milling', International Journal of Advance Manufacturing Technology, **64**, 247-261.

32. **A.I. Azmi** (2013), 'Tool Wear Predictions models during End Milling of GFRP Composites', International Journal of Advance Manufacturing Technology, **67**, 701-718.

33. **P. Praveen Raj** (2012), 'Prediction of Surface Roughness and Delamination in End Milling of GRFP using mathematical model and ANN', Indian Journal of Engineering & Materials Sciences, **19**, 107-120.

34. **S.A**. **Tobias** (1965), 'The Vibration of Radial Drilling Machines under Testing and Working Conditions', Proc. Inst. Mechanical Engineering, **170**, 232-264.

35. **Doi** (1956), 'Chatter Vibration of Lathe Tools', Transactions of the ASME, **78**, (5), 1127-1134.

36. **J.A. Tlusty** (1965), 'A Method of Analysis of Machine Tool Stability', Proc. 6th MTRD, 5-14.

37. **H.E**. **Merritt** (1965), 'Theory of self-excited machine tool chatter', Transactions of the ASME, Sec B, **87**(4), 447-454.

38. **Y. Kondo, O. Kawano and H. Sato** (1981), 'Behavior of Self-Excited Chatter due to Multiple Regenerative Effect', ASME Journal of Engineering for Industry, **103**(3), 324-329.

39. **S. Saha, A. Bandyopadhyay, P.K. Pal and D.K. Bandyopadhyay** (2002), 'Effect of Infeed on Vibration Behavior of Cylindrical Grinding Machine', proc. of the 20th AIMTDR Conference, BIT, Meshra, Ranchi, 130-135.

40. **J.S. Kin and B.H. Lee** (1991), 'An Analytical Model of Dynamic Cutting forces in Chatter Vibration', International Journal of Machine Tools and Manufacture, **31**(3), 371-380.

41. **N. Kasahara, H. Sato and Y. Tani** (1992), 'Phase characteristics of Self-excited chatter in Cutting', International Journal of Machine tools and Manufacture, **114**, 324-329.

42. **S. Malkin** (1984), 'Milling of Metals, Theory of Application', Journal of Applied Metal Working, 95-109.

43. **R**. **Aini** (1990), 'A Five Degrees of Freedom Analysis of Vibration in Precision Spindles', International Journal of Machine Tools and Manufacture, **30**, 1-18.

44. **Mohammed Alfares and Abdallah Elshakawy** (2000), 'Effect of Milling Forces on the Vibration of Grinding Machine Spindle System', International Journal of Machine Tools and Manufacture, **40**(14), 2003-2030.

45. **N. Akturk** (1993), 'Dynamics of Rigid Shaft Supported by Angular Contact Ball Bearing', Ph.D., Thesis, Imperial College of Science, Tech. and medicine, London.

46. **Y. S. Liao and L. C. Shiang** (1991), 'Computer Simulation of Self-excited and Force Vibrations in the External Cylindrical Plunge Grinding Process', Journal of Engineering for Industry, **113**, 297-304.

47. **Orynski** (1999), 'The Influence of Grinding Process on Forced Vibration Damping in head stock of Grinding Wheel of Cylindrical Grinder', International Journal of Machine Tools and Manufacture, **39**, 229-235.

48. **Drew** (2001), 'The Measurement of Forces in Grinding in the presence of Vibration', International Journal of Machine Tools and Manufacture, **41**, 509-520.

49. **J. Y. S-Ahmad** (2009), 'Machining of Polymer Composites', The Petroleum Institute, Department of Mechanical Engineering, United Arab Emirates, ISBN 978-0-387-35539-9, Ed. Springer Science, Abu Dhabi.

50. **A. Kobayashi** (1967), 'Machining of Plastics', McGraw-Hill, New York.

51. **A. James, M. Freeman and Skapura** (1999), 'Training data with Back propagation', International student edition Neural Networks, 1, First ISE reprint, Eastern Press (Bangalore) Pvt. Ltd., 103-104.

52. **A. Roushan**, (2014), 'Experimental Investigation and Parametric Optimization on Milling GFRP'- MME Thesis, Jadavpur University.

53. **P.K. Sahoo** (2003), 'Analysis of Dynamic Behavior of Cylindrical Grinding machine under different input parameters through experiments and ANN'- MME Thesis, Jadavpur University.

54. **A.B. Chattopadhyay** (2011), 'Machining and Machine Tools', 1st Edition, WILEY- India.

55.**W.D. Callister Jr. and D.G. Rechwisch** (2009), 'Material Science and Engineering- An introduction', 8th edition, WILEY - India.

56. **Y. Altintas** (2014), 'Manufacturing Automation- Metal Cutting Mechanics, MachineTool Vibration and CNC Design', 2nd Edition, Pearson- India.

57. **S.S. Rattan** (2014), 'Theory of Machines', 4th Edition, Tata McGraw-hill.

Calibration Certificate for Kistler 9272

KISTLER
measure. analyze. innovate.

Kalibrierschein
Calibration Certificate

Type Kistler 9272 Serial No. 5443685

Bearbeiter Calibration Technician	Datum Date
K. Ta	16. Oct. 2018

Referenzgeräte Reference Equipment	Typ Type	Serien Nr. Serial No.
Gebrauchsnormal Working Standard	Kistler 9251A Kistler 9369A_mod	329968 43048
Präzisionskalibrator Precision Calibrator	Kistler 5395A	605253

Umgebungstemperatur Ambient Temperature	Relative Feuchte Relative Humidity
25 °C	41 %

Messergebnisse Results of Measurement

Kalibrierter Bereich Calibrated Range	Empfindlichkeit Sensitivity	Linearität[1] Linearity[1]	Übersprechen Crosstalk			
kN	pC/N	±%FSO	→Fx[%]	→Fy[%]	→Fz[%]	→Mz[mN·m/N]
Fx 0 ... 5	-7,568	0,11		0,9	0,1	
Fx 0 ... 0,5	-7,578	0,16		0,9	-0,6	
Fy 0 ... 5	-7,555	0,11	-0,2		-0,1	
Fy 0 ... 0,5	-7,566	0,15	-0,3		-0,9	
Fz 0 ... 20	-3,641	0,35	-0,2	-0,2		0,011
Fz 0 ... 2	-3,631	0,02	-0,3	-0,2		0,016

1) Linearität einschliesslich Hysterese
linearity including hysteresis

Kalibrierter Bereich Calibrated Range	Empfindlichkeit Sensitivity	Linearität[1] Linearity[1]	Übersprechen Crosstalk
N·m	pC/N·m	±%FSO	→Fz[N/N·m]
Mz 0 ... 200	-170,6	0,18	-0,63
Mz 0 ... 20	-170,9	0,08	-0,41
Mz 0 ... -200	-170,6	0,16	-0,43
Mz 0 ... -20	-170,8	0,08	-0,34

1) Linearität einschliesslich Hysterese
linearity including hysteresis

Bestätigung Confirmation

Das oben durch die Seriennummer identifizierte Gerät entspricht der Vereinbarung der Bestellung und hält die Herstelltoleranzen gemäss den Spezifikationen der Datenblätter ein, sofern nicht anders auf dem Kalibrierschein vermerkt. Das Kistler Qualitätsmanagement System ist nach ISO 9001 zertifiziert. Das Dokument erfüllt die Anforderungen von EN 10204 Abnahmeprüfzeugnis "3.1". Die aufgeführten Referenzgeräte sind auf nationale Normale rückgeführt. Das Dokument wurde elektronisch erstellt und ist daher ohne Unterschrift gültig.

The equipment identified by Serial No. complies with the agreement of the order and meets the manufacturing tolerances specified in the data sheets, unless otherwise specified on the calibration certificate. The Kistler Quality Management System is certified per ISO 9001. This document fulfils the requirements of EN 10204 Inspection Certificate "3.1". The reference equipment is traceable to national standards. The document was issued electronically and is therefore valid without signature.

Seite Page 1 / 1

Kistler Instrumente AG
Eulachstrasse 22
8408 Winterthur
Switzerland
Tel. +41 52 224 11 11
Fax +41 52 224 14 14
info@kistler.com
ZKB Winterthur BC 732
Swift: ZKBKCHZZ80A
Account: 1132-0374.628
IBAN: CH67 0070 0113 2003 7462 8
VAT: 229 713
ISO 9001 certified
www.kistler.com

APPENDIX – B

Graphical and Surface Plots for Experiment – 2

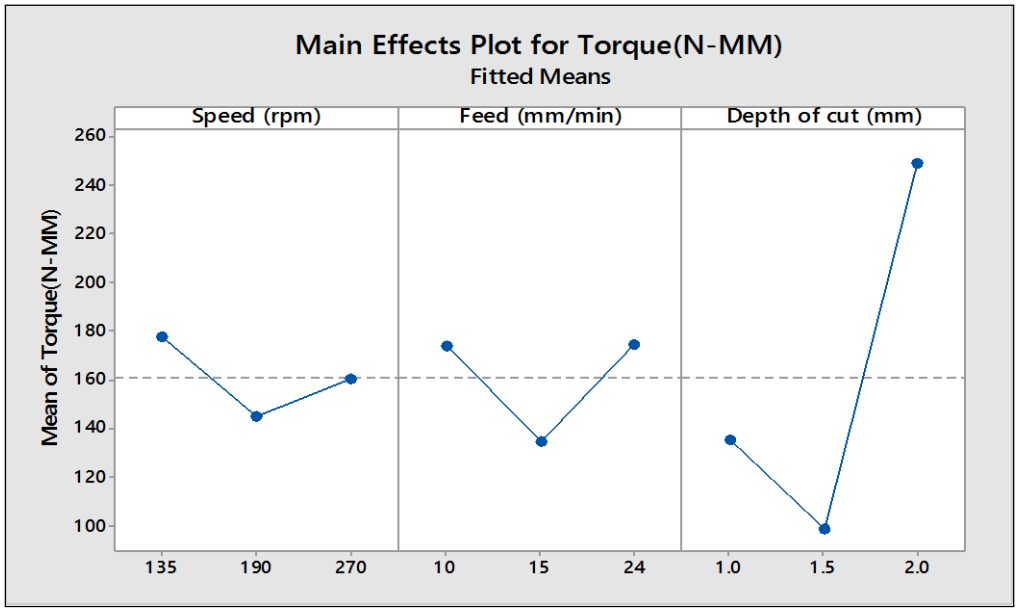

Fig- B.1 Main effect plot for Torque

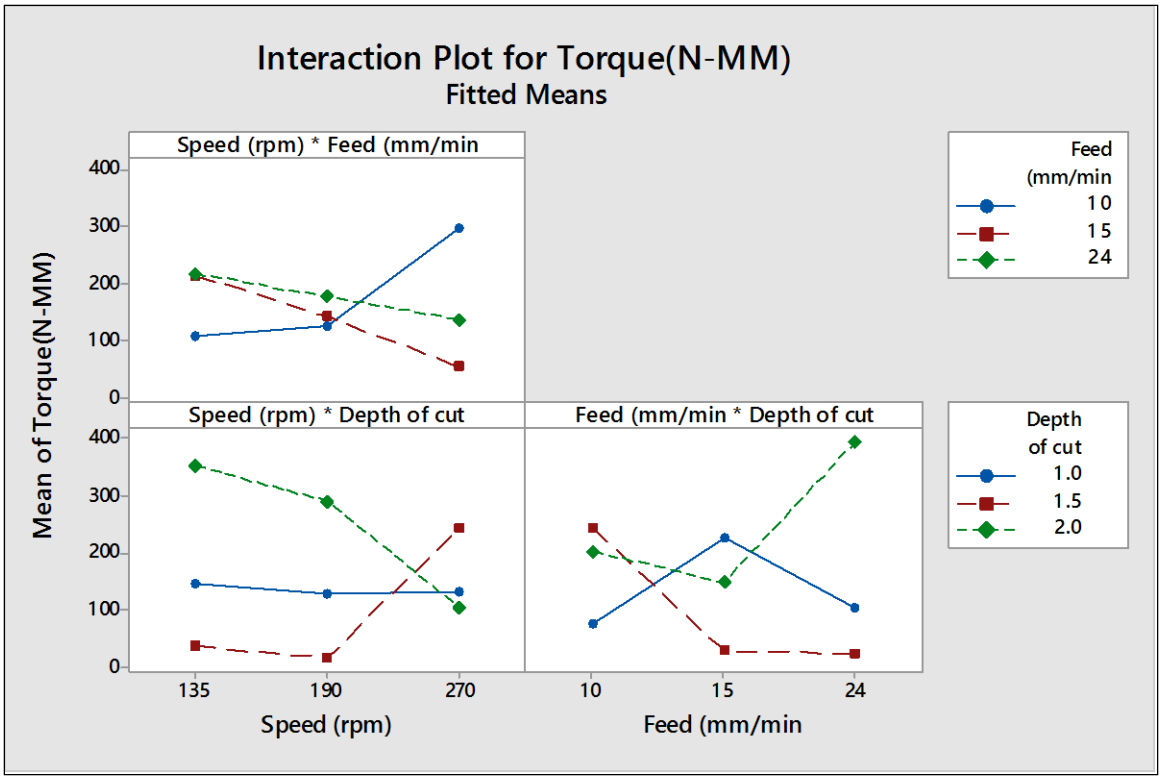

Fig - B.2 Interaction plot for Torque

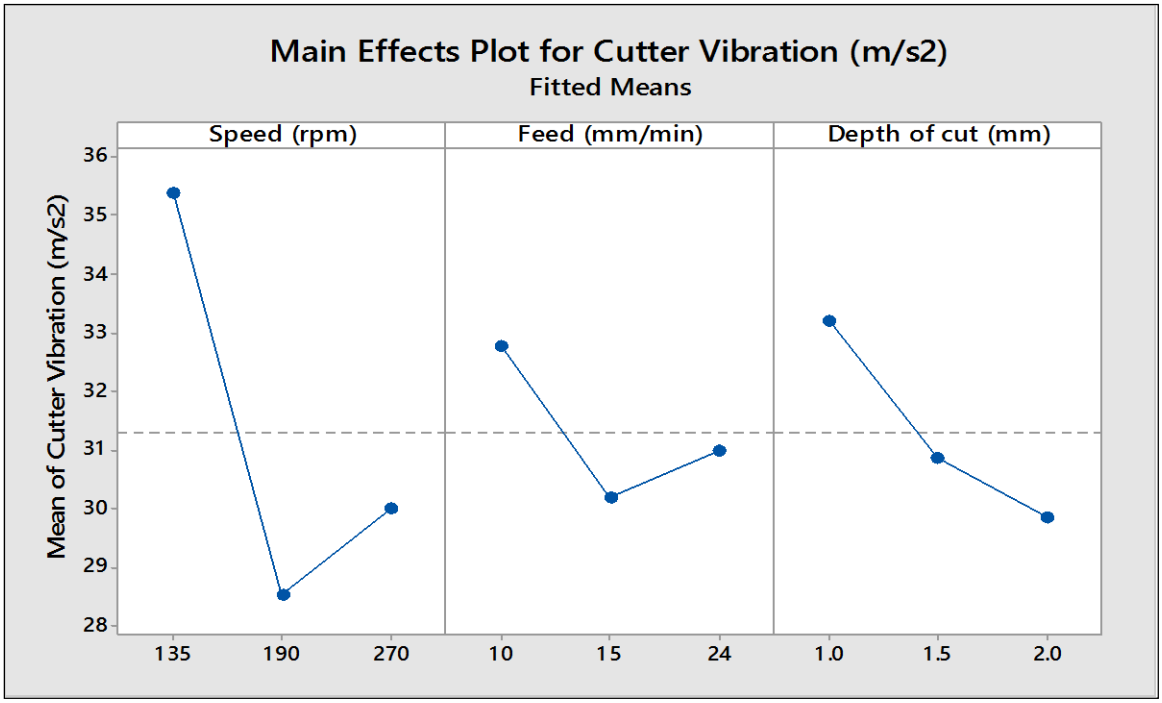

Fig- B.3 Main effect plots for milling cutter vibration

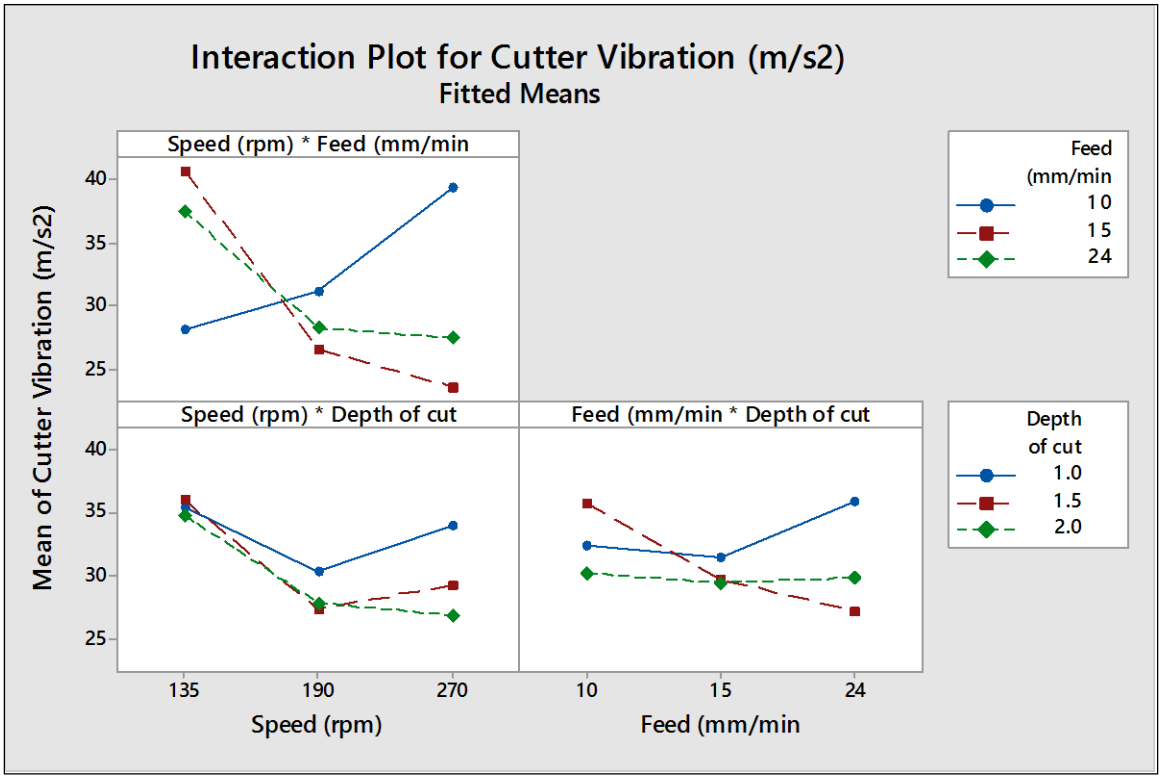

Fig- B.4 Interaction plots for milling cutter vibration

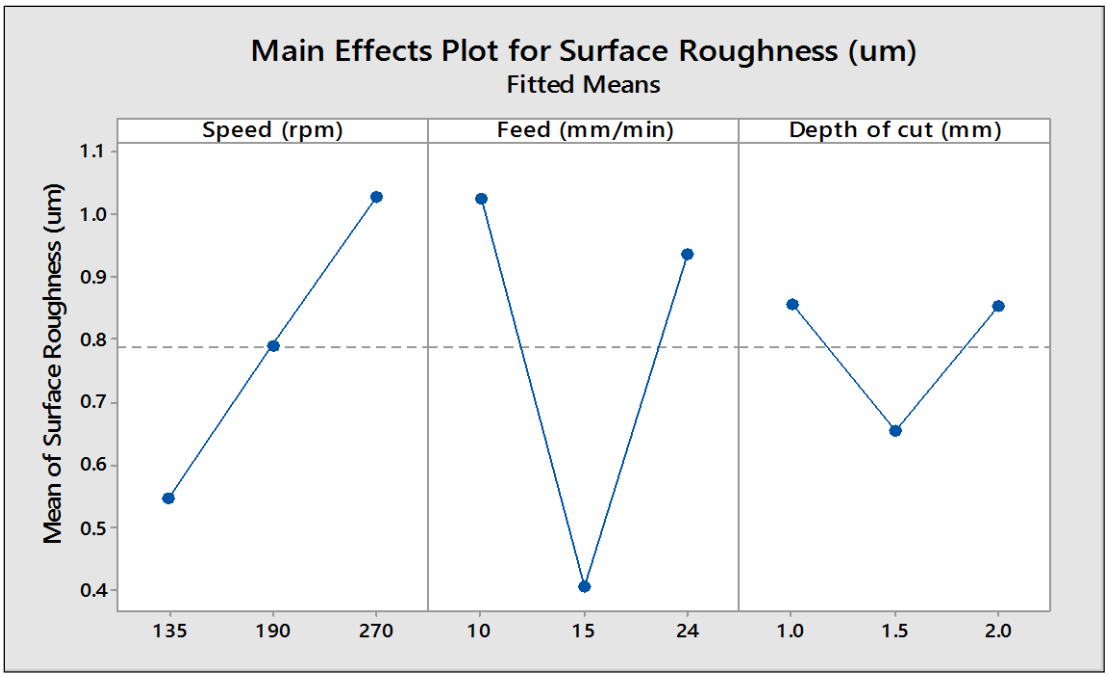

Fig- B.5 Main effect plots for Surface Roughness

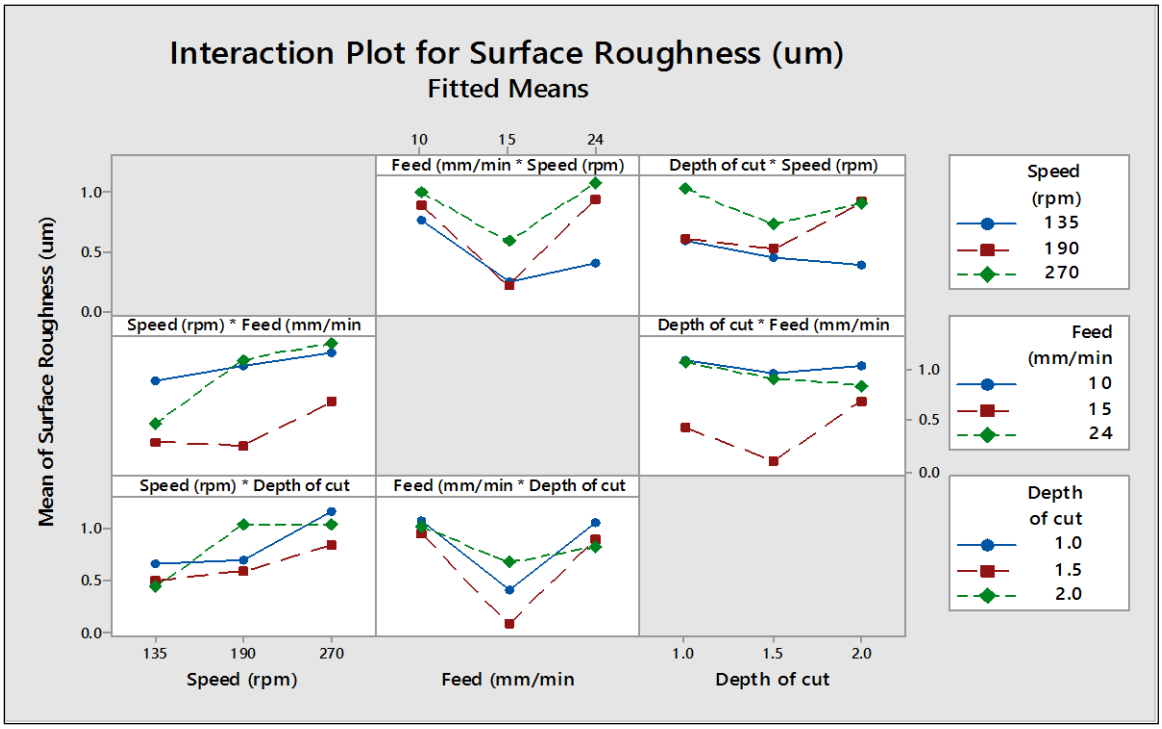

Fig- B.6 Interaction Plot for Surface Roughness

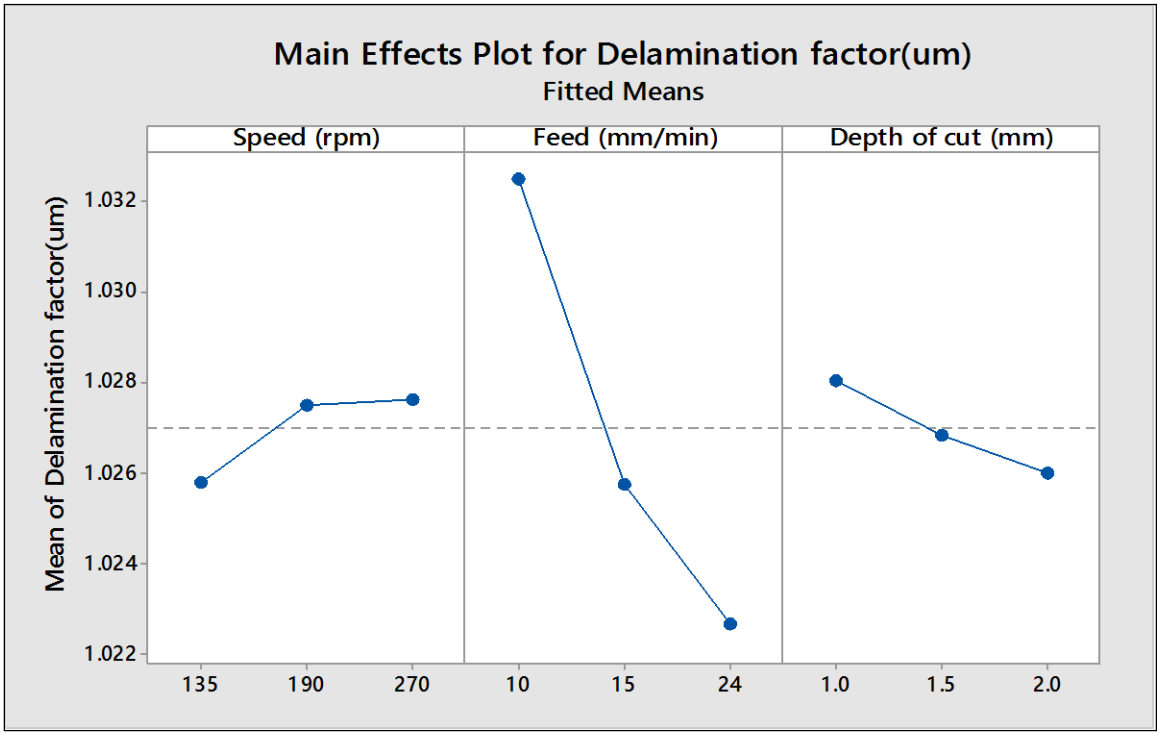

Fig- B.7 Main effect plots for Delamination Factor

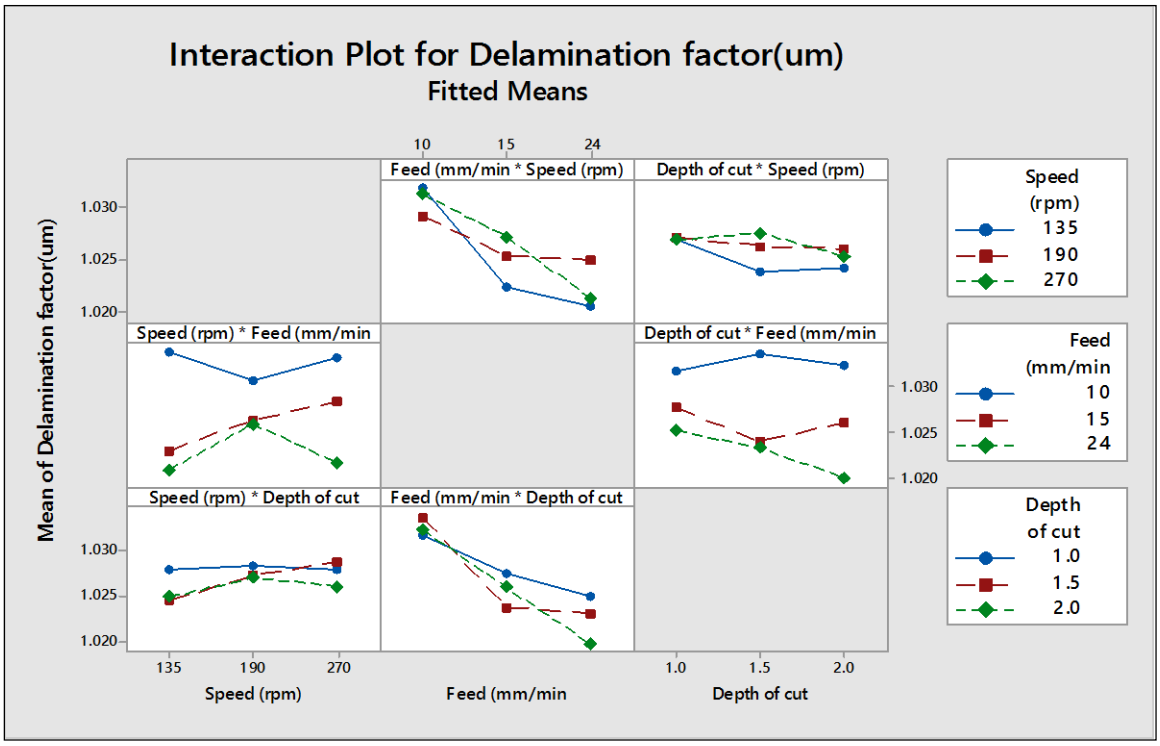

Fig- B.8 Interaction Plot for Delamination factor

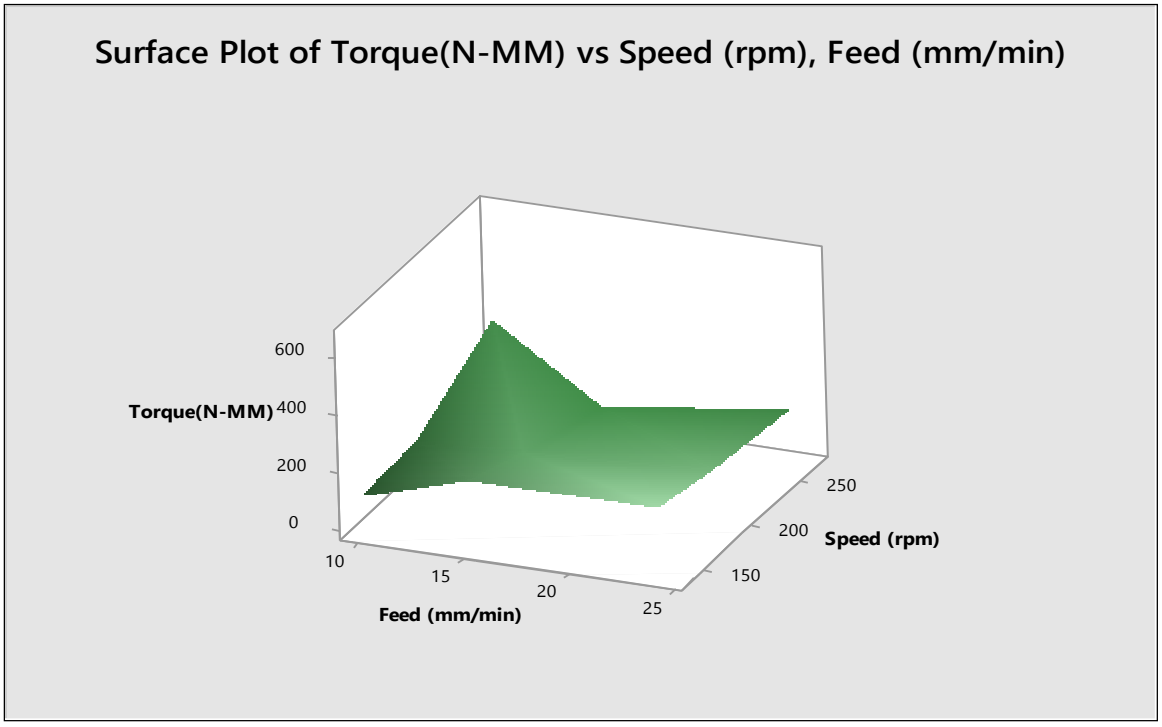

Fig- B.9 Response surface showing combined effect of rotational speed and feed rate on Torque

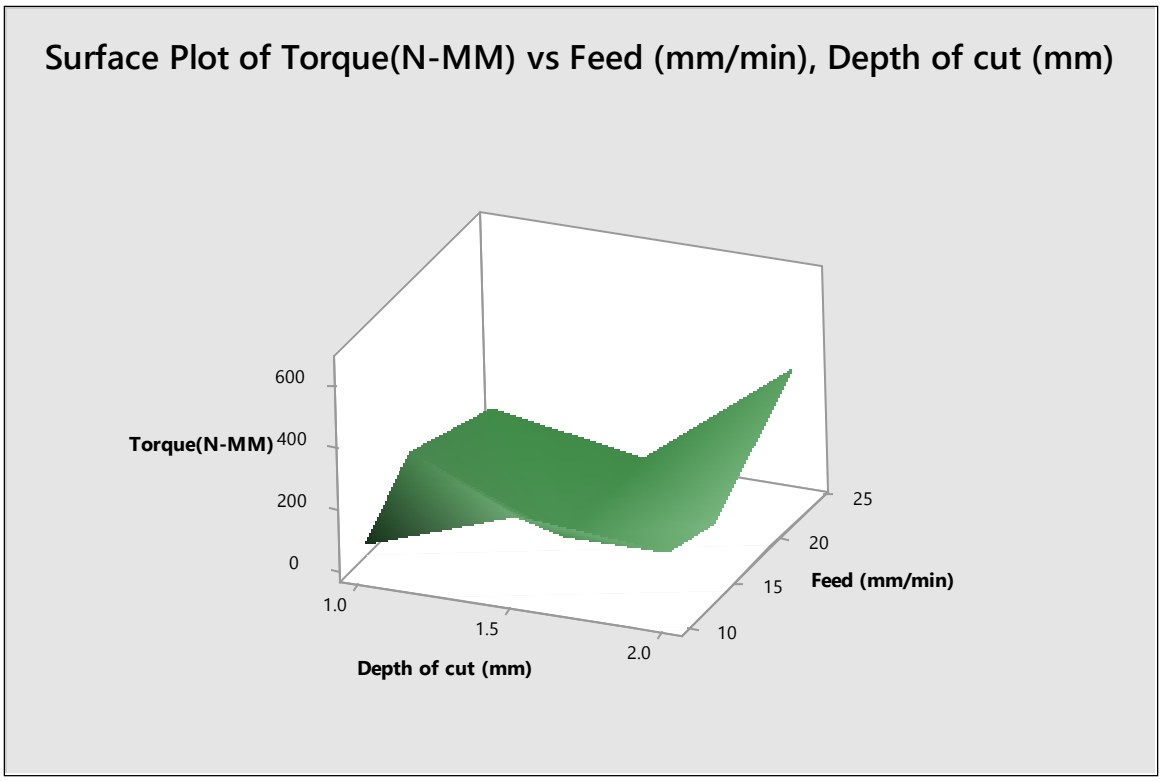

Fig– B.10 Response surface showing combined effect of feed rate and depth of cut on Torque

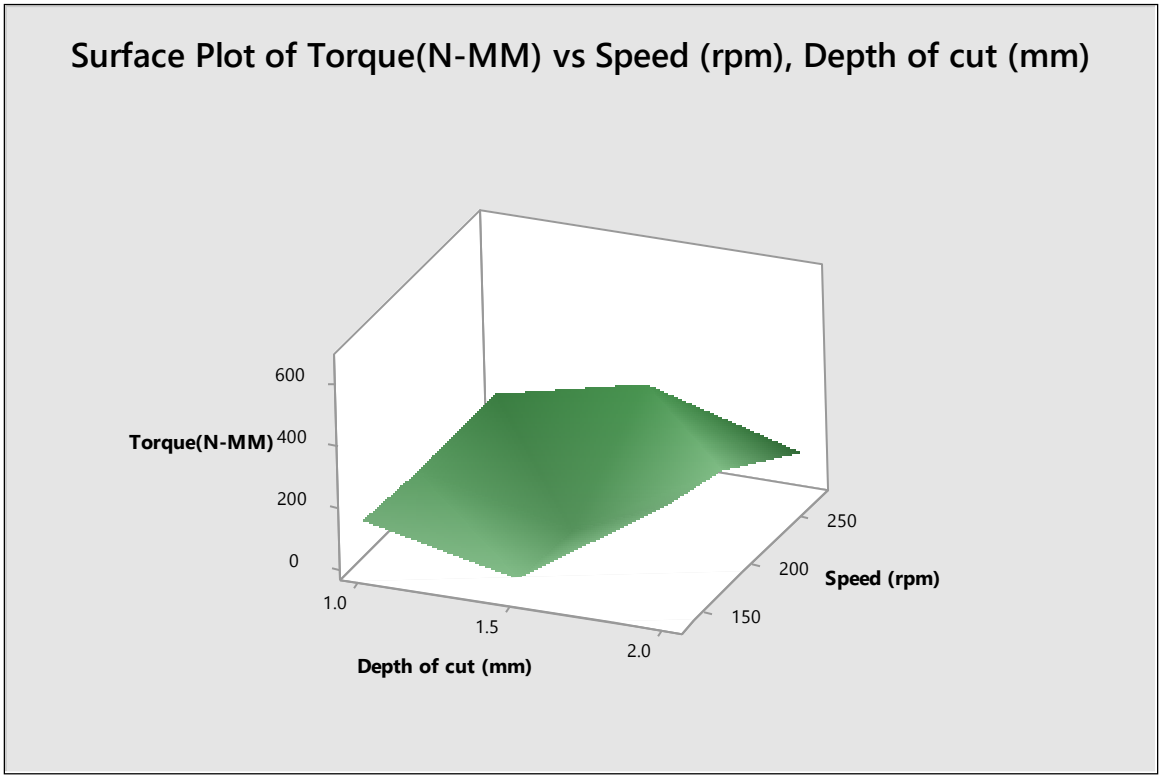

Fig- B.11 Response surface showing combined effect of speed and depth of cut on Torque

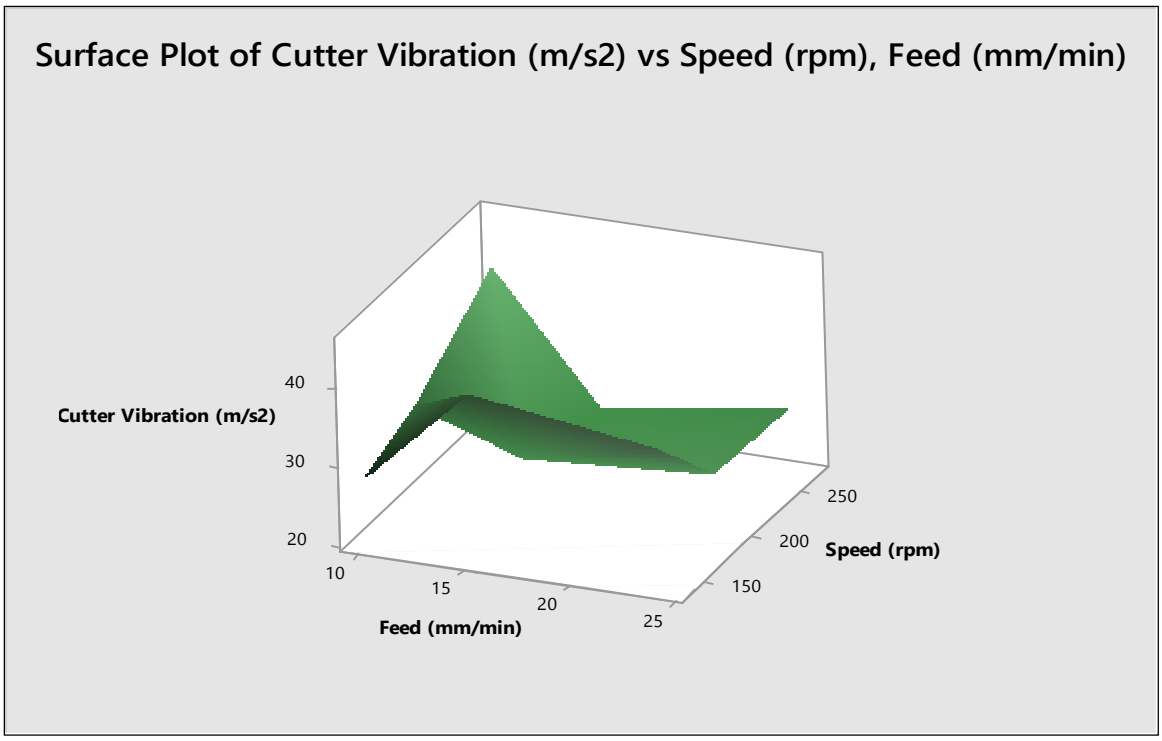

Fig– B.12 Response surface showing combined effect of rotational speed and feed rate on milling cutter vibration

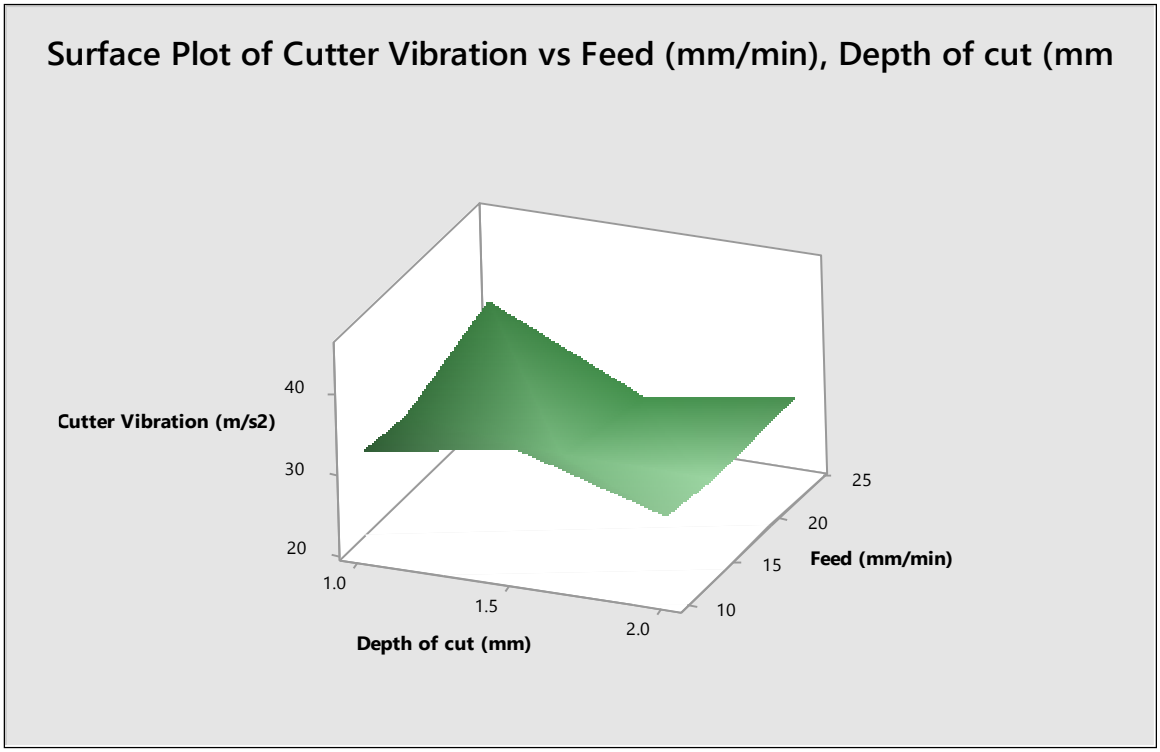

Fig – B.13 Response surface showing combined effect of Depth of cut and feed rate on milling cutter vibration

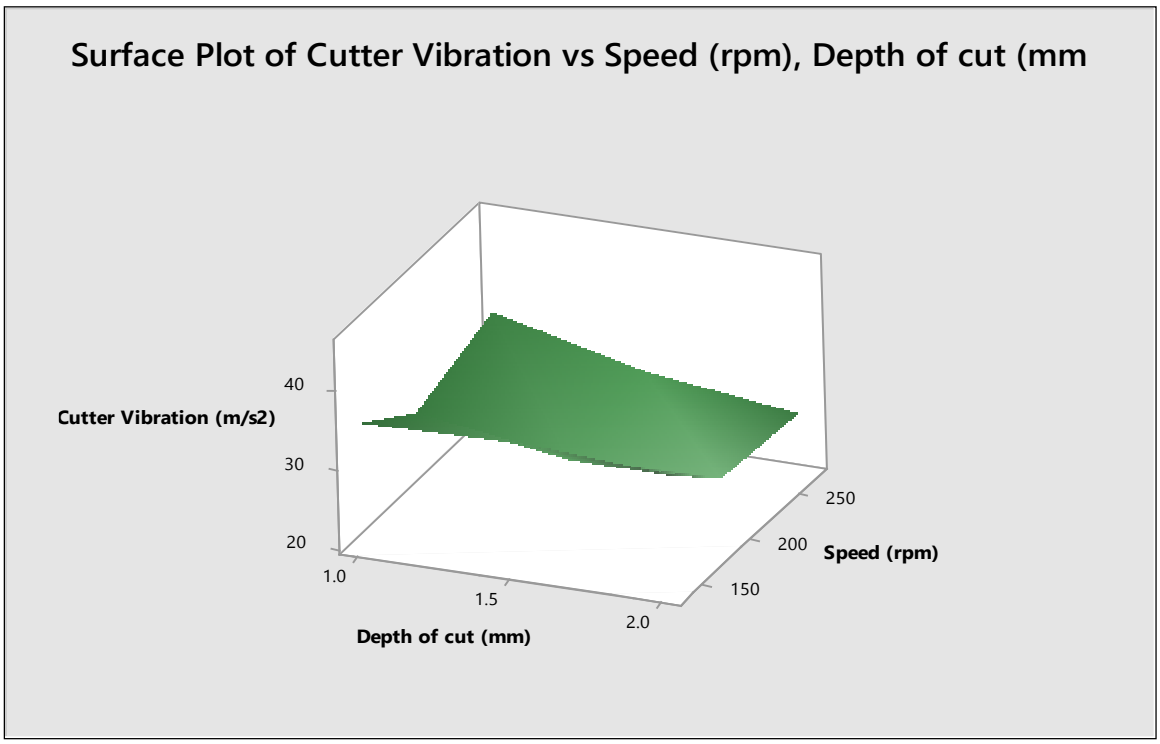

Fig – B.14 Response surface showing combined effect of rotational speed and Depth of cut on milling cutter vibration

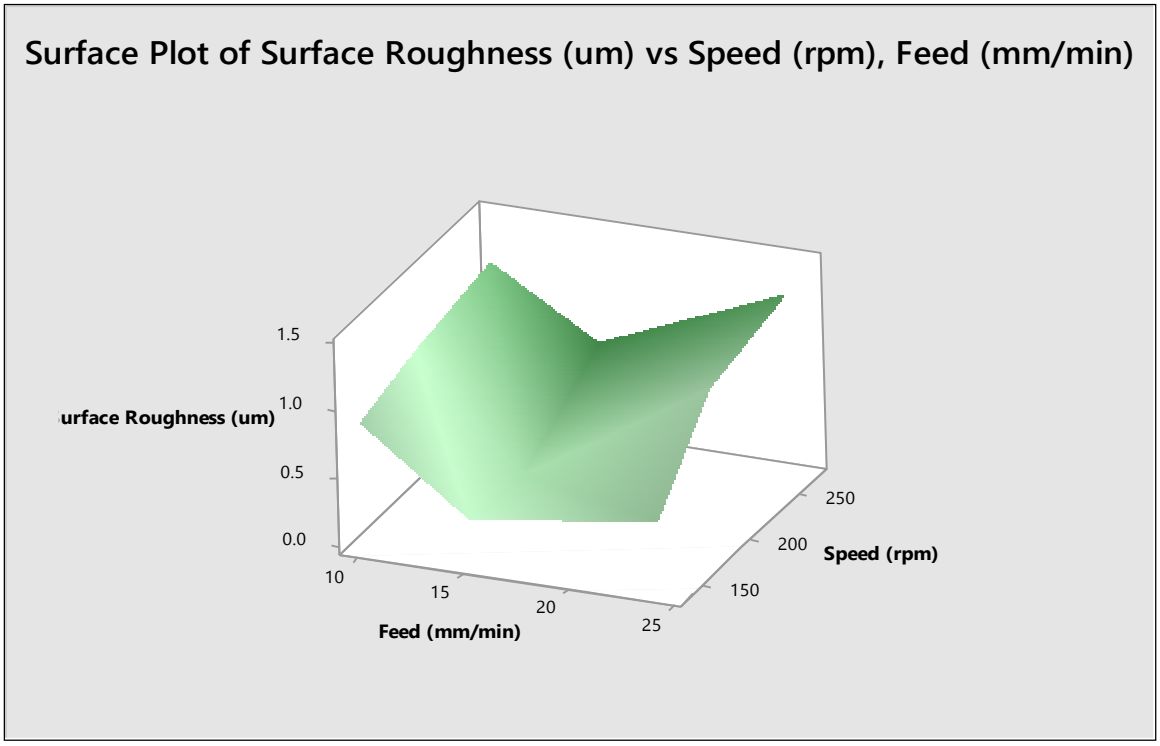

Fig – B.15 Response surface showing combined effect of rotational speed and feed rate on Surface Roughness

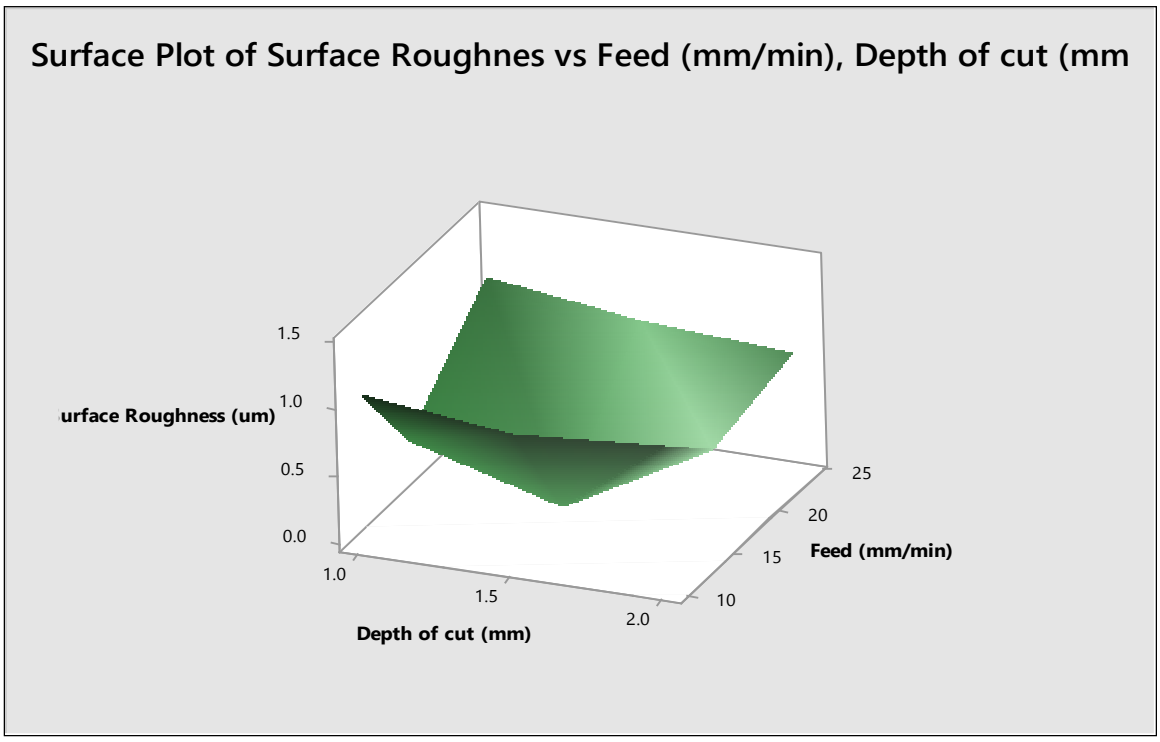

Fig – B.16 Response surface showing combined effect of Depth of cut and feed rate on Surface Roughness

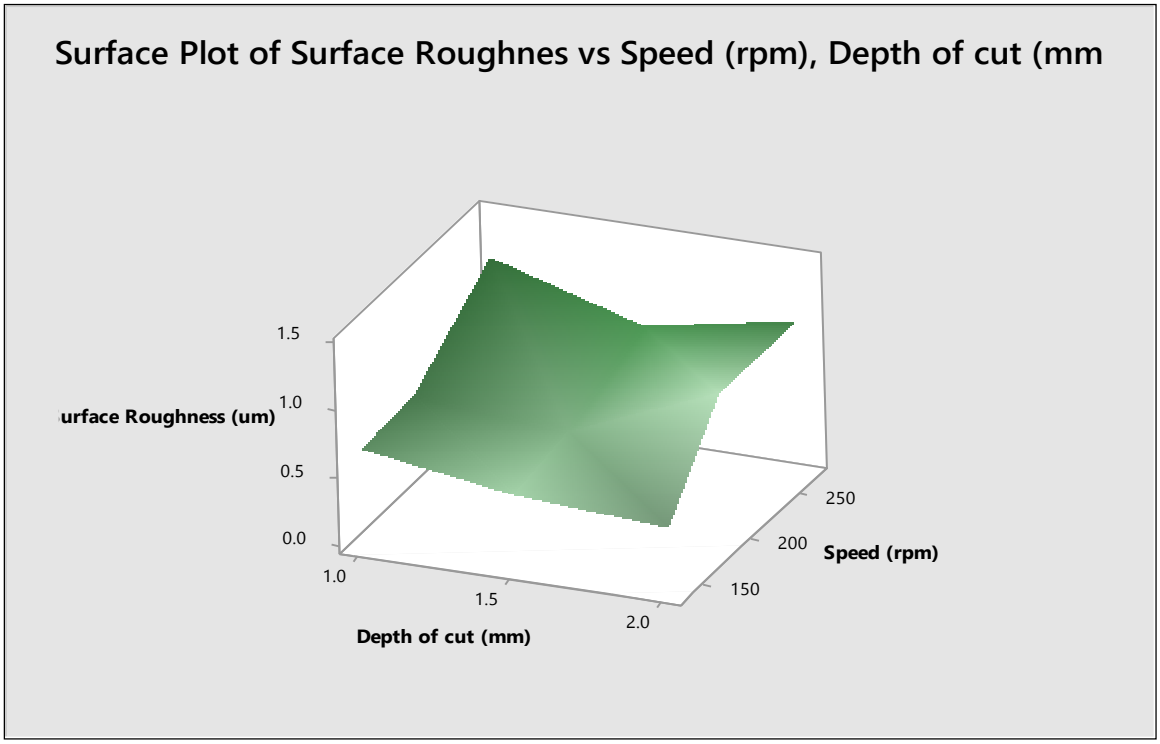

Fig – B.17 Response surface showing combined effect of rotational speed and depth of cut on Surface Roughness

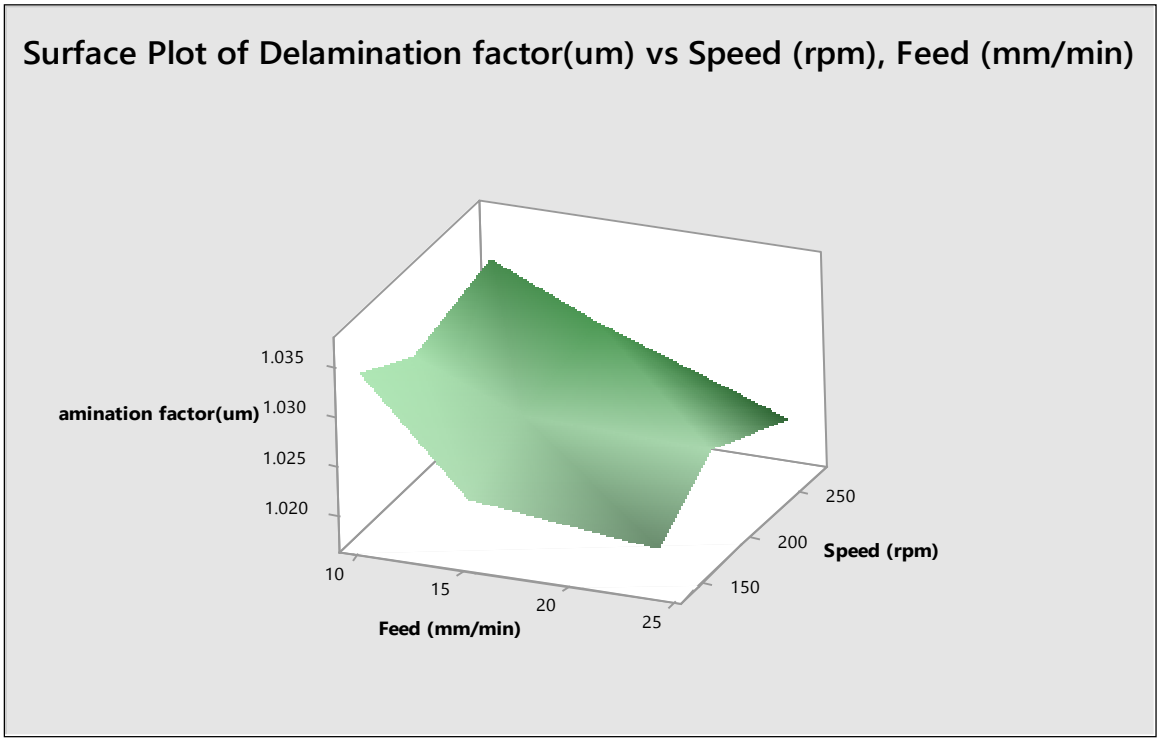

Fig – B.18 Response surface showing combined effect of rotational speed and feed rate on Delamination Factor

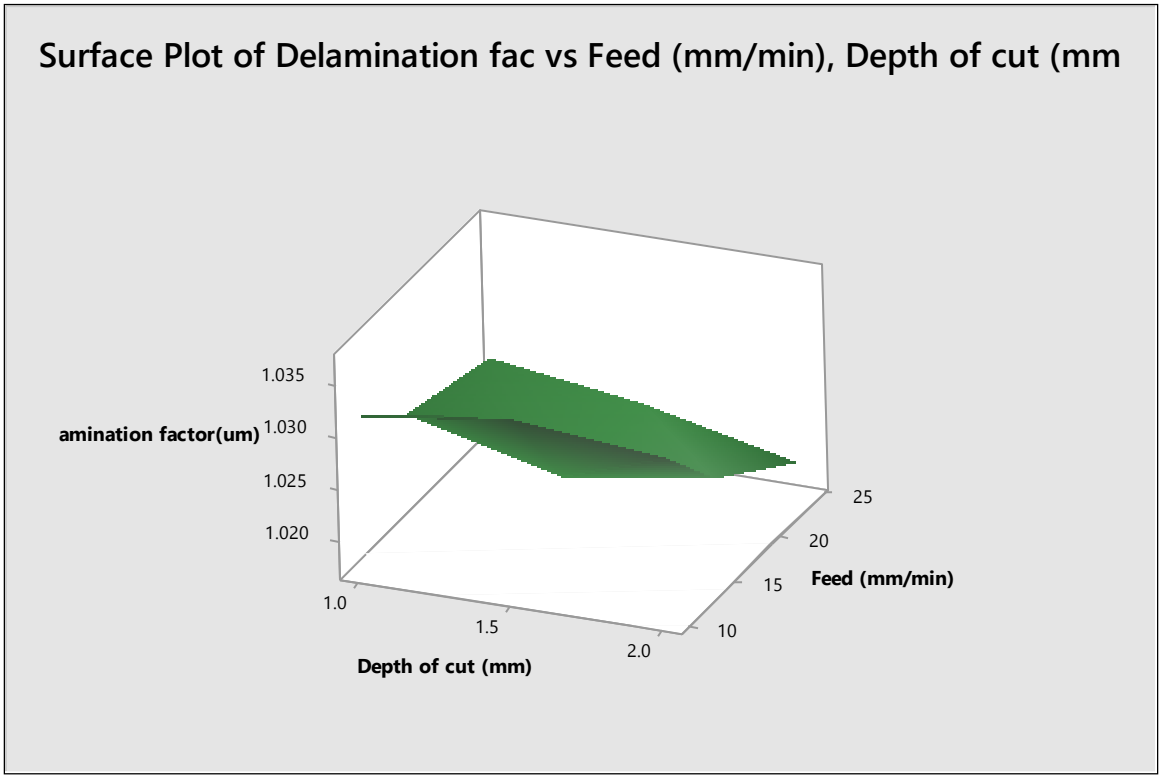

Fig – B.19 Response surface showing combined effect of depth of cut and feed rate on Delamination Factor

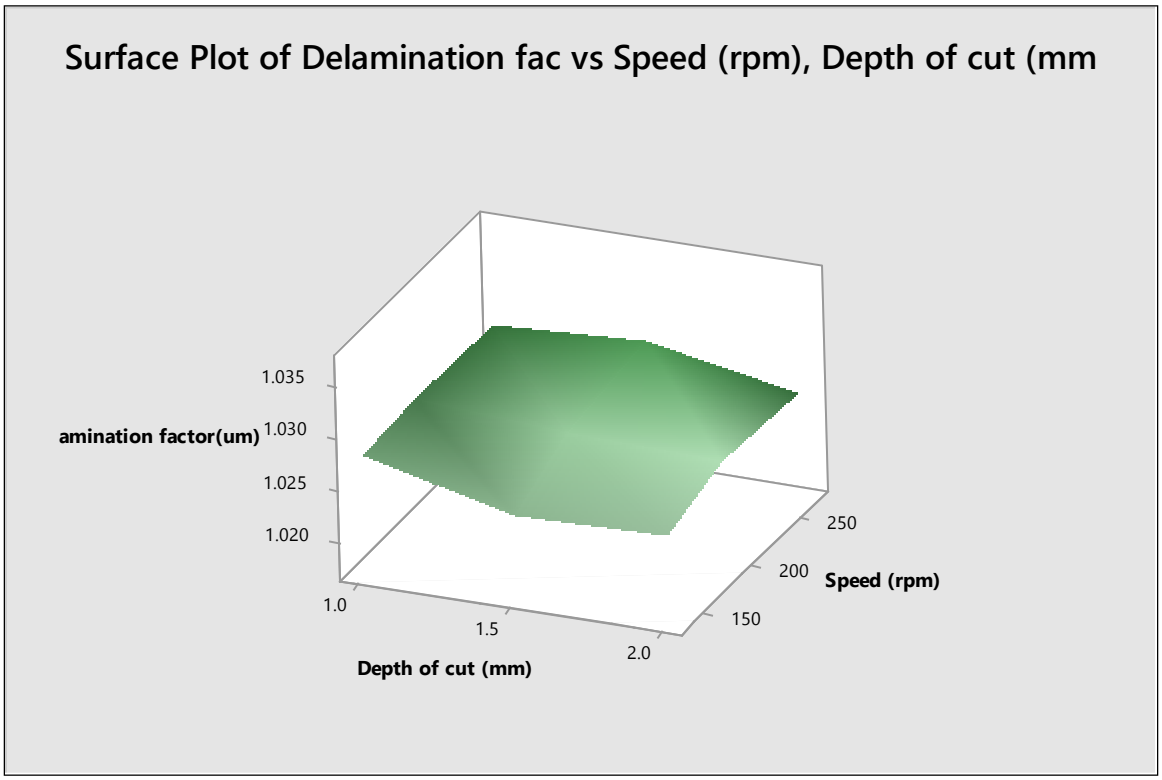

Fig – B.20 Response surface showing combined effect of rotational speed and depth of cut on Delamination Factor

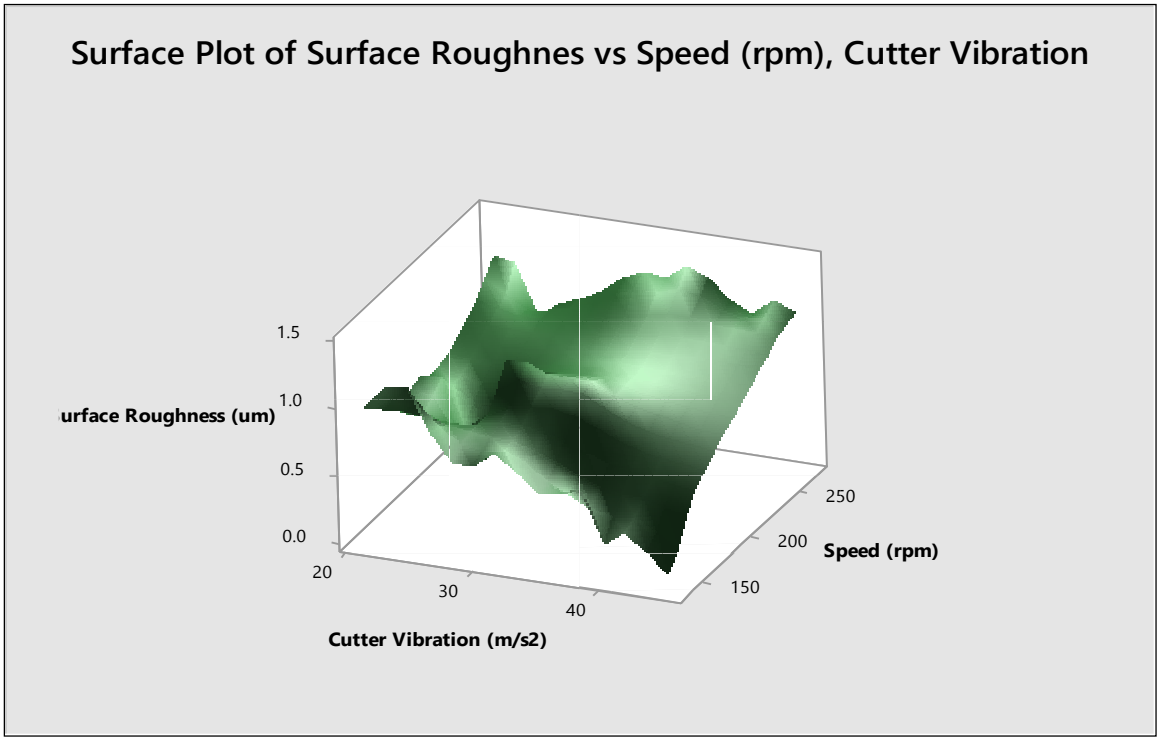

Fig – B.21 Response surface showing combined effect of Cutter vibration and Rotational speed on Surface Roughness

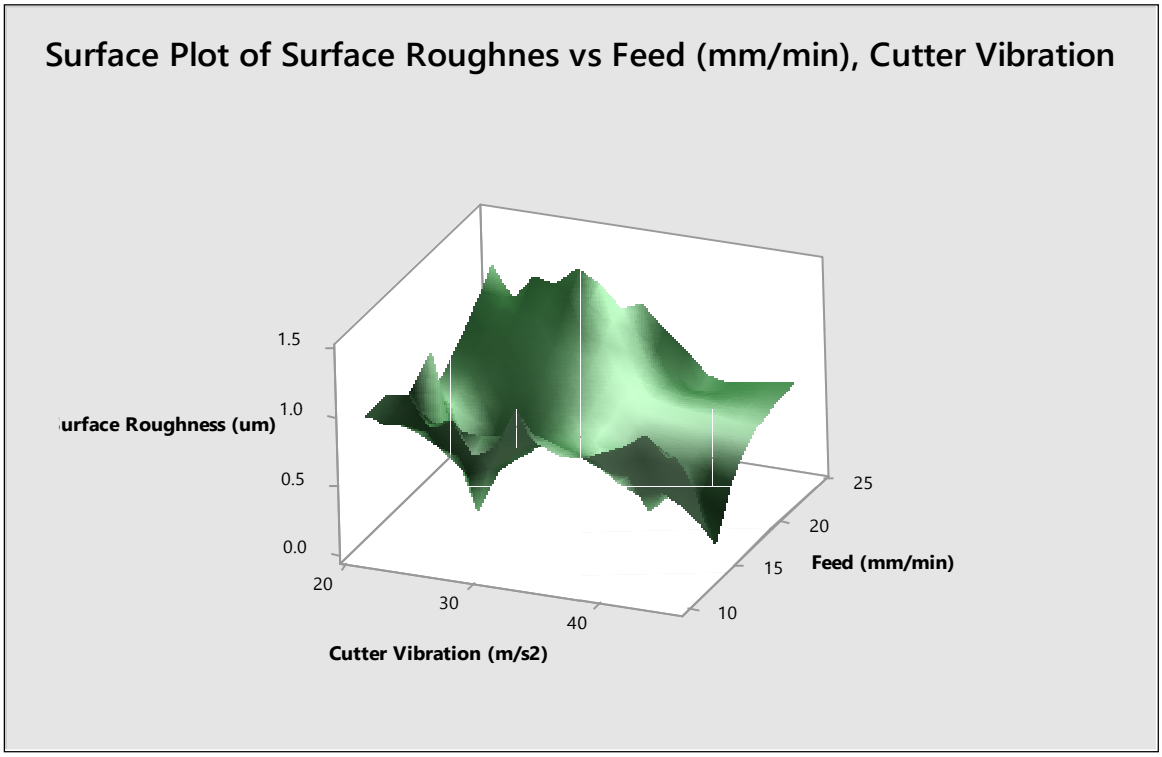

Fig – B.22 Response surface showing combined effect of Cutter vibration and Feed rate on Surface Roughness

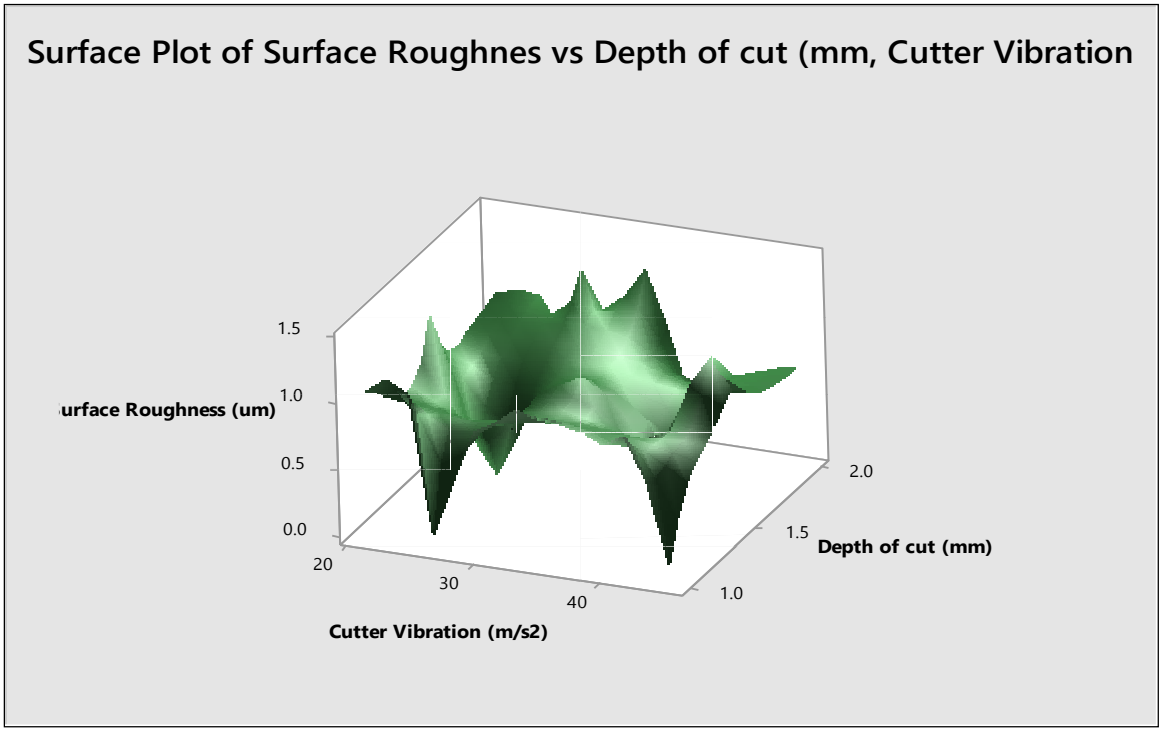

Fig – B.23 Response surface showing combined effect of Cutter vibration and Depth of cut on Surface Roughness

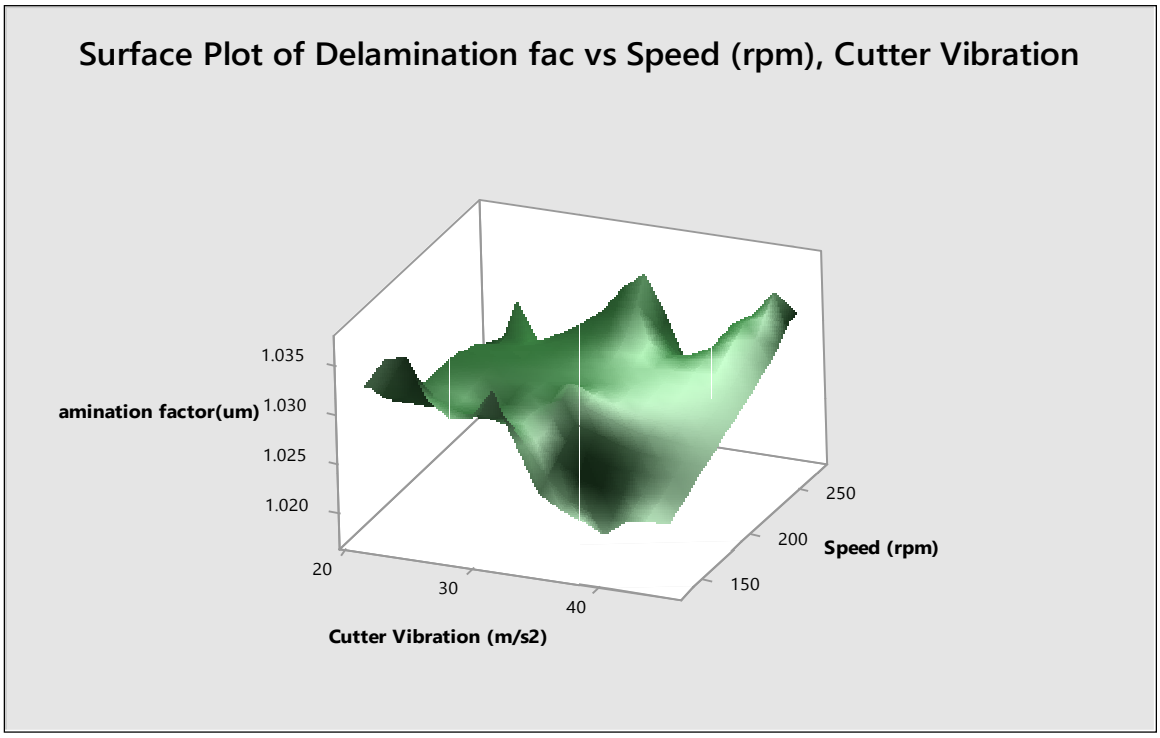

Fig – B.24 Response surface showing combined effect of Cutter vibration and Rotational speed on Delamination Factor

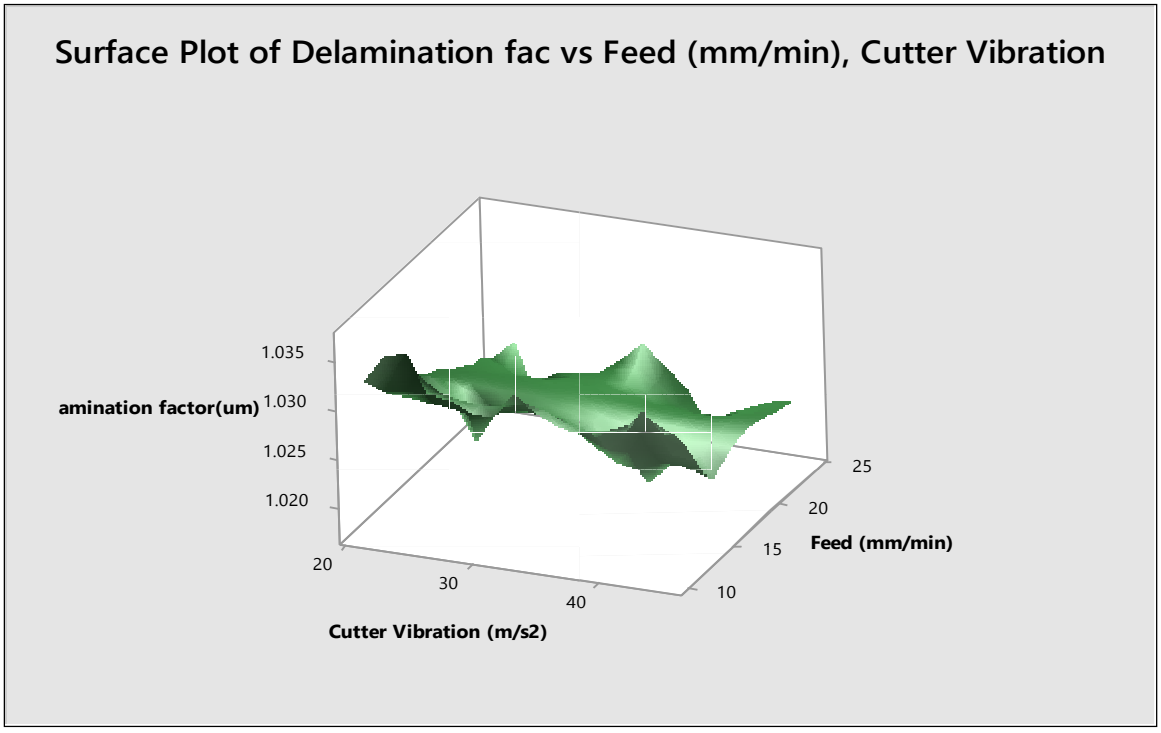

Fig – B.25 Response surface showing combined effect of Cutter vibration and Feed rate on Delamination Factor

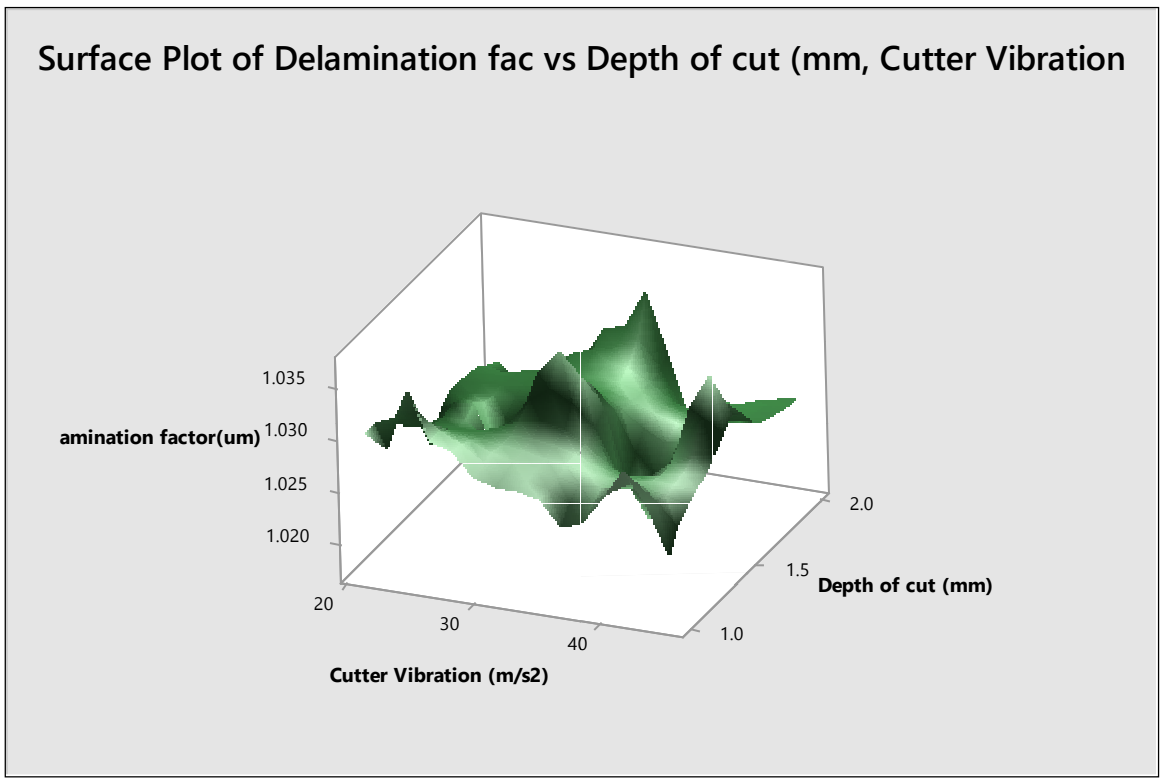

Fig – B.26 Response surface showing combined effect of Cutter vibration and Depth of cut on Delamination Factor